ESPOO 2007 VTT RESEARCH NOTES 2385

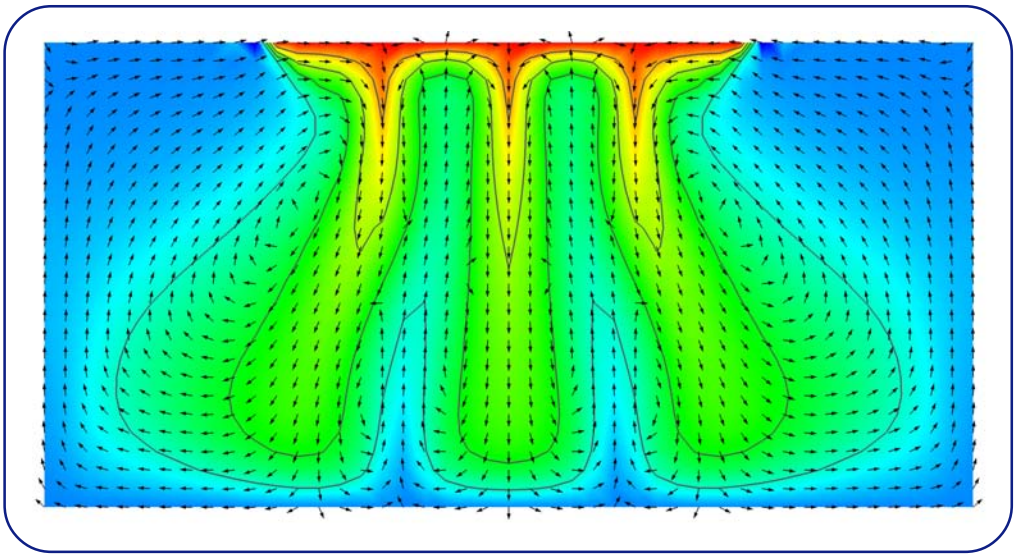

Jari Löfman, Vesa Keto & Ferenc Mészáros

FEFTRA™

Verification

VTT TIEDOTTEITA – RESEARCH NOTES 2385

FEFTRA™

Verification

Jari Löfman & Vesa Keto
VTT

Ferenc Mészáros
The Relief Laboratory

ISBN 978-951-38-6919-9 (soft back ed.)
ISSN 1235-0605 (soft back ed.)

ISBN 978-951-38-6920-5 (URL: http://www.vtt.fi/publications/index.jsp)
ISSN 1455-0865 (URL: http://www.vtt.fi/publications/index.jsp)

JULKAISIJA – UTGIVARE – PUBLISHER

VTT, Vuorimiehentie 3, PL 1000, 02044 VTT
puh. vaihde 020 722 111, faksi 020 722 4374

VTT, Bergsmansvägen 3, PB 1000, 02044 VTT
tel. växel 020 722 111, fax 020 722 4374

VTT Technical Research Centre of Finland, Vuorimiehentie 3, P.O.Box 1000, FI-02044 VTT, Finland
phone internat. +358 20 722 111, fax +358 20 722 4374

VTT, Otakaari 3 A, PL 1000, 02044 VTT
puh. vaihde 020 722 111, faksi 020 722 6390

VTT, Otsvängen 3 A, PB 1000, 02044 VTT
tel. växel 020 722 111, fax 020 722 6390

VTT Technical Research Centre of Finland, Otakaari 3 A, P.O. Box 1000, FI-02044 VTT, Finland
phone internat. +358 20 722 111, fax +358 20 722 6390

Edita Prima Oy, Helsinki 2007

Löfman, Jari, Keto, Vesa & Mészáros, Ferenc. FEFTRA™. Verification. Espoo 2007. VTT Tiedotteita – Research Notes 2385. 103 p. + app. 4 p.

Keywords modelling, groundwater flow, solute transport, heat transfer, nuclear waste, disposal

Abstract

FEFTRA is a finite element program package developed at VTT for the analyses of groundwater flow in Posiva's site evaluation programme that seeks a final repository for spent nuclear fuel in Finland. The code is capable of modelling steady-state or transient groundwater flow, solute transport and heat transfer as coupled or separate phenomena. Being a typical research tool used only by its developers, so far the FEFTRA code has been short of a competent testing system and precise documentation of the verification of the code.

The objective of this work was to reorganise all the material related to the existing verification cases and place them into the FEFTRA program path under the version-control system. The work also included development of a new testing system, which automatically calculates the selected cases, checks the new results against the old approved results and constructs a summary of the test run. All the existing cases were gathered together, checked and added into the new testing system. The documentation of each case was rewritten with the LaTeX document preparation system and added into the testing system in a way that the whole test documentation (this report) can easily be generated in a postscript or pdf-format.

At the moment the report includes mainly the cases related to the testing of the primary result quantities (i.e. hydraulic head, pressure, salinity concentration, temperature). The selected cases, however, represent typical hydrological applications, in which the program package has been and will be employed in the Posiva's site evaluation programme, i.e. the simulations of groundwater flow, solute transport and heat transfer as separate or coupled phenomena. The comparison of the FEFTRA results to the analytical, semianalytical and/or other numerical solutions proves the capability of FEFTRA to simulate such problems.

The report is available both in a printed and electronic format. As the report is in a constant state of evolution resulting from the current code development, the printed form represents a "snapshot" of its content at the date of publishing, while the electronic format represents always the most up-to-date version of the report.

Löfman, Jari, Keto, Vesa & Mészáros, Ferenc. FEFTRA™. Verification. Espoo 2007. VTT Tiedotteita – Research Notes 2385. 103 s. + liitt. 4 s.

Keywords modelling, groundwater flow, solute transport, heat transfer, nuclear waste, disposal

Tiivistelmä

FEFTRA on VTT:llä kehitetty elementtimenetelmään perustuva numeerinen virtausten simulointiohjelmisto. Posiva Oy:n käytetyn ydinpolttoaineen loppusijoituspaikka-tutkimuksiin liittyviin pohjaveden virtausongelmiin suunniteltua ohjelmistoa voidaan soveltaa moniin erityyppisiin tapauksiin, jotka edellyttävät esimerkiksi veteen liuenneiden aineiden ja/tai veden lämpötilaeroista aiheutuvien veden tiheyserojen huomioimista. Koska ohjelmisto on ollut ennenkaikkea kehittäjiensä ja ylläpitäjiensä käyttöön tarkoitettu työkalu, siitä on tähän asti puuttunut kunnollinen testijärjestelmä sekä yksityiskohtainen dokumentaatio verifioinnista.

Tämän työn tavoitteena oli järjestää uudelleen FEFTRAn hajallaan ollut verifiointi-materiaali ja liittää se ohjelmistopakettiin versionhallintaohjelmiston hallintaan. Työssä kehitettiin testijärjestelmä, joka automaattisesti laskee halutut tapaukset, vertaa tuloksia aikaisemmin laskettuihin ja oikeaksi todettuihin tuloksiin sekä konstruoi yhteenveto-raportin suoritetuista testiajoista ja niiden tarkastuksesta. Olemassaoleva hajallaan oleva testimateriaali koottiin yhteen, tarkistettiin ja liitettiin uuteen järjestelmään. Kustakin tapauksesta kirjoitettiin LaTeX-ohjelmalla uusi yksityiskohtainen dokumentaatio, joka liitettiin kehitettyyn järjestelmään siten, että koko dokumentti (tämä raportti) voidaan helposti generoida joko postscript tai pdf-formaatissa.

Tämä raportti sisältää tällä hetkellä pääasiassa perustulossuureisiin (hydraulinen korkeus, paine, suolapitoisuus, lämpötila) liittyviä tapauksia, jotka kuitenkin edustavat sellaisia pohjaveden virtaukseen, suolan kulkeutumiseen ja lämmönsiirtymiseen liittyviä tilanteita, joiden simulointiin ohjelmistoa sovelletaan ydinjätteen loppusijoitukseen liittyvissä paikkatutkimuksissa. Lasketut tapaukset osoittavat FEFTRA-ohjelmiston soveltuvan hyvin kyseisten ongelmien simulointiin.

Raportti on saatavissa sekä painettuna että sähköisessä muodossa. Painettu versio kuitenkin edustaa ainoastaan julkaisuhetkeä, kun taas sähköistä versiota tullaan jatkuvasti päivittämään ohjelmankehityksen mukana.

Preface

Acknowledgement is given to Mr. Lasse Koskinen (VTT) for his critical review of this report.

Contents

1. Introduction

Background

Posiva Oy (a company responsible for nuclear waste management in Finland) is preparing for the final disposal of spent nuclear fuel into the crystalline bedrock in Finland. The site for the repository will be chosen on the basis of the site investigations. Preliminary site investigations (SITU stage) were carried out at five sites during 1986–1992. Three sites (Romuvaara in Kuhmo, Kivetty in Äänekoski, Olkiluoto in Eurajoki) were chosen for more detailed and comprehensive investigations (PATU stage) performed in 1993–1996. In addition, Hästholmen in Loviisa was included in the site selection programme in 1997. In 1999, the latest investigations were finished for the four sites, and Olkiluoto was proposed to be the primary site for the repository and subject to further detailed characterisation. Currently the site investigation programme is focused on the construction of an underground rock characterisation and research facility (ONKALO) in Olkiluoto. The facility will consist of a 9000 m long and 520 m deep system of tunnels, to be potentially extended with the drifts of the repository (Posiva 2006b). At the moment (mid-March 2007) 1900 metres of the tunnels, extending to a depth of 180 metres, have been excavated (http://www.posiva.fi).

The repository will be excavated in the bedrock at a depth of 400–700 m. The spent fuel will be encapsulated in double layered copper-cast iron canisters. If the canisters fail, radioactive material could be released from the repository into the biosphere as a result of dissolution in the groundwater and subsequent migration along with the groundwater flow to surface water systems. In addition, the amount of the groundwater flowing through the repository and in its immediate vicinity affects the long-term durability of engineered barriers as well as the rate of the dissolution of the spent fuel. Therefore, an analysis of groundwater flow deep in the bedrock is an important part of the ongoing work for the site investigation programme.

The open tunnel system may constitute a hydraulic disturbance to the site's groundwater system for hundreds of years (e.g. inflow of groundwater into the open tunnels and drawdown of groundwater table, intrusion of surface water containing oxygen and carbon dioxide deep into the bedrock, upconing of deep saline groundwater). The essential part of the site investigation programme is the analyses of the possible hydrological impacts of the excavation of the ONKALO and repository tunnels.

The groundwater flow analyses carried out at VTT are based on representation of the physical processes governing flow by the mathematical models. The applied models depend on the characteristics of the area to be investigated. If density of water can be taken to be constant (as in the Kivetty and Romuvaara sites), groundwater flow can be described by flow equation only. However, consideration of density variations caused by a varying salinity concentration of water (as in the Hästholmen and Olkiluoto sites) requires solving coupled equations for flow and solute transport. Also, if the effects of the temperature rise of the repository caused by the decay heat of spent nuclear fuel are to be considered in the analyses, a heat transfer equation has to be included in the model as well.

FEFTRA program package

FEFTRA (Taivassalo et al. 1991; Löfman & Taivassalo 1993; Koskinen et al. 1996) is a finite element program package developed at VTT for groundwater flow analyses in the site investigation programme seeking a final repository of spent nuclear fuel (Figure 1.1). The code is capable of modelling steady-state or transient groundwater flow, solute transport and heat transfer as coupled or separate phenomena. The mathematical model consists of partial differential equations written for hydraulic head/pressure, solute concentration and temperature. The equations in the coupled cases are linked to each other by means of the Darcy velocity as well as temperature and concentration-dependent properties such as fluid density and viscosity. When simulating solute transport, the effect of matrix diffusion can be taken into account, while highly convective cases can be handled with different upwind methods. The water table drawdown caused by the excavation of the tunnels can be simulated by employing the free-surface approach. The time discretisation in FEFTRA is based on the finite difference approximation. The matrix equations resulting from the finite element formulation can be solved either using the direct frontal solver or various iterative solvers. In coupled cases, a set of nonlinear algebraic equations is solved applying the Picard iterative approach with options for the relaxation.

The FEFTRA code uses linear or quadratic one-, two- and three-dimensional elements. Two-dimensional elements can also be applied in a three-dimensional mesh and one-dimensional elements in both two and three-dimensional meshes. For example, in three-dimensional groundwater flow simulations, the sparsely fractured rock between the hydrogeological zones can be described by three-dimensional elements, the zones or other planar structures by two-dimensional elements and drillholes by one-dimensional elements. An advanced preprocessor includes the *quadtree/octree* algorithm, which enables an efficient local refinement of mesh around natural and engineered bedrock structures (e.g. hydrogeological zones, tunnels, drillholes, sinks, etc.) (static mode) or at locations with high hydraulic gradient (dynamic mode).

The most recent studies, in which the code has been applied, consist of the simulation of hydraulic impact of ONKALO and repository (Löfman & Mészáros 2005a; Löfman 2005; Löfman & Mészáros 2005b; Posiva 2007). In addition, supporting groundwater flow analyses have been conducted for a description of the Olkiluoto site before the excavation of the ONKALO (Posiva 2007) and for an expected evolution of a spent nuclear fuel repository at Olkiluoto (Posiva 2006a).

Overview of the report

Being a typical research tool used only by its developers, the FEFTRA code has so far been short of a competent testing system and a precise documentation of the verification of the code. The FEFTRA program package has evolved during long-term development and application work since the early 1980's. The features of the first versions of the code were quite limited, but the application of the program package to the various groundwater flow analyses has required extensive further development. Thus, the new features have

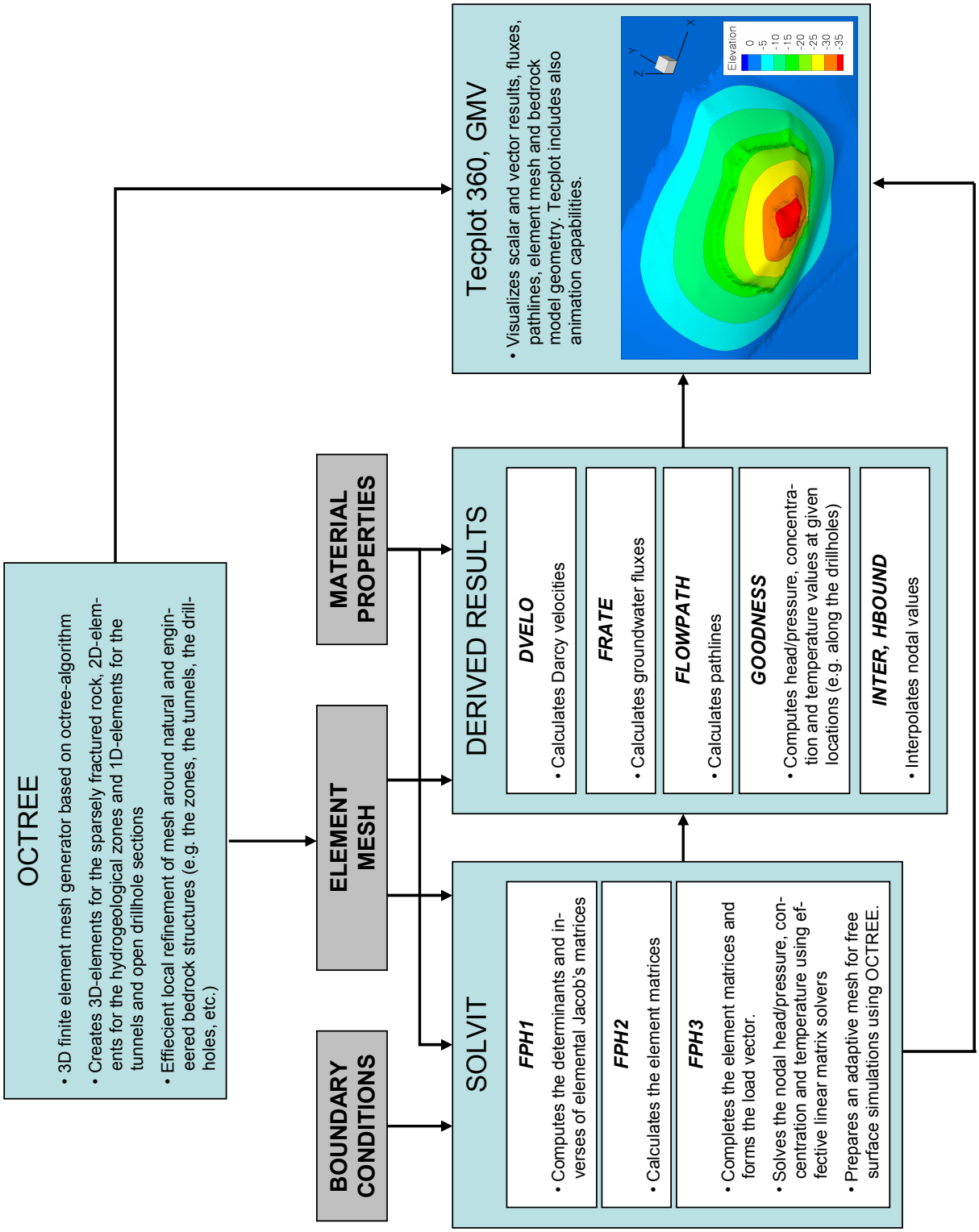

Figure 1.1. A schematic description of the components of the FEFTRA code.

been added, tested and documented within several different projects and reports (mostly in Finnish). Accordingly, individual test cases (input/output files) have also been located in several different project related directories, so the test runs and the examination of the results of the cases have not been convenient.

The objective of this work is to reorganise all the material related to the existing verification cases of FEFTRA and place them to the FEFTRA program path under the CVS version control system (CVS 2007). The work also includes a development of a new testing system, which automatically computes and documents all the test cases (see Appendix). All the existing cases are gathered together, checked and added into the new testing system. The documentations of the cases are rewritten and added into the system. Finally not only the test run can be carried out automatically but also the test documentation (this report) can easily be generated.

At the moment the report includes mainly the cases related to the testing of the primary result quantities (i.e. hydraulic head, pressure, salinity concentration, temperature, location of groundwater table) in the FEFTRA module *solvit*, but more cases for the other modules will be added in the future. The selected cases, however, represent the applications, in which FEFTRA has been employed.

The report is available both in a printed and electronic format. However, the report is in a constant state of evolution resulting from the current code development. Thus, the printed form represents a "snapshot" of its content at a date of publishing, while the electronic format, which belongs to the FEFTRA package, represents always the most up-to-date version of the report.

2. Groundwater flow

2.1 Radial steady-state flow

de Marsily (1986) presented analytical solutions for various groundwater flow problems. The case with a radial steady-state flow was selected to verify the capability of the FEFTRA code to use various types of elements (2D and 3D) and boundary conditions (flow rates and fluxes).

The test case is located in the FEFTRA program path as follows:

- *feftra/solvit/t/head/th3Dst_v* (flow rate boundary condition in 3D)
- *feftra/solvit/t/head/th3Dst* (flux boundary condition in 3D)
- *feftra/solvit/t/head/th2Dst_v* (flow rate boundary condition in 2D)
- *feftra/solvit/t/head/th2Dst* (flux boundary condition 2D).

Definition of the problem

The case concerns a steady-state groundwater flow in a homogeneous and isotropic discoid structure (Figure 2.1). The disc is pumped from the centre at a constant rate, while a zero hydraulic head is used on an outer boundary. The density of water is assumed to be constant. The resulting quantity is hydraulic head.

Mathematical model

A steady-state flow equation for hydraulic head is written as follows (Bear 1979; Huyakorn & Pinder 1983; de Marsily 1986)

$$\nabla \cdot (\boldsymbol{K} \nabla h) + Q = 0, \tag{2.1}$$

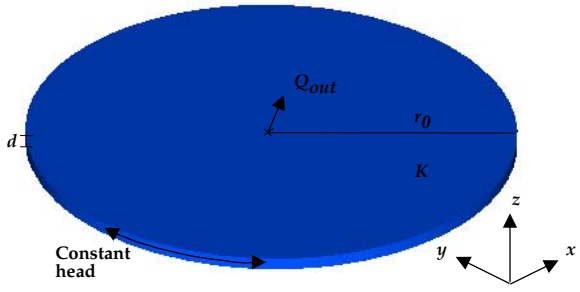

Figure 2.1. Schematic figure of the radial steady-state flow problem.

Table 2.1. Input parameters for the radial steady-state flow problem.

Symbol	*Parameter*	*Equation*	*Value*
$\boldsymbol{K}$	Hydraulic conductivity	2.1, 2.3	10^{-8} m s^{-1}
d	Thickness of modelled disc	2.3	100 m
r_0	Radius of modelled disc	2.3	2000 m
Q_{out}	Pumping rate	2.3	$1.0 \cdot 10^{-5}$ m^3 s^{-1}

where $\boldsymbol{K}$ is the hydraulic conductivity [m/s], h the hydraulic head [m] and Q the rate of flow per unit volume [1/s]. The parameter values are given in Table 2.1.

Numerical solution method

Due to the symmetry of the problem, only a sector of 11.25° of the disc was included into the model, which gave an outflow rate

$$Q_s = -Q_{out} \cdot \frac{11.25^\circ}{360^\circ} = -3.125 \cdot 10^{-7}\text{m}^3\text{/s} \tag{2.2}$$

at the vertex.

In order to test various elements and boundary conditions, different 2D and 3D element meshes were constructed. The elements used in the meshes were hexahedrals, wedges, quadrilaterals and trilaterals (Figure 2.2). The flow rate boundary condition was assigned to the vertex nodes in the cases shown in Figures 2.2(a) and 2.2(c). In the cases shown in Figures 2.2(b) and 2.2(d) the modelled sector was selected to begin at the distance of 20 m from the vertex, and flux q was specified through the innermost face/edge of the innermost element. Table 2.2 summarises the use of the flow rate and flux boundary conditions.

The partial differential equation (2.1) describing groundwater flow was solved numerically employing the conventional Galerkin technique with linear elements (Huyakorn & Pinder 1983). The linear matrix equation resulting from the finite element formulation was solved using the direct frontal method (Hinton & Owen 1977; Bathe 1982).

Table 2.2. Flow rates and fluxes given in the FEFTRA input files for different cases.

Case	*Flow rate [m^3/s]*	*Flux q*	*Comment*
3D; vertex	Q_s/2=$-1.563 \cdot 10^{-7}$		2 nodes at the vertex
3D; no vertex		Q_s/A=$-7.97 \cdot 10^{-10}$ m/s	face A=392.0459 m^2
2D; vertex	Q_s=$-3.125 \cdot 10^{-7}$		1 node at the vertex
2D; no vertex		Q_s/L=$-7.97 \cdot 10^{-8}$ m^2/s	edge L=3.920459 m

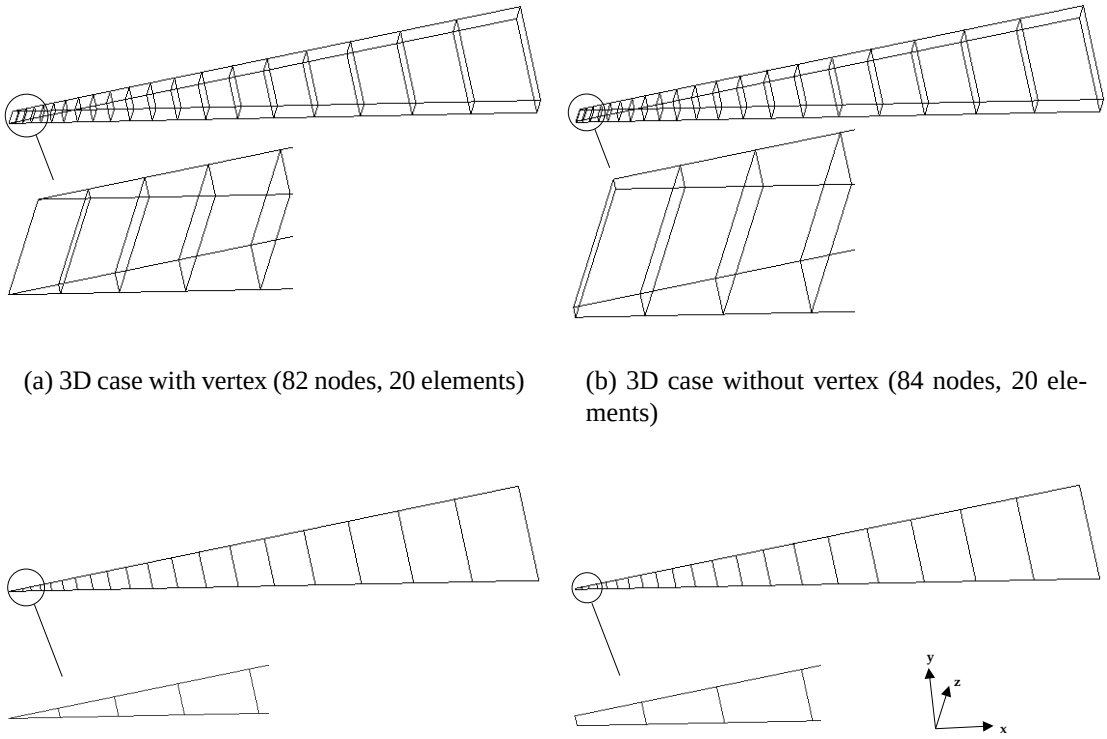

(a) 3D case with vertex (82 nodes, 20 elements)

(b) 3D case without vertex (84 nodes, 20 elements)

(c) 2D case with vertex (41 nodes, 20 elements)

(d) 2D case without vertex (42 nodes, 20 elements)

Figure 2.2. Finite element meshes in different cases with and without vertex.

Results

The simulated values were compared against the analytical drawdown of steady-state hydraulic head h as a function of radius r [m] (de Marsily 1986)

$$\Delta h(r) = h(r_0) - h(r) = \frac{Q_{out}}{2\pi K d} \ln(\frac{r_0}{r}), \tag{2.3}$$

where r_0 is the radius [m] and d the thickness [m] of the modelled disc. The hydraulic heads are presented in Figure 2.3, which shows that the numerical results compare very well with the analytical solution in all the cases considered.

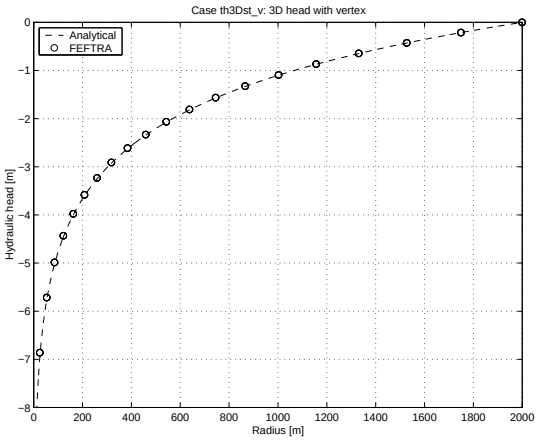

(a) 3D case with vertex

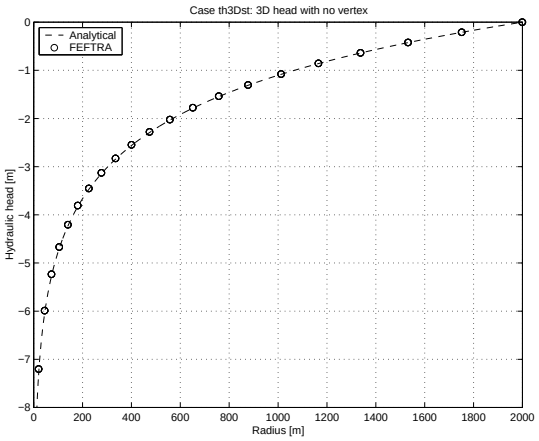

(b) 3D case without vertex

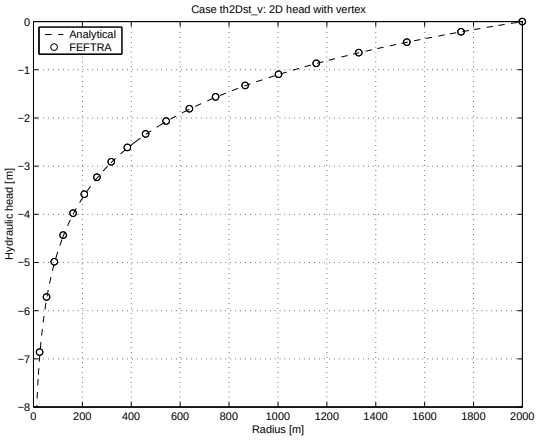

(c) 2D case with vertex

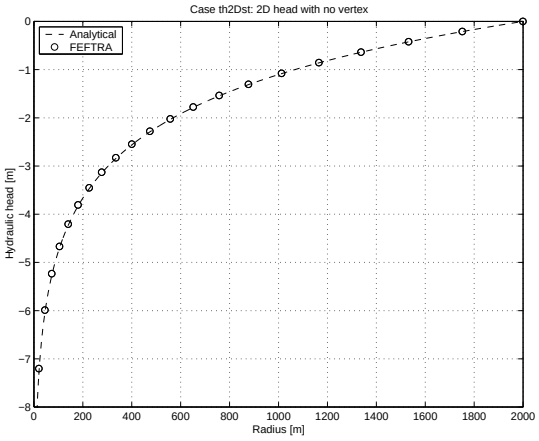

(d) 2D case without vertex

Figure 2.3. Simulated and analytical hydraulic head as a function of radius. The corresponding meshes of different cases are shown in Figure 2.2.

2.2 Radial transient flow

Theis (1935) considered temperature change of an infinite plane with an instantaneous line-source coinciding with the normal of the plane. An analogous hydrologic problem (de Marsily 1986; Ségol 1994) examines transient change of hydraulic head induced by an injection of water. The problem is used to verify the capability of the FEFTRA code to simulate time-dependent problems and to use various types of elements (2D and 3D) and boundary conditions (flow rates and fluxes).

The test case is located in the FEFTRA program path as follows:

- *feftra/solvit/t/head/th3Dtr_v* (flow rate boundary condition in 3D)

- *feftra/solvit/t/head/th3Dtr* (flux boundary condition in 3D)
- *feftra/solvit/t/head/th2Dtr_v* (flow rate boundary condition in 2D)
- *feftra/solvit/t/head/th2Dtr* (flux boundary condition in 2D).

Definition of the problem

In the hydrologic analogue of the Theis' problem (de Marsily 1986; Ségol 1994), water is injected at a constant rate to the centre of a discoid structure with infinite boundaries. The structure is assumed to be homogeneous and isotropic. The density of water is assumed to be constant. Initially hydraulic head is constant in the structure, but it starts to increase with the injection.

Mathematical model

The flow equation for hydraulic head h [m] is written as (Bear 1979; Huyakorn & Pinder 1983; de Marsily 1986)

$$\nabla \cdot (\boldsymbol{K} \nabla h) + Q = S_s \frac{\partial h}{\partial t}, \tag{2.4}$$

where $\boldsymbol{K}$ is the hydraulic conductivity [m/s], Q the flow rate per unit volume [1/s] and S_s the specific storage of the medium [1/m]. The parameter values are given in Table 2.3.

Theis (1935) presented a solution for the case with an infinite structure. If the injection of water is supposed to take place in a line segment with negligible diameter running through the structure, the increase of hydraulic head h on the radius r [m] at time t [s] is (de Marsily 1986; Ségol 1994)

$$\Delta h(r,t) = \frac{Q_{in}}{4\pi K d} \int_0^t \frac{e^{-\frac{r^2 S_s}{4K\tau}}}{\tau} d\tau, \tag{2.5}$$

where Q_{in} is the injection rate [m^3/s] and d the thickness of the modelled structure [m].

Let

$$u = \frac{r^2 S_s}{4Kt} \tag{2.6}$$

in Equation 2.5. Thus

$$\Delta h(r,t) = \frac{Q_{in}}{4\pi K d} \int_u^\infty \frac{e^{-\tau}}{\tau} d\tau = \frac{Q_{in}}{4\pi K d} W(u). \tag{2.7}$$

The integral $W(u)$ is the so-called Theis function, the values of which have been tabulated (Ségol 1994; de Marsily 1986). They can also be given in the form (Gradshteyn & Ryzhik 1980)

$$W(u) = -E_i(-u) = -0.5772 - \ln(u) - \sum_{k=1}^{\infty} \frac{(-u)^k}{k k!}, \tag{2.8}$$

Table 2.3. Input parameters for the case with a radial transient flow.

Symbol	*Parameter*	*Equation*	*Value*
$\boldsymbol{K}$	Hydraulic conductivity	2.4, 2.5, 2.6, 2.7	10^{-8} m s^{-1}
S_s	Specific storage	2.4, 2.5, 2.6	10^{-9} m^{-1}
d	Thickness	2.5, 2.7	100 m
Q_{in}	Injection rate	2.5, 2.7	$1.0 \cdot 10^{-5}$ m^3 s^{-1}

where E_i is an exponential integral function. Note that the series in Equation 2.8 is valid only, if the parameter $u > 0$.

Numerical solution method

Due to the symmetry of the problem, only a sector of 11.25° of the disc was included into the model, which gave the injection rate

$$Q_s = Q_{in} \cdot \frac{11.25^\circ}{360^\circ} = 3.125 \cdot 10^{-7}\text{m}^3\text{/s} \tag{2.9}$$

at the vertex. The boundary of the model was selected to be far enough (2000 m) from the centre of the sector to not affect the results in short modelling periods.

In order to test various elements and boundary conditions, different 2D and 3D element meshes were constructed. The elements used in the meshes were hexahedrals, wedges, quadrilaterals and trilaterals (Figure 2.4). Initially the hydraulic head was zero in the structure. The constant injection rate was set from the first time step onwards. The flow rate boundary condition was assigned to the vertex nodes in the cases shown in Figures 2.4(a) and 2.4(c). In the cases shown in Figures 2.4(b) and 2.4(d) the modelled sector begins at the distance of 20 m from the vertex, and flux q was specified through the innermost face/edge of the innermost element. Table 2.4 summarises the use of the flow rate and flux boundary conditions.

The partial differential equation (2.4) describing groundwater flow was solved numerically employing the conventional Galerkin technique with linear elements (Huyakorn & Pinder 1983). The fully implicit difference scheme was applied in the time discretisation. The mass matrix resulting from the transient finite element formulation was formed by a diagonalisation procedure known as "lumping" (Huyakorn & Pinder 1983), which gives a more stable solution in practical problems than a "consistent" matrix. Finally, the linear matrix equation was solved employing the conjugate-gradient method (Atkinson 1988).

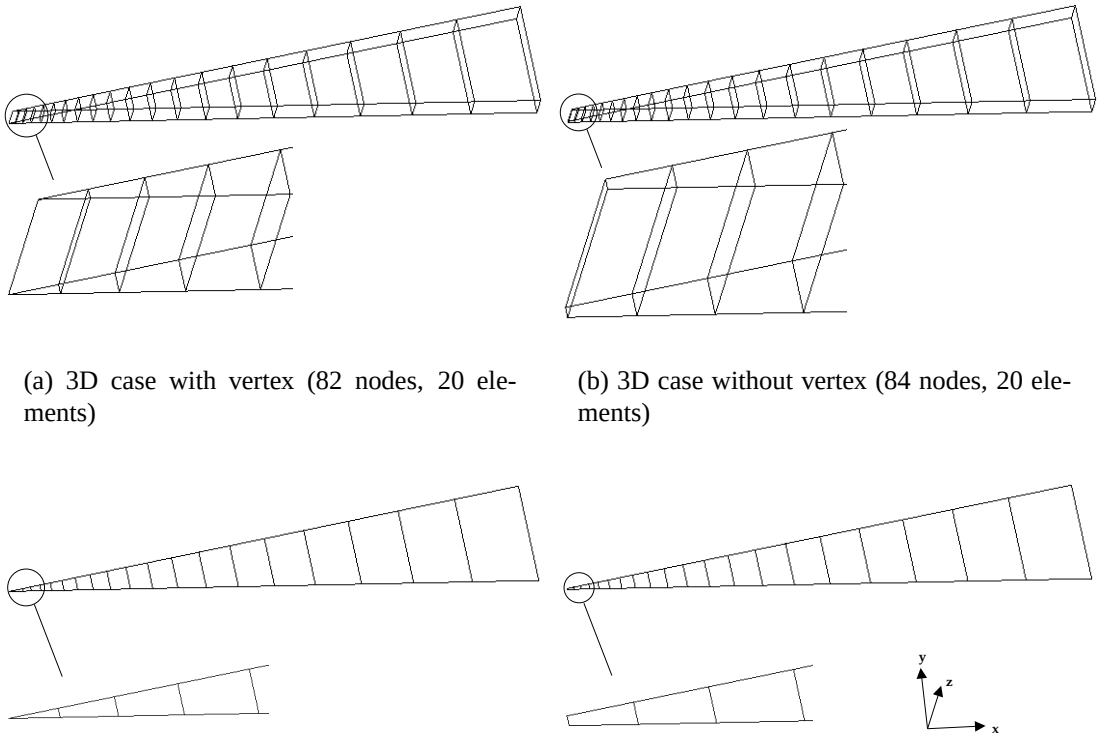

(a) 3D case with vertex (82 nodes, 20 elements)

(b) 3D case without vertex (84 nodes, 20 elements)

(c) 2D case with vertex (41 nodes, 20 elements)

(d) 2D case without vertex (42 nodes, 20 elements)

Figure 2.4. Finite element meshes in different cases with and without vertex.

Table 2.4. Flow rates and fluxes given in the FEFTRA input files for different cases.

Case	*Flow rate [m^3/s]*	*Flux q*	*Comment*
3D; vertex	Q_s/2=$1.563 \cdot 10^{-7}$		2 nodes at the vertex
3D; no vertex		Q_s/A=$7.97 \cdot 10^{-10}$ m/s	face A=392.0459 m^2
2D; vertex	Q_s=$3.125 \cdot 10^{-7}$		1 node at the vertex
2D; no vertex		Q_s/L=$7.97 \cdot 10^{-8}$ m^2/s	edge L=3.920459 m

Results

The simulated and analytical (Equation 2.7) hydraulic heads are presented in Figure 2.5. The results representing an increase of head as a function of time at the distance of 20 m from the injection point comprised 2D and 3D cases with flow rate or flux boundary conditions. At the beginning the FEFTRA code overestimates hydraulic head slightly, resulting probably from the instant increase of the injection rate from zero to the maximum value. The difference between the simulated and analytical solution could be decreased

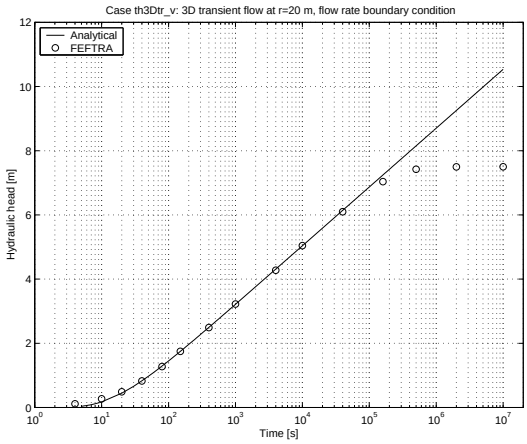

(a) 3D case with vertex

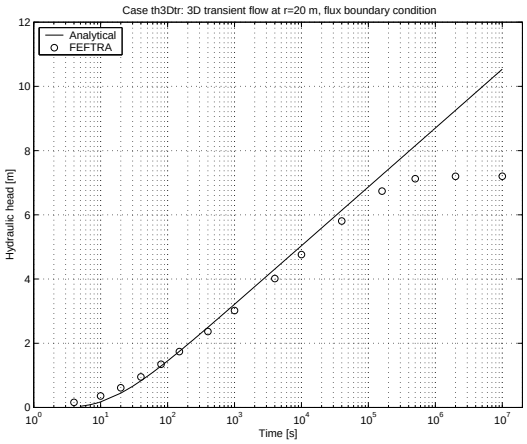

(b) 3D case without vertex

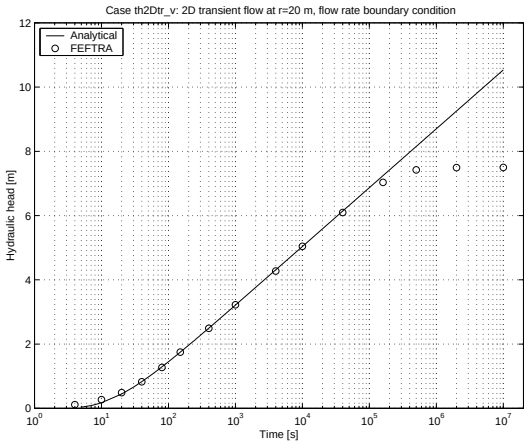

(c) 2D case with vertex

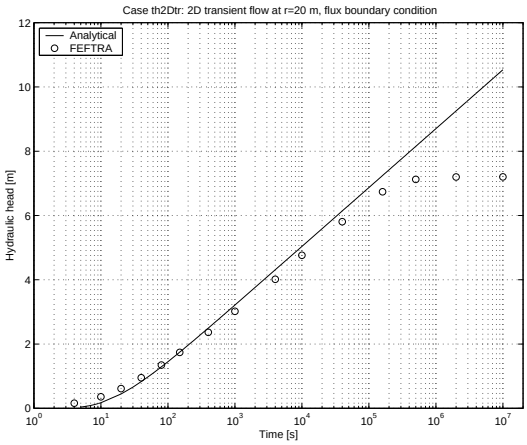

(d) 2D case without vertex

Figure 2.5. Simulated and analytical hydraulic head at r = 20 m. The corresponding meshes of different cases are shown in Figure 2.4.

by optimizing the time steps. At later time steps the numerical results compare fairly well with the analytical solution, until the effect of the injection reaches the boundary and the model attains the steady state. Then, the model is not anymore compatible with the Theis problem and the difference between the results starts to increase.

2.3 Transient flow from a borehole in a fractured permeable medium

This test case was introduced in the international hydrologic code intercomparison project (HYDROCOIN 1988) as the Case 1 of Level 1, and it concerns a transient groundwater flow from a borehole penetrating a confined aquifer. The objective of the case was to

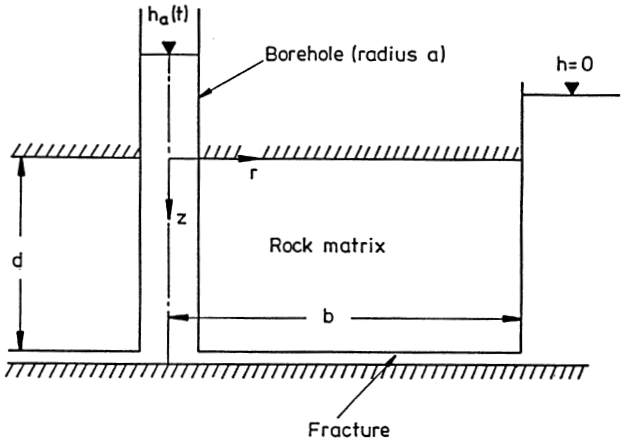

Figure 2.6. Schematic figure of the problem Hydrocoin Level 1 Case 1 (HYDROCOIN 1988).

verify the ability of codes to model transient pumping tests in boreholes in order to get information about the hydraulic properties of a rock mass. The case was explicitly designed to code testing rather than a realistic modelling.

The test case is located in *feftra/solvit/t/head/th_hydrocoin_l1c1* in the FEFTRA program path.

Definition of the problem

A vertical and finite-radius borehole is assumed to penetrate a cylindrical volume of permeable rock (Figure 2.6). The saturated rock is underlain by a single horizontal fracture and confined between impermeable horizontal boundaries. The pumping of water results in a flow from the borehole to the fracture and the rock matrix and further to the boundary of the modelled region. Due to the pumping hydraulic head in the borehole also changes continuously from initial to final value. The top and bottom boundaries of the model are impermeable to water, while a constant hydraulic head is specified on the vertical boundary. Initially the same hydraulic head is applied in the borehole and the vertical boundary. Both the matrix and the fracture are assumed to be homogeneous and isotropic. The matrix is characterised by a hydraulic conductivity and a specific storage, while the fracture is characterised by a transmissivity and a storage coefficient.

Mathematical model

The flow equation for hydraulic head h [m] is written as (Bear 1979; Huyakorn & Pinder 1983; de Marsily 1986)

$$\nabla \cdot (\boldsymbol{K} \nabla h) + Q = S_s \frac{\partial h}{\partial t}, \tag{2.10}$$

where $\boldsymbol{K}$ is the hydraulic conductivity [m/s], Q the rate of flow per unit volume [1/s] and S_s the specific storage of the medium [1/m]. The input parameter values are given in Table 2.5. For the time-dependent hydraulic head imposed in the borehole a smooth function is used

$$h_a(t) = h(\infty)(1 - e^{-\frac{t}{\tau}}), \tag{2.11}$$

where $h(\infty)$ is the value that the hydraulic head approaches asymptotically and τ is a time constant.

The analytical solution for the problem is presented by Hodgkinson & Barker (1985).

Numerical solution method

Due to the symmetry of the problem, only a sector of 11.25° of the cylinder was included into the model. The modelled volume, which started from the distance of borehole radius a, was discretised to mesh with 408 linear hexahedral elements for the rock matrix and 24 linear quadrangular elements for the fracture (Figure 2.7). The mesh consisted of 900 nodes. In the x-y plane the size of the elements increased towards the outer boundary, while in the z direction the mesh was refined near the fracture.

The radial sides were assumed impermeable to water. The hydraulic head $h = 1 \cdot 10^{-10}$ m was initially applied to both nodes representing the borehole and the nodes on the outer boundary. The simulation period from 0 to 10 000 s was discretised into 21 time steps the length of steps increasing from 0.001 to 5 000 s. The time steps and hydraulic head in the borehole (Equation 2.11) are shown in Table 2.6.

Table 2.5. Input parameters for the problem Hydrocoin Level 1 Case 1 (HYDROCOIN 1988). Compared to the base case tenfold transmissivity was used for the fracture.

Symbol	*Parameter*	*Equation*	*Value*
T	Transmissivity of fracture		10^{-7} m^2 s^{-1}
S	Storage coefficient of fracture		10^{-10}
$\boldsymbol{K}$	Hydraulic conductivity of matrix	2.10	10^{-9} m s^{-1}
S_s	Specific storage of matrix	2.10	10^{-7} m^{-1}
a	Borehole radius		0.1 m
b	Distance between borehole and boundary		10 m
d	Thickness of rock matrix		5 m
τ	Time constant for borehole head	2.11	0.1 s

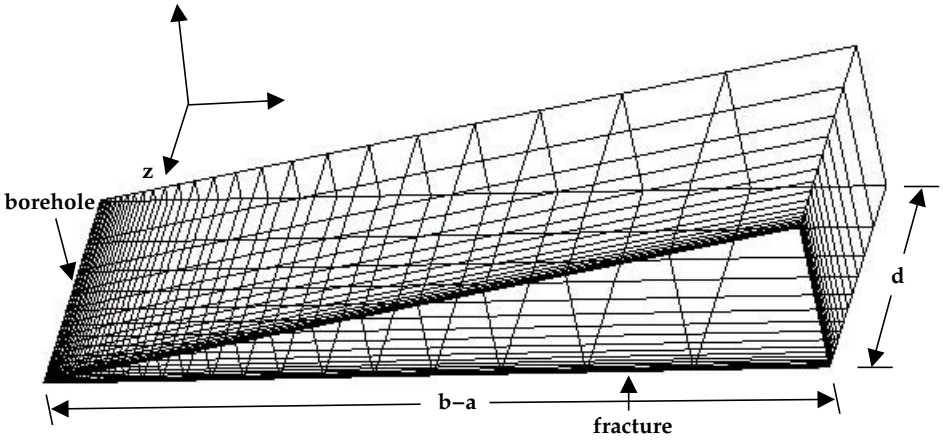

Figure 2.7. Finite element mesh for the problem Hydrocoin Level 1 Case 1 (HYDROCOIN 1988).

Table 2.6. Time steps and hydraulic head in the borehole (Equation 2.11).

Time t [s]	*Hydraulic head [m]*	*Time t [s]*	*Hydraulic head [m]*
0.0	$1 \cdot 10^{-10}$	5	1.0
0.001	0.00995	10	1.0
0.005	0.0488	20	1.0
0.01	0.095	50	1.0
0.02	0.181	100	1.0
0.05	0.393	200	1.0
0.1	0.632	500	1.0
0.2	0.865	1000	1.0
0.5	0.993	2000	1.0
1	1.0	5000	1.0
2	1.0	10000	1.0

The partial differential equation (2.10) describing groundwater flow was solved numerically employing the conventional Galerkin technique (Huyakorn & Pinder 1983). The fully implicit difference scheme was applied in the time discretisation. The linear matrix equation was solved employing the direct frontal method (Hinton & Owen 1977; Bathe 1982).

Results

The computed hydraulic head was compared to the analytical solution provided by Hodgkinson & Barker (1985). Hydraulic heads as a function of time at a midpoint of the rock matrix ($r = 5$ m, $z = 2.5$ m) and in the fracture ($r = 5$ m, $z = 5$ m) are presented in Figure 2.8(a). In addition, heads as a function of radius one metre above the horizontal

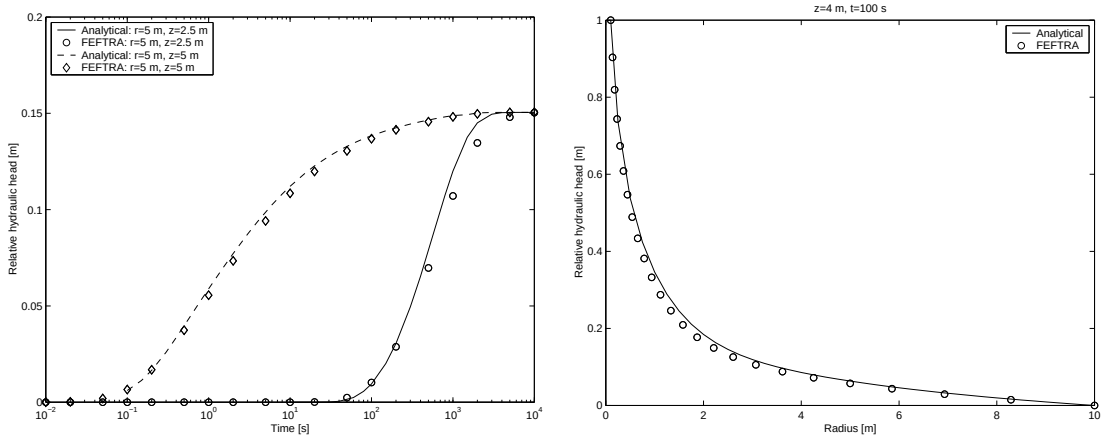

(a) Relative hydraulic head at a midpoint of the rock matrix ($r = 5$ m, $z = 2.5$ m) and in the fracture ($r = 5$ m, $z = 5$ m) as a function of time.

(b) Relative hydraulic head one metre above the horizontal fracture ($z = 4$ m, $t = 100$ s) as a function of radius.

Figure 2.8. Results for the problem Hydrocoin Level 1 Case 1 HYDROCOIN (1988).

fracture ($z = 4$ m, $t = 100$ s) is shown in Figure 2.8(b). The computed heads compare well with the analytical solution.

2.4 Steady-state flow in a rock mass intersected by fracture zones

In the international hydrologic code intercomparison project (HYDROCOIN 1988) a case with steady-state flow in a two-dimensional slice of a fractured bedrock was considered as the Case 2 of Level 1. The case is used to verify the capability of the FEFTRA code to model heterogeneous flow problems with large permeability contrasts. In addition, the test case is employed to assess the performance of different representations of zones in the finite element mesh. In the *base* case mesh both rock matrix and fracture zones were represented by 2D elements. The FEFTRA code provides two additional approaches, in which the elements of different dimensions can be used in the same mesh, i.e. 1D elements for fracture zones and 2D elements for rock matrix. In the first, 1D elements were located only along the edges of 2D elements (*quadtree* case), and in the second both along the edges and diagonal of 2D elements (*diagonal* case). Corresponding three-dimensional cases were also included to demonstrate the possibility of combining 2D elements with 3D elements.

The test case is located in the FEFTRA program path as follows:

- *feftra/solvit/t/head/th_hydrocoin_l1c2_2Dr2Dfz* (2D base case, head field)
- *feftra/solvit/t/head/th_hydrocoin_l1c2* (2D quadtree case, head field)
- *feftra/solvit/t/head/th_hydrocoin_l1c2_pa* (2D diagonal case, head field)

- *feftra/solvit/t/head/th_hydrocoin_l1c2_3Dr3Dfz* (3D base case, head field)
- *feftra/solvit/t/head/th_hydrocoin_l1c2_3D* (3D quadtree case, head field)
- *feftra/solvit/t/head/th_hydrocoin_l1c2_pa_3D* (3D diagonal case, head field)
- *feftra/solvit/t/velo/tq_hydrocoin_l1c2_3Dr3Dfz* (3D base case, velocity field)
- *feftra/solvit/t/velo/tq_hydrocoin_l1c2_3D* (3D quadtree case, velocity field)
- *feftra/solvit/t/velo/tq_hydrocoin_l1c2_pa_3D* (3D diagonal case, velocity field)
- *feftra/flowpath/t/tfp_hydrocoin_l1c2_3Dr3Dfz* (3D base case, flow path)
- *feftra/flowpath/t/tfp_hydrocoin_l1c2_3D* (3D quadtree case, flow path)
- *feftra/flowpath/t/tfp_hydrocoin_l1c2_pa_3D* (3D diagonal case, flow path)

The pressure, concentration and temperature analogues of this problem were solved in *quadtree case*s and they are located in:

- *feftra/solvit/t/press/tp_hydrocoin_l1c2* (2D, pressure field)
- *feftra/solvit/t/conc/tc_hydrocoin_l1c2* (2D, concentration field)
- *feftra/solvit/t/temp/tt_hydrocoin_l1c2* (2D, temperature field)
- *feftra/solvit/t/press/tp_hydrocoin_l1c2_3D* (3D, pressure field)
- *feftra/solvit/t/conc/tc_hydrocoin_l1c2_3D* (3D, concentration field)
- *feftra/solvit/t/temp/tt_hydrocoin_l1c2_3D* (3D, temperature field)

Definition of the problem

The problem is an idealisation of the hydrogeological conditions encountered at a potential site for a deep repository in bedrock. The case concerns steady-state flow in a two-dimensional slice of a fractured bedrock intersected by two fracture zones with different widths (10 m and 15 m) and inclinations (Figure 2.9). The zones intersect deep in the modelled 2D cross-section of rock and meet the surface in two valleys. A simple and symmetric topography consisting of straight lines is assumed. The surface near the top corners is horizontal for the first ten metres to define an unambiguous horizontal derivative at the top corners. Flow governed by Darcy's law is influenced by the asymmetry of the fracture zones. Both the zones and the rock matrix are homogeneous and isotropic. The rainfall is assumed to cause the water table to be coincident with the surface. The vertical and bottom boundaries are impermeable to flow.

Mathematical model

The steady-state flow equation is written for hydraulic head as follows (Bear 1979; Huyakorn & Pinder 1983; de Marsily 1986)

$$\nabla \cdot (\boldsymbol{K} \nabla h) = 0, \tag{2.12}$$

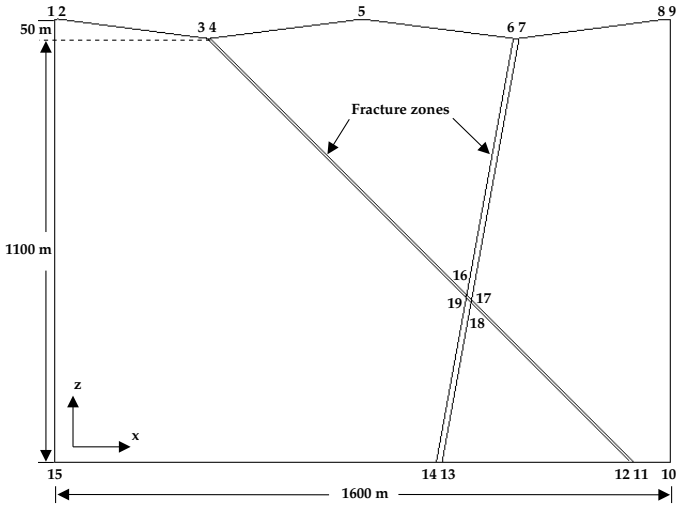

Figure 2.9. Schematic description of the problem Hydrocoin Level 1 Case 2 (HYDROCOIN 1988). The coordinates of the numbered points are given in Table 2.7.

Table 2.7. Coordinates of the numbered points in the modelled region of the problem described Figure 2.9.

Point	x *[m]*	z *[m]*	*Point*	x *[m]*	z *[m]*
1	0.0	150.0	11	1505.0	-1000.0
2	10.0	150.0	12	1495.0	-1000.0
3	395.0	100.0	13	1007.5	-1000.0
4	405.0	100.0	14	992.5	-1000.0
5	800.0	150.0	15	0.0	-1000.0
6	1192.5	100.0	16	1071.35	-566.35
7	1207.5	100.0	17	1084.04	-579.04
8	1590.0	150.0	18	1082.5	-587.5
9	1600.0	150.0	19	1069.81	-574.81
10	1600.0	-1000.0			

where $\boldsymbol{K}$ is the hydraulic conductivity [m/s] and h the hydraulic head [m]. Hydraulic head

$$h(x, z) = z \tag{2.13}$$

representing the elevation of water table (Figure 2.9) is used as the boundary condition on the top boundary, while no-flow conditions are applied to the vertical ($x = 0$ m and $x = 1600$ m) and the bottom ($z = -1000$ m) boundaries. The input parameters are given in Table 2.8. The Darcy velocity $\boldsymbol{q}$ [m/s] required in the flow path calculations is expressed as follows:

$$\boldsymbol{q} + \boldsymbol{K}\nabla h = 0. \tag{2.14}$$

Table 2.8. Input parameters for the problem Hydrocoin Level 1 Case 2 (HYDROCOIN 1988).

Symbol	*Parameter*	*Equation*	*Value*
$\boldsymbol{K_f}$	Hydraulic conductivity of the fracture zones	2.12, 2.14	$1.0 \cdot 10^{-6}$ m/s
$\boldsymbol{K_r}$	Hydraulic conductivity of the rock matrix	2.12, 2.14	$1.0 \cdot 10^{-8}$ m/s
$\boldsymbol{T_1}$	Transmissivity of the fracture zones	2.15, 2.16	$1.0 \cdot 10^{-5}$ m/s
$\boldsymbol{T_2}$	Transmissivity of the fracture zones	2.15, 2.16	$1.5 \cdot 10^{-5}$ m/s

Numerical solution method

The finite element method with linear elements was applied when solving the case numerically. In order to assess the performance of different representations of zones, the finite element mesh was constructed with three different approaches. In the *base* case both rock matrix and fracture zones were represented by triangular 2D elements (Figure 2.10(a)). The elements for rock matrix were approximately of uniform size and the zone elements followed exactly the given geometry including the physical thickness.

In the *quadtree* (Figure 2.10(b)) and *diagonal* (Figure 2.10(c)) cases, the elements of different dimensions were used in the same mesh, i.e. 1D elements for the fracture zones and 2D elements for the rock matrix. The *quadtree* case applied an adaptive and recursive *tree* algorithm, which enables an efficient local refinement of mesh near desired locations (e.g. fracture zones, sinks, tunnels). 1D elements were located along the edges of triangular 2D elements and the fracture zones in the mesh followed exactly the given geometry, except the physical thickness. In the *diagonal* case, the uniform mesh with quadrilateral elements for the rock matrix was constructed first. 1D fracture zone elements were embedded to the mesh afterwards both along the edges and the diagonals of the 2D matrix elements. Due to the (finite) size of 2D elements, the lines representing the zones were somewhat stepped compared to the given geometry.

As the 1D elements did not have physical thickness, the thickness of the zones was assigned in the transmissivity $\boldsymbol{T}$ $[\mathrm{m}^2/\mathrm{s}]$ for the flow equation and the Darcy velocity, which for 1D elements are written as follows

$$\nabla \cdot (\boldsymbol{T} \nabla h) = 0 \tag{2.15}$$

and

$$\boldsymbol{q} + \boldsymbol{T} \nabla h = 0. \tag{2.16}$$

Corresponding three-dimensional cases were also included to demonstrate the possibility of combining 2D elements with 3D elements. Thus, the 3D *base* case comprised of wedge elements for both the rock matrix and the fracture zones. In the 3D *quadtree* and *diagonal* cases the rock matrix was modelled with wedges and hexahedrals, respectively, while the fracture zones were described with quadrilaterals in both cases. In the 3D case, the flow in 3D elements was expressed by Equations (2.12) and (2.14), and in 2D elements by Equations (2.15) and (2.16).

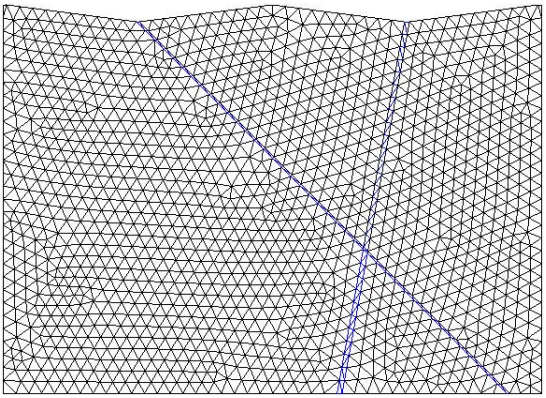

(a) 2D mesh for the base case (1554 nodes, 2957 elements).

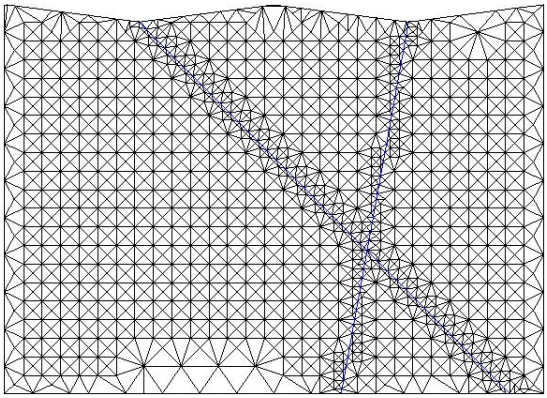

(b) 2D mesh for the quadtree case (1450 nodes, 2940 elements).

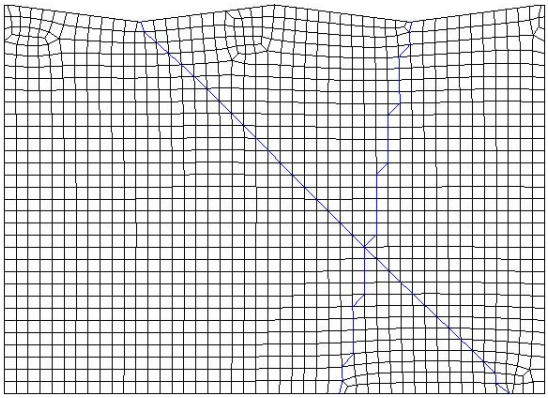

(c) 2D mesh for the diagonal case (1537 nodes, 1520 elements).

Figure 2.10. Finite element meshes for the problem Hydrocoin Level 1 Case 2 (HYDROCOIN 1988).

The partial differential equations (2.12) and (2.15) describing groundwater flow was solved numerically employing the conventional Galerkin technique (Huyakorn & Pinder 1983). The matrix equation resulting from the finite element formulation was solved employing the conjugate-gradient method (Atkinson 1988). The flow paths (in 3D cases only) were computed with the algorithm that uses the continuous Darcy velocity field obtained by treating $\boldsymbol{q}$ as an unknown variable and applying the finite element method to Equations (2.14) and (2.16) (Yeh 1981).

Results

Due to the complex geometry, no attempt was made to find an analytical solution for this problem in HYDROCOIN (1988). Thus, the computed FEFTRA results were compared to numerical solutions by the HYDROCOIN (1988) groups and Grundfelt (1984), which

provided an initial attempt to solve the case using quadratic finite elements in a proposal for a test problem. The computed hydraulic heads along horizontal lines are presented in Figure 2.11, showing a good agreement between the FEFTRA and other results. The *base* results by FEFTRA are nearly identical to those by Grundfelt (1984), whereas the *quadtree* and *diagonal* cases give slightly lower heads (especially deeper in the bedrock). Corresponding 3D heads were identical to the 2D results.

One flow path (no. 2 in HYDROCOIN (1988)) starting at point ($x = 100$ m, $z = -200$ m) in the modelled region and accumulated distance as a function of accumulated time are presented in Figure 2.12, which shows that the FEFTRA paths are in line with those computed by the HYDROCOIN (1988) groups. However, in the *quadtree* and *diagonal* cases, FEFTRA resulted in slightly shorter travel times, although the accumulated distance was about the same.

The results proved that the representation of the fracture zones by lower dimensional elements (1D elements in the 2D mesh and 2D elements in the 3D mesh) is a feasible and efficient alternative to the use of uniform dimensional elements, which was already shown by some HYDROCOIN (1988) groups.

2.5 Groundwater flow to a horizontal well in an unconfined aquifer

The underground rock characterization facility ONKALO is currently being constructed at Olkiluoto to investigate the suitability of the bedrock as a location for a final repository of spent nuclear fuel (Posiva 2006b). The ONKALO will consist of a tunnel system extending to a depth of 520 m. The open tunnels will act as a sink in the groundwater system and will therefore constitute a hydraulic disturbances to the site's groundwater system. For example, an inflow of groundwater into the open tunnel system might cause a drawdown of the groundwater table. The FEFTRA code employs a free surface approach (Huyakorn & Pinder 1983) to simulate the water table drawdown and its recovery to the undisturbed conditions.

Zhan & Zlotnik (2002) considered a problem of water table drawdown caused by constant-rate pumping at a horizontal well in an unconfined aquifer. The problem resembles the disturbance of the ONKALO in the groundwater system of Olkiluoto, and is therefore suitable for testing the free surface module of FEFTRA. Zhan and Zlotnik presented a semianalytical solution for transient drawdown of the water table for their problem. The solution was based on the inverse Laplace transformation and is available as a Fortran 77 code WHI (WHI 2003).

The test case is located in the FEFTRA program path *feftra/solvit/t/head/tfs_ZhanZlotnik*.

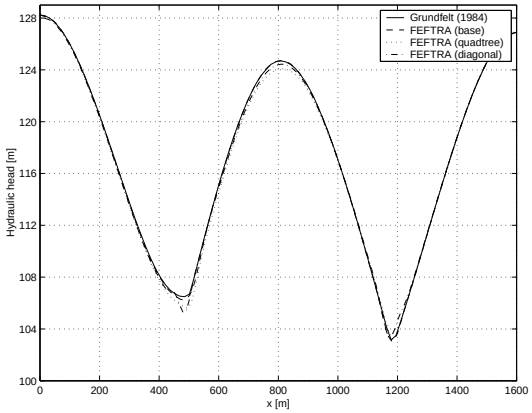

(a) $z = 0$ m

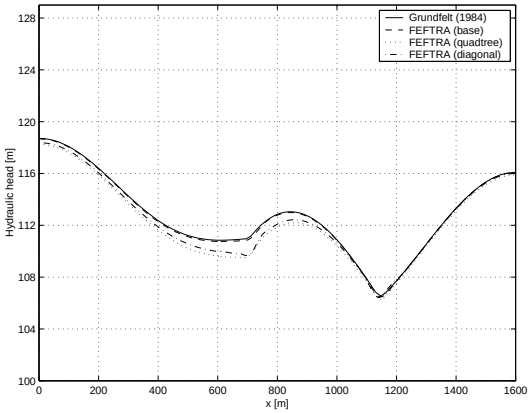

(b) $z = -200$ m

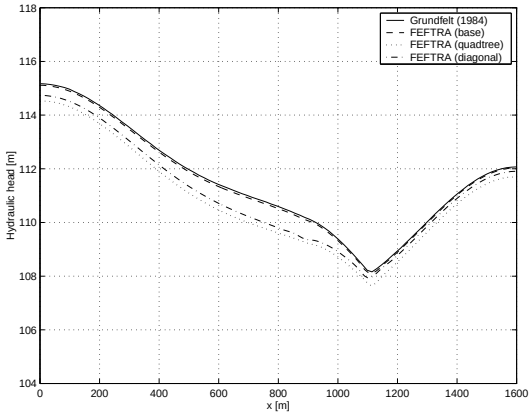

(c) $z = -400$ m

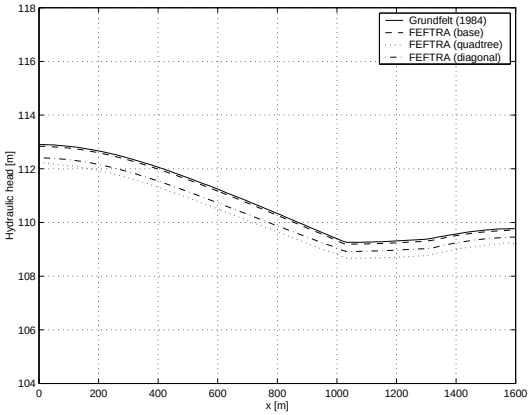

(d) $z = -800$ m

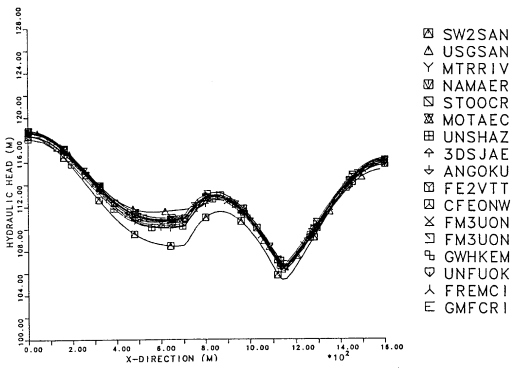

(e) $z = -200$ m

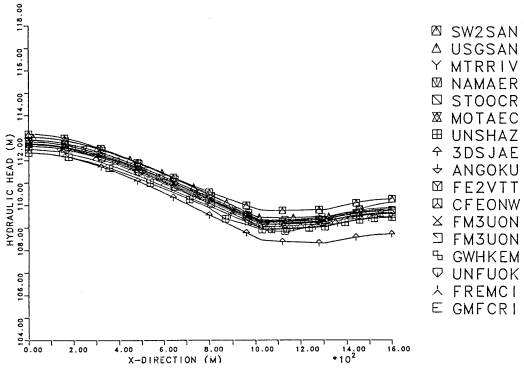

(f) $z = -800$ m

Figure 2.11. Computed hydraulic heads along horizontal lines. The results by FEFTRA and Grundfelt (1984) are presented in subfigures (a)–(d), whereas subfigures (e) and (f) include the heads computed by the HYDROCOIN (1988) groups with the finest meshes.

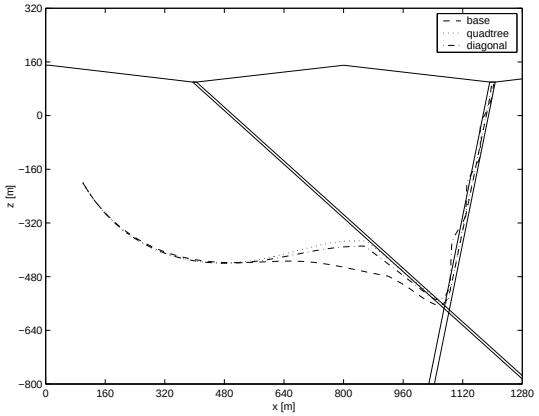

(a) Flow paths by FEFTRA

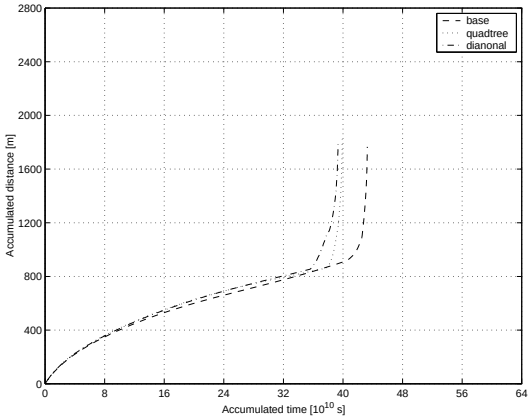

(b) Distance by FEFTRA

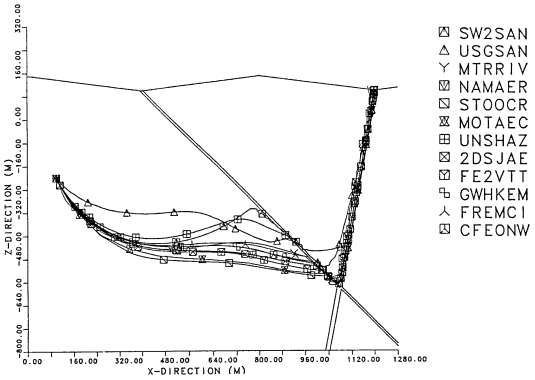

(c) Flow paths by the HYDROCOIN (1988) groups

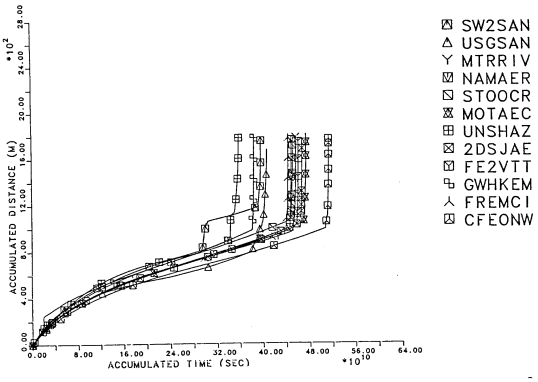

(d) Distance by the HYDROCOIN (1988) groups

Figure 2.12. Path lines starting at point ($x = 100$ m, $z = -200$ m) in the modelled region and accumulated distance as a function of accumulated time. The FEFTRA results in subfigures (a) and (b) were computed with 3D meshes.

Definition of the problem

The simulation case concerns water table depression caused by constant-rate pumping at a horizontal well located near the water table. Model geometry and boundary conditions are illustrated in Figure 2.13. The initial model domain is an 800 m $\times$ 800 m $\times$ 50 m box, with a horizontal well of length 40 m located at the centre of the domain at a depth of 10 m. The initial groundwater table is assumed to be completely flat.

A free surface boundary condition is assigned at the surface of the model, whereas a constant hydraulic head boundary condition ($h = 0$ m) is applied for the lateral boundaries. The base of the model is treated as impermeable using a no-flow boundary condition. Infiltration is ignored in this problem.

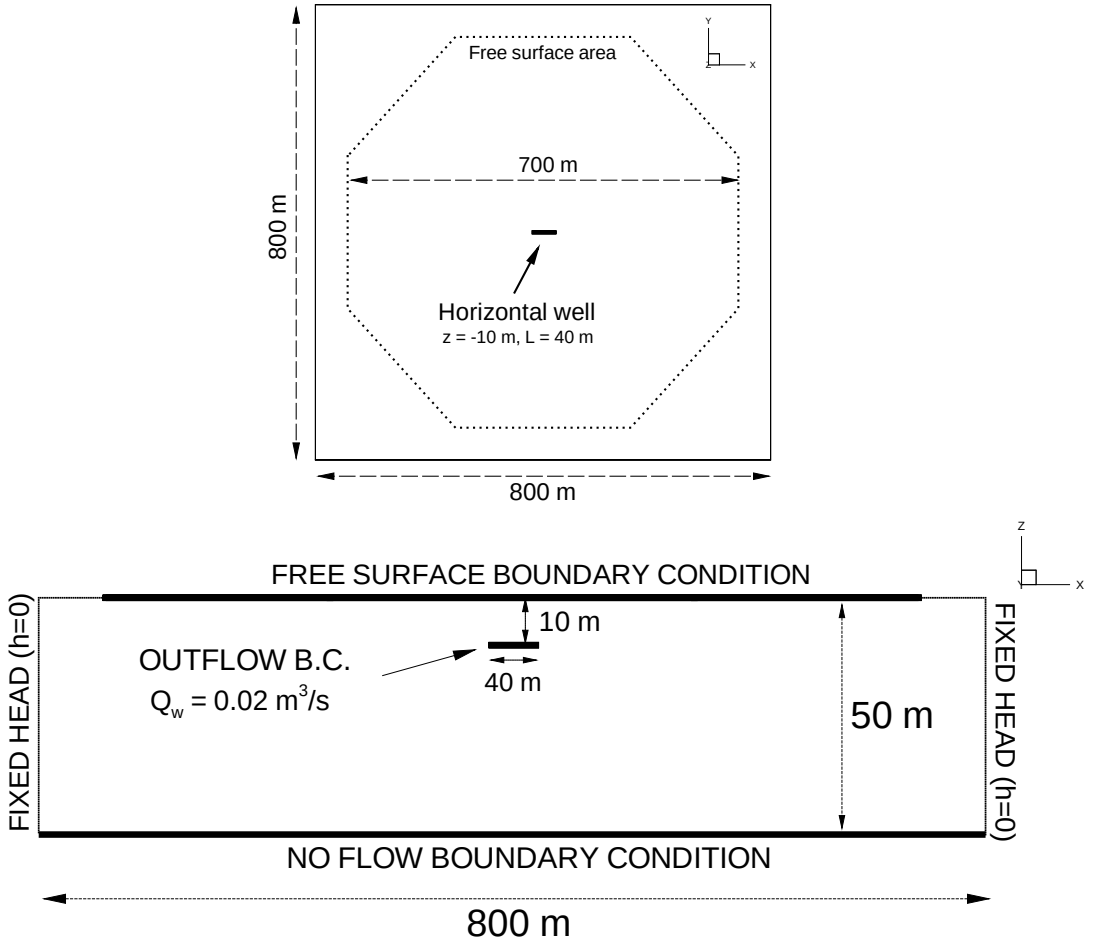

Figure 2.13. Schematic illustration of the initial model domain and applied boundary condition types for the horizontal well case. The model domain is an 800 m $\times$ 800 m $\times$ 50 m box with an octagon-shaped free surface area at the models' surface. A horizontal well of length 40 m is located at the center of the model domain at a depth 10 m.

Mathematical model

The water table drawdown caused by the well is simulated by employing a free surface approach, in which only the saturated part of the bedrock is included in the modelled volume and the transiently moving water table constitutes a free surface. The effect of storativity is assumed to be negligible compared to that of the specific yield, and hence the groundwater flow under the water table is governed by the steady-state flow equation (Bear 1979; Huyakorn & Pinder 1983)

$$\nabla \cdot \left(\boldsymbol{K} \nabla h \right) + Q_w = 0, \tag{2.17}$$

where $\boldsymbol{K}$ is the hydraulic conductivity tensor of rock [$\mathrm{m/s}$], h is the hydraulic head [m] and Q_w is the rate of water flowing out of the model by pumping [m^3/s].

The flow equation (2.17) is subject to various boundary conditions (Neuman & Witherspoon 1971; Huyakorn & Pinder 1983). On the free surface, of which location and

Table 2.9. Input data for simulation of the horizontal well case.

Symbol	*Parameter*	*Equation*	*Value*
K	Hydraulic conductivity	2.17	1.0×10^{-4} m/s
Q_w	Outflow rate by pumping	2.17	0.02 m^3/s
S_y	Specific yield (porosity)	2.19	0.2
$\zeta(x, y, 0)$	Initial free surface elevation	2.19	0 m

geometric shape are *a priori* unknown, the atmospheric and the continuity condition must be satisfied. Thus the following two boundary conditions must be simultaneously satisfied at the free surface:

$$h = \zeta \tag{2.18}$$

$$\big(\boldsymbol{K}\nabla h\big) \cdot \mathbf{n} = -S_y \frac{\partial \zeta}{\partial t} n_z \tag{2.19}$$

where $\zeta = \zeta(x, y, t)$ is the elevation of the free surface [m], $\mathbf{n}$ is the unit normal vector of the free surface [–] and S_y is the specific yield [–], which is approximated with the flow porosity. The transient behaviour of the system follows from the conditions at the moving free surface. Infiltration is not considered in this problem.

The flow equation (2.17) is a steady-state equation and needs no initial conditions, but the transient continuity equation (2.19) has to be complemented with the initial condition $\zeta(x, y, 0) = 0$ m, indicating that the initial water table is completely flat.

The numerical values of all constants are presented in Table 2.9.

Numerical solution method

The finite element method with linear elements was applied in solving the case numerically. In the implicit scheme suggested and treated in detail by (Neuman & Witherspoon 1971) and (Huyakorn & Pinder 1983) each time step involves a meshing and a finite element analysis phase, of which the latter is further divided into two stages.

Meshing phase The meshing phase discretises the actual saturated zone bounded from above by the free surface (the top of the water table). The discretisation of the irregular free surface was based on the recursive *octree*-algorithm. The FEFTRA/*octree* mesh generator applies the algorithm to successively divide the saturated zone in tetrahedral elements until the desired level of refinement is achieved. At the location of the free surface, the element resolution is set significantly higher than elsewhere in the model to successfully discretize the changing surface of the model. The meshing process of the free surface concludes by removing all finite elements from above the free surface (i.e. those representing the unsaturated zone). The initial mesh is shown in Figure 2.14 and the adaptive meshing procedure is illustrated in Figure 2.15.

Finite element analysis phase The finite element analysis phase receives the discretised model from the meshing phase, uses the static hydrogeological properties defined in the model input and prescribes the boundary conditions. The FEM-phase is divided in two iteration stages. The task of the first stage is to re-create the results of the previous time step on the actual mesh, which are needed in calculating the transient term in Equation 2.19 during the second stage. The task of the second stage of the iteration is to actually compute the new location of the free surface. This is accomplished by prescribing an implicit and as yet unknown flux boundary condition (Equation (2.19)) over the free surface. The new geometry for the free surface is then obtained from the solution of the flow equation (2.17), and a new adaptive mesh is constructed by continuing to the meshing phase.

The water table drawdown at the surface of the model is assumed to be restricted inside an octagon, which is centred at the well (Figure 2.13). Outside the octagon, the water table is assumed to remain at its initial position. At the free surface, the element size 1.6 m proved out to be sufficient. Element sizes as small as 0.4 m were tested, but identical results were obtained in both cases. In the vicinity of the well the mesh was refined to element size 0.8 m (Figure 2.14). The horizontal well was modelled as a set of nodes located along the well screen. To model pumping, the total outflow rate $Q_w = 0.02$ m^3/s was distributed evenly at these nodes.

The simulation was run until the steady-state was reached. Time step sizes for the first three time steps were $\Delta t_1 = 100.0$ s, $\Delta t_2 = 900.0$ s and $\Delta t_3 = 1000.0$ s, after which they were increased steadily by the rule $\Delta t_{i+1} = \sqrt{2}\Delta t_i$, $i = 4, 5, \ldots$. Using this time stepping scheme, the steady-state was reached in 26 time steps (80 days in simulation time).

Results

The FEFTRA results are compared to the semianalytical solution calculated with Zhan's Fortran 77 program (WHI 2003). The WHI code is based on the numerical inversion of the Laplace transformation, which is prone to numerical errors and instabilities close to the well (Zhan & Zlotnik 2002). Therefore the results should not be compared in the immediate vicinity of the well, but at some distance apart. The semianalytical WHI results were obtained by constructing a regular grid of observation points at a distance 2 m apart from each other, calculating the semianalytical solution at each of the observation points and finally interpolating the solution linearly between the points to construct a surface.

Figure 2.16 compares the simulated water table with the semianalytical one along the vertical cross–sections at $x = 0$ m and $y = 1$ m at four time steps (the horizontal well is centred at $x = y = 0$ m and oriented along the x-axis). Location $y = 1$ m was selected instead of $y = 0$ m, since the well is oriented parallel to this plane and the semianalytical solution would be erroneous were it calculated over the well, see the manual of the semianalytical code (WHI 2003).

The results calculated with FEFTRA compare well with the semianalytical ones. At early times, the peak drawdown close to the well lags behind the semianalytical solution, but the

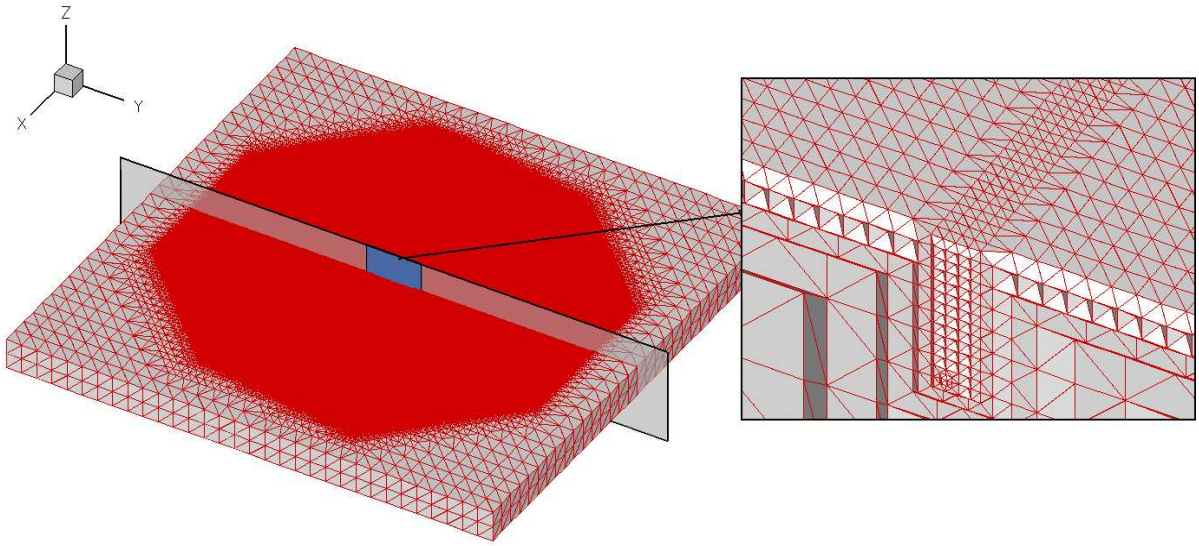

Figure 2.14. The initial computational mesh used in the horizontal well case. The initial mesh comprises of 3400000 *tetrahedral elements ranging from* 0.8 *m (close to the well) to* 35.0 *m (lateral boundaries). As the water table depresses with time, the top of the mesh is deformed to match with the free surface. The subfigure illustrates the mesh refinement near the horizontal well. The well is oriented along the x-axis at a depth of* 10 *m at the centre of the model.*

shape of the curves already at a distance of 10 m from the well are indistinguishable. With increasing time, the curves approach each other and, as the steady-state is reached, they are almost identical. The actual calculated (FEFTRA and WHI) free surface representing the water table is shown in Figure 2.17.

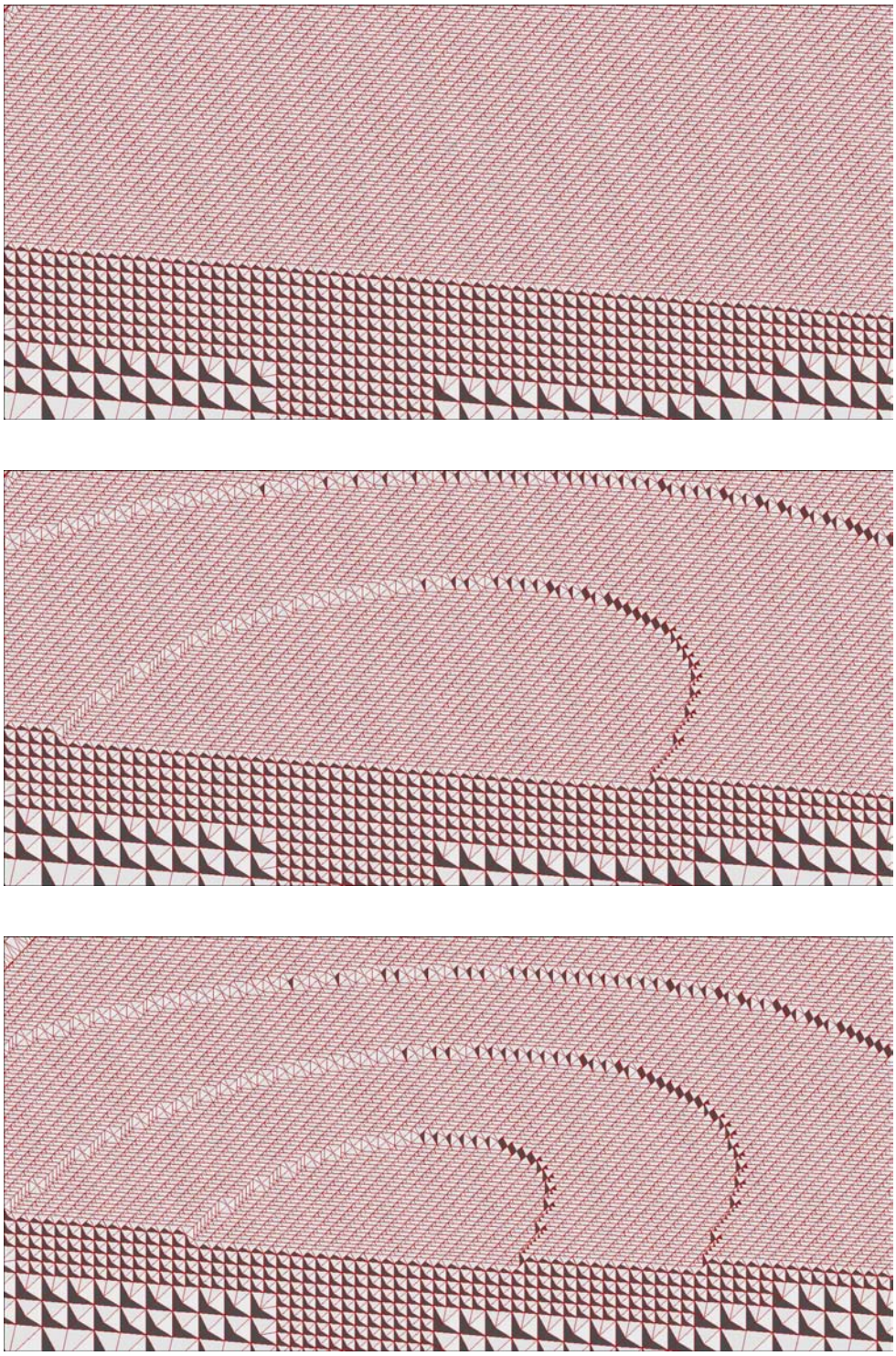

Figure 2.15. The illustration of the adaptive meshing phase that discretizes the models' surface to match with the current free surface at the time steps $t = 100$ *min,* $t = 700$ *min and* $t = 22$ *h. The location of the free surface at each time step is obtained from the solution of the flow equation* (2.17) *subject to the atmospheric pressure (Equation* (2.18)*) and the continuity (Equation* (2.19)*) boundary conditions on the free surface. For illustrational purposes only half of the mesh is shown here.*

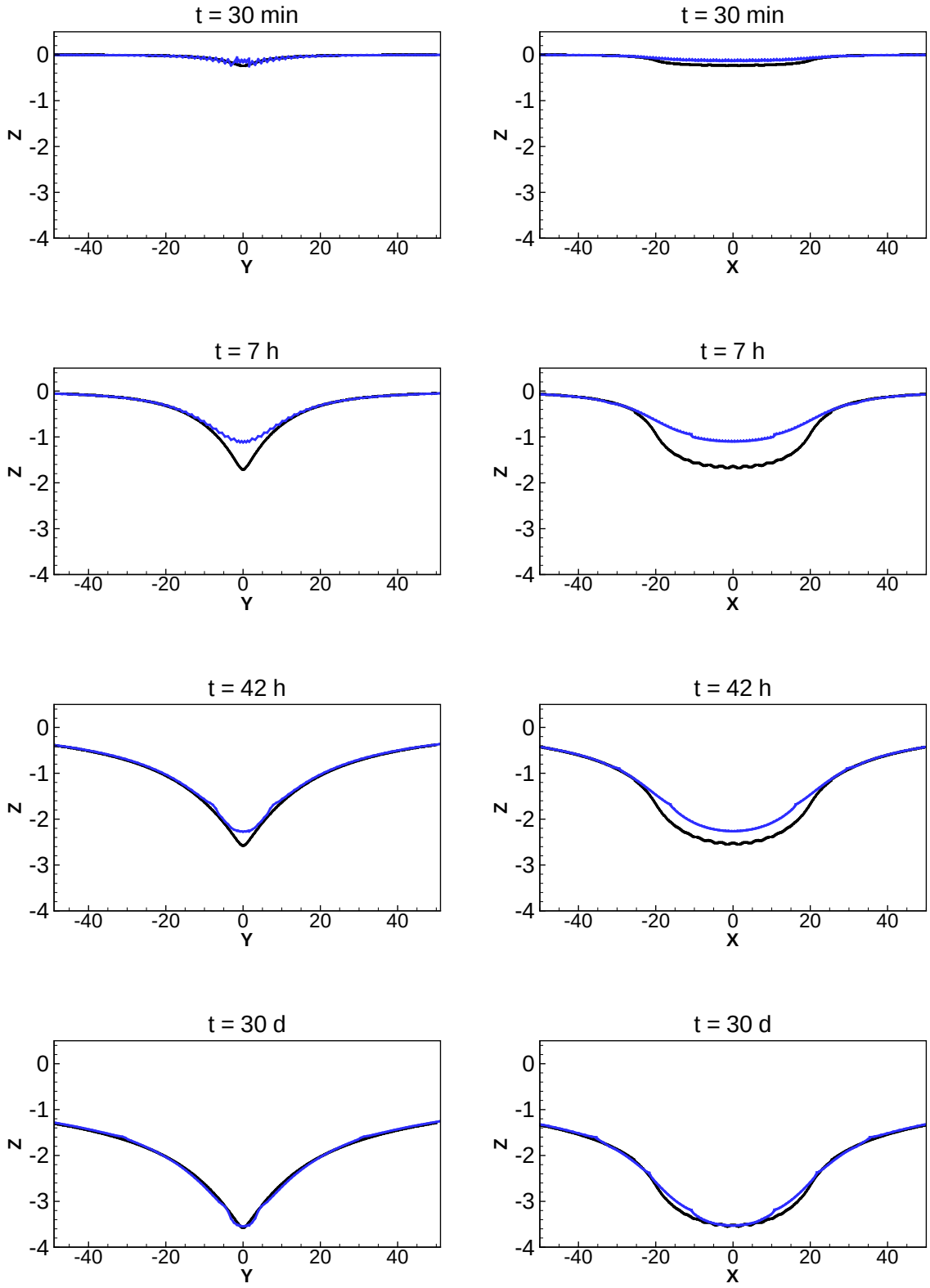

Figure 2.16. The calculated free surface (the water table) along the vertical cross sections $x = 0$ m (left) and $y = 1$ m (right). The horizontal well is centred at $x = y = 0$ m and oriented along the x-axis. The FEFTRA results are presented in blue, whereas the black curves denote the semianalytical approximation calculated with the WHI code (WHI 2003).

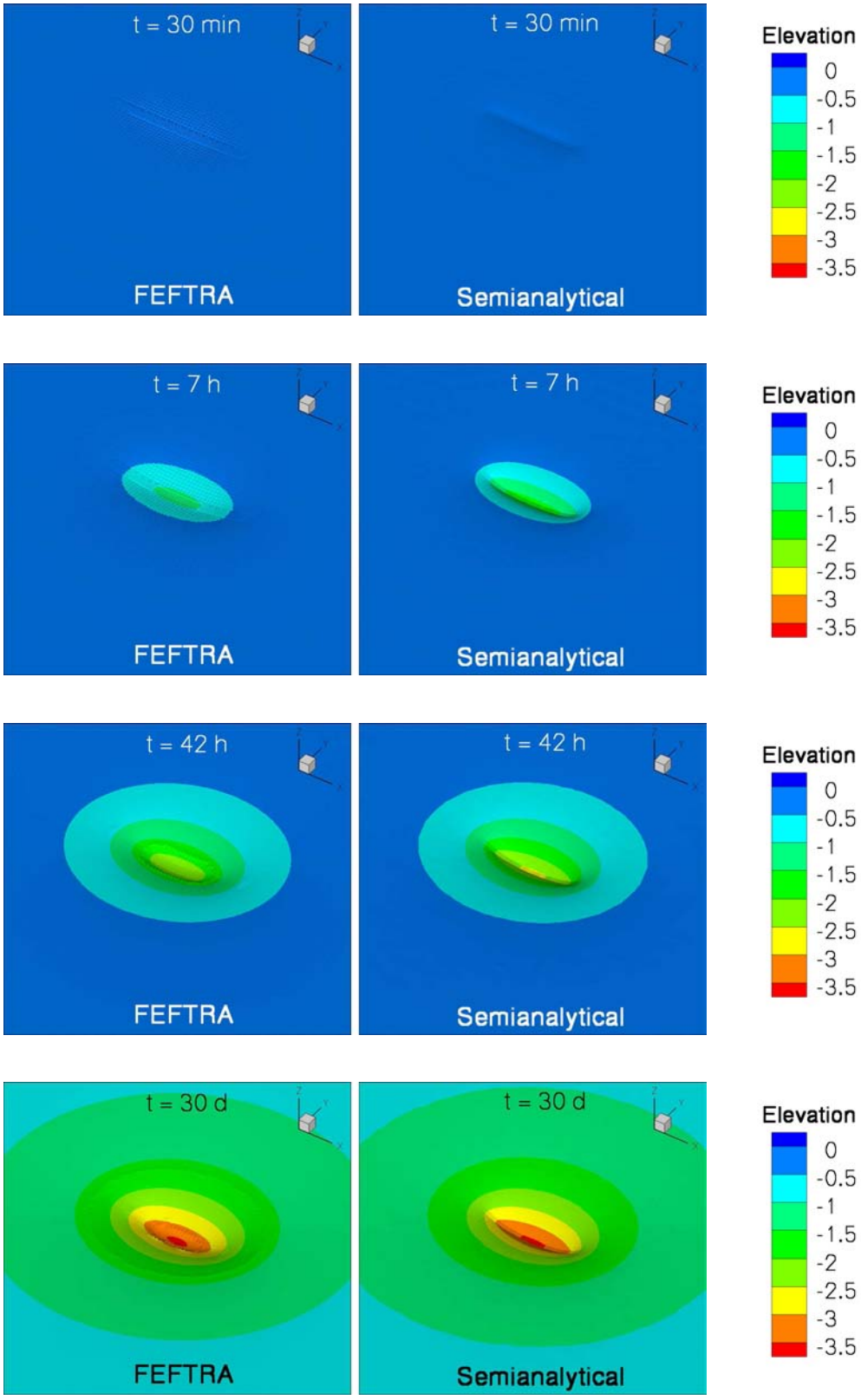

Figure 2.17. The free surface (the water table) calculated with the FEFTRA code (left) and the semianalytical WHI approximation (right).

2.6 Mariño's experiment

Mariño conducted laboratory investigations of the growth and decay of groundwater ridges using the Helen-Shaw model under the effect of infiltration (Ségol 1994). Mariño set up a 2D experiment, applied a constant recharge on the top and made systematic measurements of the water table height as a function of time. He also compared the observed results to an analytical solution of the corresponding mathematical problem. Neglecting the effect of the unsaturated zone, this experiment along with the analytical solution is suitable for testing the free surface module of FEFTRA both with 2D and 3D elements.

The test case is located in the FEFTRA program path as follows:

- *feftra/solvit/t/head/tfs_marino2D (2D mesh)*
- *feftra/solvit/t/head/tfs_marino3D (3D mesh)*

Definition of the problem

The problem concerns transient development of a free surface (water table) due to infiltration into the soil. The initial domain is assumed to be a rectangular, vertical cross section taken through a homogeneous and isotropic medium (Figure 2.18). For the simulation with 3D elements the domain is extended in the third spatial dimension. A constant recharge is applied as a flux boundary condition at the left part of the surface while keeping all other boundaries closed. As water cannot exit the model, the water content of the system increases by recharge and a ridge begins to develop at the free surface.

Mathematical model

The growth of the groundwater ridge with a recharge of water is simulated by employing a free surface approach, in which only the saturated part is included in the modelled volume

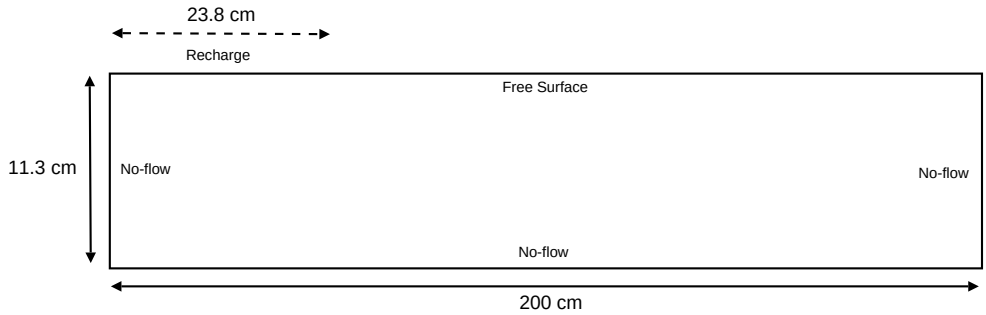

Figure 2.18. The initial model domain and boundary conditions for the simulation of Mariño's Experiment. The initial domain is a rectangle with a recharge-strip at the top-left corner. For the simulation with 3D elements, this domain is extended in the third spatial dimension by 160 *cm.*

Table 2.10. Input data for the Mariño's case.

Symbol	*Parameter*	*Equation*	*Value*
K	Hydraulic conductivity	2.20	4.2×10^{-3} m/s
S_y	Specific yield (porosity)	2.22	1.0
I	Infiltration rate	2.22	5.6×10^{-4} m/s
	Initial free surface height		11.3 cm

and the transiently moving water table constitutes a free surface. Assuming that the effect of storativity is negligible compared to that of the specific yield, steady-state groundwater flow is governed by the well-known equation (Bear 1979; Huyakorn & Pinder 1983)

$$\nabla \cdot \big(\boldsymbol{K} \nabla h\big) = 0, \tag{2.20}$$

where $\boldsymbol{K}$ is the hydraulic conductivity tensor of rock $[\mathrm{m/s}]$ and h is the hydraulic head [m].

The flow equation (2.20) is subject to the following boundary conditions (Neuman & Witherspoon 1971; Huyakorn & Pinder 1983). On the free surface, of which location and geometric shape are *a priori* unknown, the atmospheric and the continuity condition must be satisfied

$$h = \zeta \tag{2.21}$$

$$\big(\boldsymbol{K} \nabla h\big) \cdot \mathbf{n} = \Big(I - S_y \frac{\partial \zeta}{\partial t}\Big) n_z, \tag{2.22}$$

where $\zeta = \zeta(x, y, t)$ is the elevation of the free surface [m], $\mathbf{n}$ is the unit normal vector of the free surface [–], I is the rate of vertical infiltration through the free surface $[\mathrm{m/s}]$ and S_y is the specific yield [–], which is approximated with the flow porosity. The transient behaviour of the system follows from the conditions at the moving free surface.

Numerical solution method

The implicit scheme suggested and treated in detail by Neuman & Witherspoon (1971) and Huyakorn & Pinder (1983) was employed. Each time step involves a meshing and a finite element analysis phase, of which the latter is further divided into two stages.

Meshing phase The meshing phase discretises the actual saturated zone bounded from above by the free surface (the top of the water table). The discretisation of the irregular free surface was based on the recursive *quadtree/octree*-algorithm. The FEFTRA/*quadtree* mesh generator applies the algorithm to successively divide the saturated zone in triangular elements until the desired level of refinement is achieved (2D case). The FEFTRA/*octree* mesh generator applies the same algorithm to successively divide the saturated zone in tetrahedral elements for the 3D simulations. At the location of the free surface the element resolution is set significantly higher than elsewhere in the model to

successfully discretize the changing surface of the model. The meshing process of the free surface concludes by removing all finite elements from above the free surface (i.e. those representing the unsaturated zone).

Finite element analysis phase The finite element analysis phase receives the discretised model from the meshing phase, uses the static hydrogeological properties defined in the model input and prescribes the boundary conditions. The FEM-phase is divided in two iteration stages. The task of the first stage is to re-create the results of the previous time step on the actual mesh, which are needed in calculating the transient term in Equation (2.22) during the second stage. The task of the second stage of the iteration is to actually compute the new location of the free surface. This is accomplished by prescribing an implicit and as yet unknown flux boundary condition (Equation (2.22)) over the free surface. The new geometry for the free surface is then obtained from the solution of the flow equation (2.20), and a new adaptive mesh is constructed by continuing to the meshing phase.

The initial domain for the 2D finite element simulation was chosen to be a rectangle (Figure 2.18). For 3D simulation this domain was extended in the third dimension. The time discretization was set up using 23 time steps of length of 30.0 s with total simulation time of 660 seconds. This time stepping proved to be fine enough to ensure the convergence of the proposed iterative solution method in this application.

On the vertical sides and the bottom of the model, a no-flow boundary condition was assumed, whereas at the top of the model a free surface boundary condition was applied. A constant infiltration rate was applied at the 23.8 cm long strip over the top of the model, providing a recharge of water into the model.

Results

The evolution of the watertable during the simulation is shown in Figure 2.19. The groundwater ridge develops steadily during the simulation period. Initially the watertable rises only under the recharge strip, but as the simulation proceeds and the recharge water re-distributes, the watertable begins to rise also further away from the strip.

The results from the simulations are compared to the analytical solution provided by Mariño (Ségol 1994) at two locations x = 0.0 cm and x = 60.0 cm (Table 2.11 and 2.12, Figure 2.20). The computed results are in good agreement with the analytical solution, regardless of a small deviation. The difference between the analytical and simulated results is almost constant at the beginning of the simulation but increase as the simulation proceeds, indicating a small cumulative error in the numerical solution.

For 3D-simulation the error is a bit higher than for the 2D-simulation, because, in 2D simulation, the actual free surface is discretized faithfully by adjusting the location of the nodes at the free surface to correspond with the exact elevation of the surface, whereas, in the 3D model, the surface is approximated by tetrahedral elements to the size of a few centimetres and the location of the surface is determined by the calculated head at the

surface nodes. However, the error is small and qualitative results compare well with the analytical results.

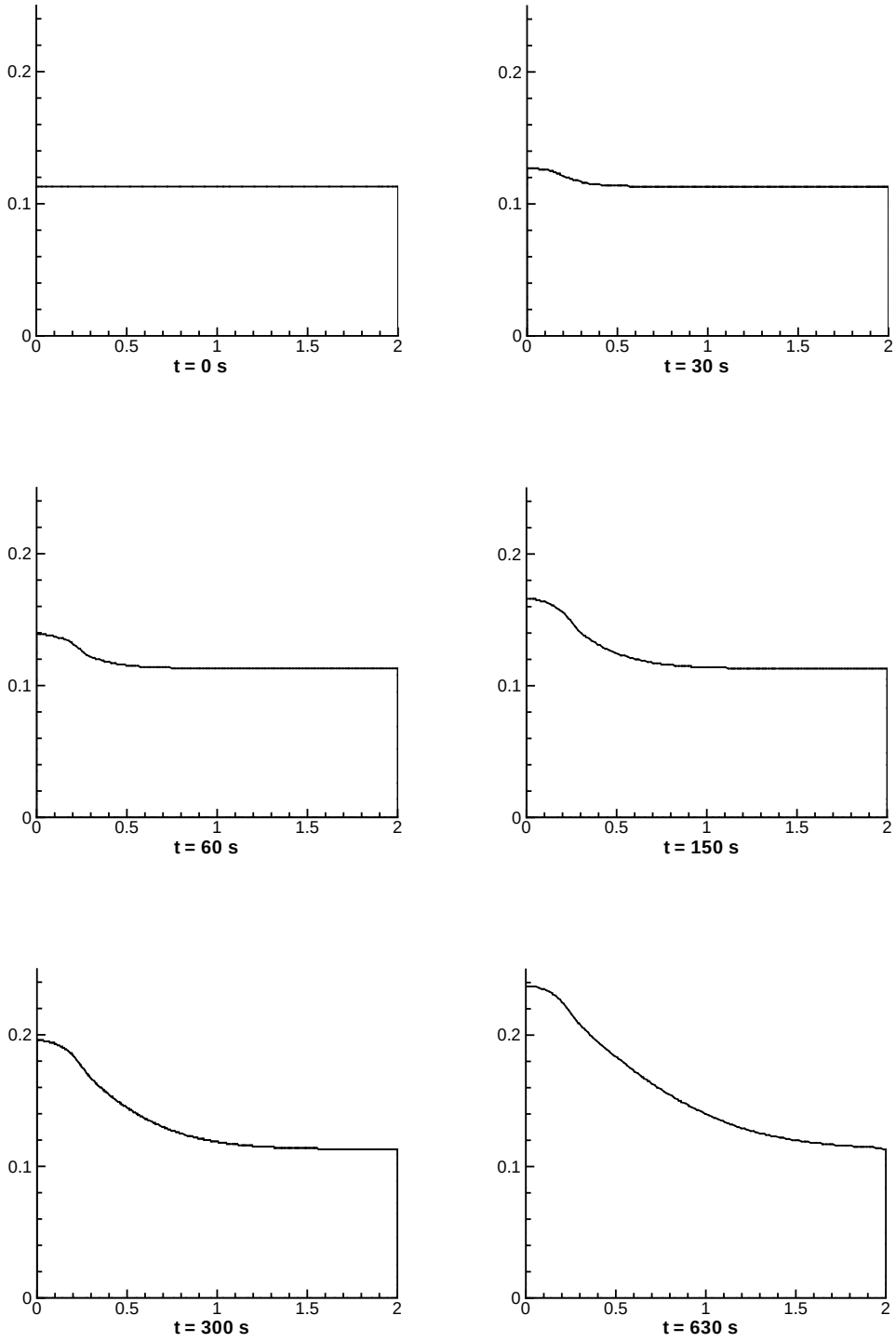

Figure 2.19. The simulated height of the watertable at different time-steps in the Mariño's Experiment (2D case). Note the different scales at the vertical and horizontal axis.

Table 2.11. The analytical (Ségol 1994) and simulated results at point x = 0.0 cm in the Mariño's Experiment.

Time [s]	Analytical [cm]	FEFTRA 2D [cm]	FEFTRA 3D [cm]
30	12.9	12.7	12.8
60	14.2	13.9	14.0
120	16.1	15.8	15.9
180	17.5	17.3	17.9
270	19.4	19.1	19.3
360	20.8	20.5	20.1
450	22.1	21.8	21.3
540	23.2	22.8	22.3

Table 2.12. The analytical (Ségol 1994) and simulated results at point x = 60.0 cm in the Mariño's Experiment.

Time [s]	Analytical [cm]	FEFTRA 2D [cm]	FEFTRA 3D [cm]
90	11.5	11.6	11.7
150	12.0	12.0	12.5
210	12.6	12.6	13.6
300	13.5	13.6	14.8
390	14.5	14.7	15.6
480	15.3	15.7	16.6
570	16.3	16.7	17.6

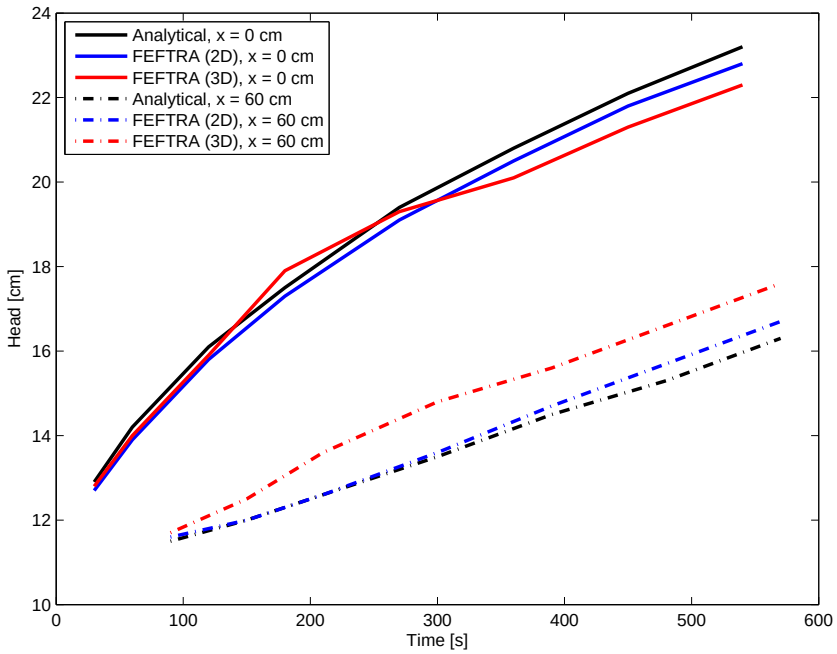

Figure 2.20. The analytical (Ségol 1994) and simulated results at points x = 0 cm and x = 60.0 cm in the Mariño's Experiment.

2.7 Site-scale flow at the Olkiluoto site

Site-scale groundwater flow modelling has been an essential part of the site investigation programme for seeking the repository for the final disposal of spent nuclear fuel. The objective of the modelling has been to characterise the overall groundwater flow conditions at the investigation sites as well as provide support and site-specific data for the safety analyses.

The study by Hartley et al. (2002) consisted of a site-scale model testing, in which a steady-state 3D groundwater flow (without a consideration of salinity) was calculated for the Olkiluoto site. The simulations were carried out with the NAMMU program package (NAMMU 2007). In this section the corresponding FEFTRA simulations (Löfman & Mészáros 2002) are presented and the results are compared against those obtained with NAMMU. The case is introduced to compare FEFTRA to a similar code in a real-life, site-scale groundwater flow problem in 3D. In addition, as the fracture zones are represented by 3D elements in NAMMU and 2D elements in FEFTRA, the performance of the differing representations of the zones can also be assessed with this case.

The test case is located in the FEFTRA program path as follows:

- *feftra/solvit/t/press/tp3Dst_olkiluoto* (pressure field)
- *feftra/solvit/t/velo/tp3Dst_olkiluoto* (velocity field)
- *feftra/flowpath/t/tp3Dst_olkiluoto* (flow paths)
- *feftra/frate/t/tp3Dst_olkiluoto* (flow rates)

Definition of the problem

The case was comprised of a steady-state site-scale simulation of groundwater flow assuming freshwater conditions. As a site-specific flow model is practically identical to the one employed in the latest study by Löfman (1999), most of the details are omitted here and only a summary and modifications to the previous model are presented.

The size of the modelled bedrock volume was 6.3 km $\times$ 4.3 km $\times$ 1.5 km (Figure 2.21). The modelled area and the inner refined area (the area covered by the borehole investigations) were slightly enlarged compared to (Löfman 1999). The modelled bedrock volume was conceptually divided into the hydrogeological zones and the sparsely fractured rock between the zones (Figure 2.22). The equivalent-continuum model was applied separately for each hydrogeological zone and the sparsely fractured rock, which were assumed to consist of five hydrological layers (Tables 2.13–2.15). The geometry of the 33 planar zones was based on a revised bedrock model by Saksa et al. (1998). The following slight modifications were made to some of the zones compared to (Löfman 1999):

- AR3, AR6, AR8, R1, R4, R4I, R5 and R27 were extended to the outer boundary of the model
- AR5 was excluded, because of the location near R5

- AR1, AR6, R1, R4, R7 were slightly simplified
- R6L was included in the name R6, and R18L in R18 (no changes)
- zone R28A and R28B renamed to R28AB (no changes)

The internal structure of the repository located at a depth of 500 metres was not considered in detail, but the repository was modelled as a two-dimensional structure (Figure 2.23) based on the layout by Löfman (1999). Specified pressure corresponding to the elevation of the groundwater table relative to the sea level (where water table data was available) or a simple linear transformation of the topography ($watertable = 0.56 \cdot topography$, where water table data was not available) was applied on the surface (Figure 2.24), and no flow on other boundaries.

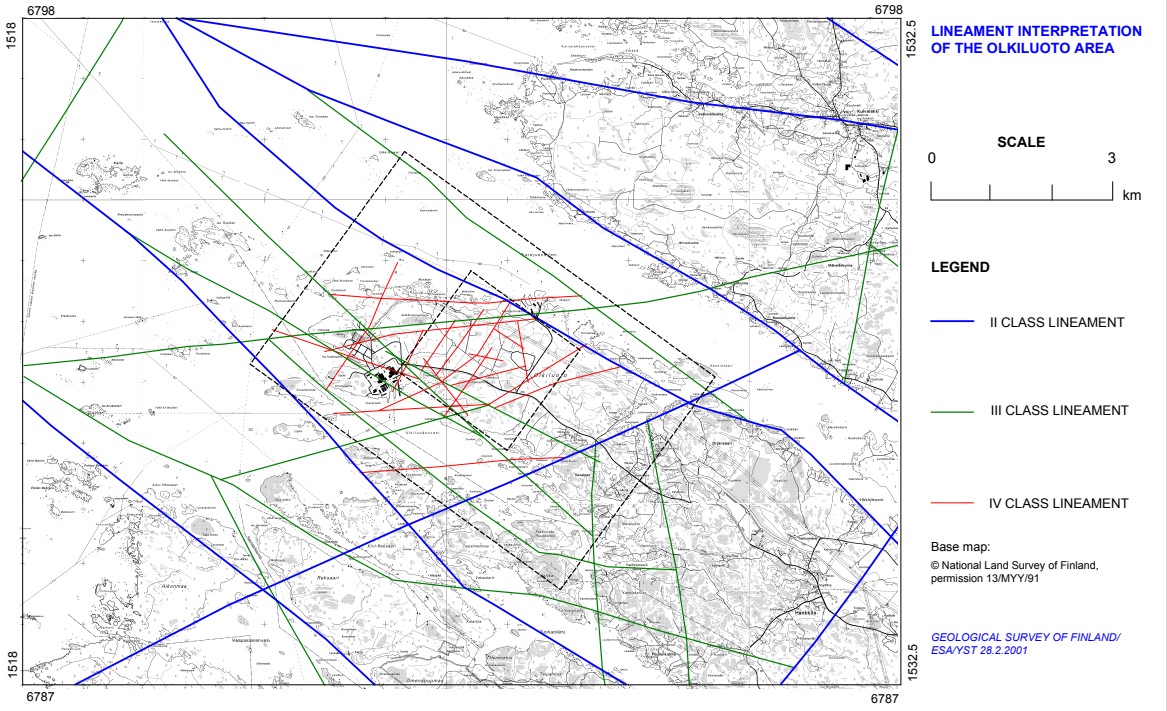

Figure 2.21. Outlines of the modelled area and the inner refined area on the ground surface.

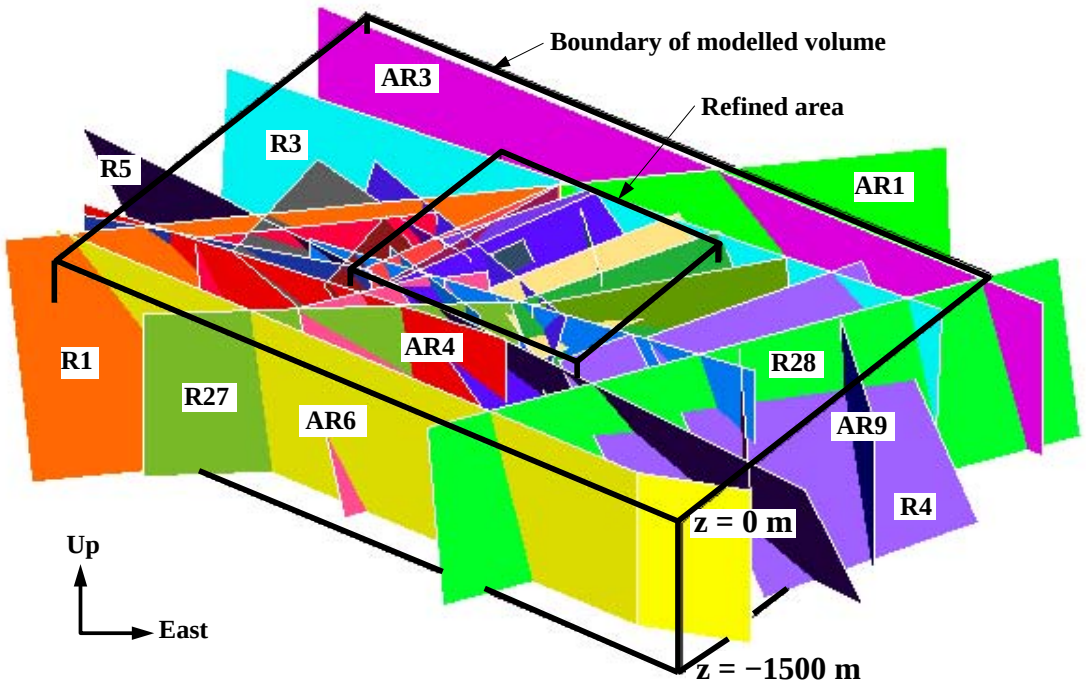

Figure 2.22. Conceptual geometry of the hydrogeological zone for the Olkiluoto site.

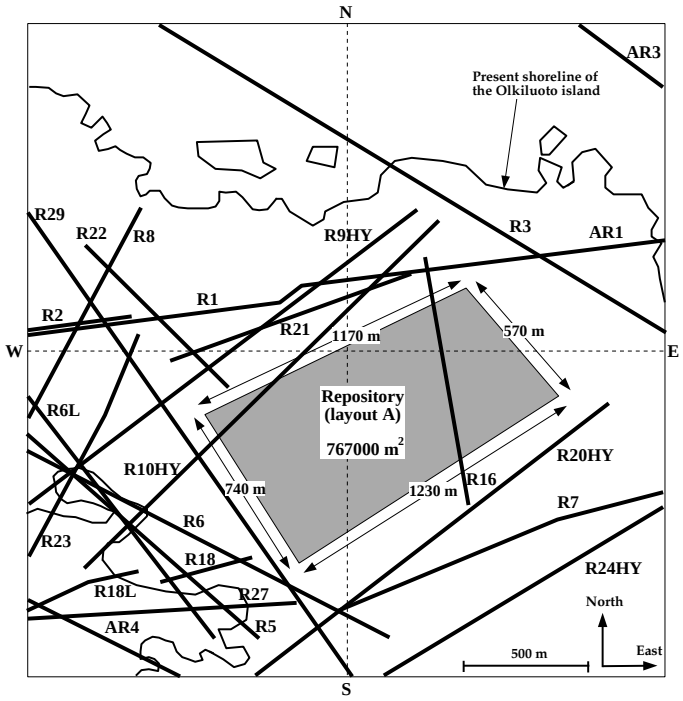

Figure 2.23. The layout for the repository located at a depth of 500 meters.

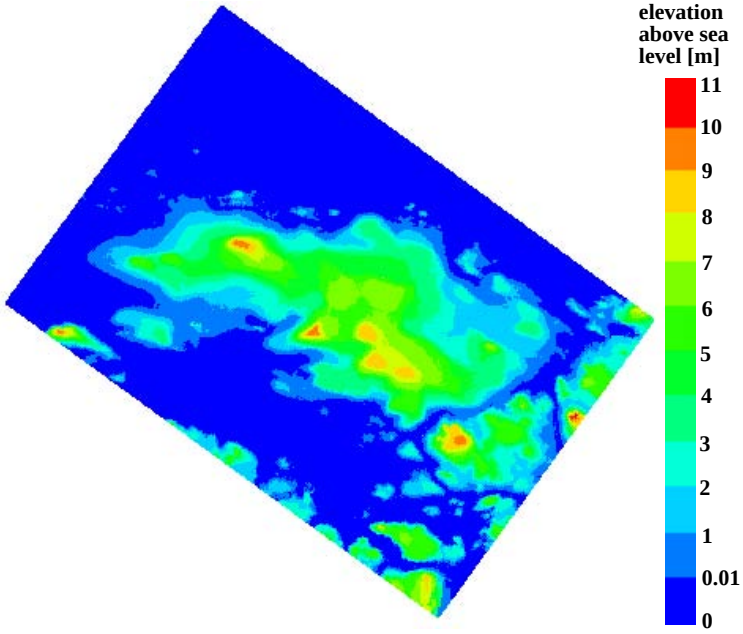

Figure 2.24. The present groundwater table of the Olkiluoto island on the surface of the model (Posiva 2005). The values are based on the measured means of hydraulic head in shallow boreholes and multilevel piezometers.

Mathematical model

The flow equation in a steady-state is written for the residual pressure p_r [Pa] (the total pressure without the hydrostatic component of freshwater) as follows (Bear 1979; Huyakorn & Pinder 1983; de Marsily 1986)

$$\nabla \cdot \left(\frac{\rho \boldsymbol{k}}{\mu} \left(\nabla p_r + (\rho - \rho_0) g \nabla z \right) \right) = 0, \tag{2.23}$$

where ρ is the density of water [$\mathrm{kg/m^3}$], ρ_0 is the density of the freshwater [= 998.6 $\mathrm{kg/m^3}$], $\boldsymbol{k}$ is the permeability tensor of rock [$\mathrm{m^2}$], μ is the dynamic viscosity of water [= $1.0{\cdot}10^{-3}\mathrm{kg/m/s}$], g is the gravitational acceleration [= 9.81 $\mathrm{m/s^2}$], and z is the elevation relative to the sea level [m].

The velocity required in the flow path calculations is expressed in terms of the residual pressure as follows

$$\boldsymbol{v} + \frac{\boldsymbol{k}}{\mu \phi} \left(\nabla p_r + (\rho - \rho_0) g \nabla z \right) = 0, \tag{2.24}$$

where ϕ is the flow porosity $[-]$.

The permeability $\boldsymbol{k}$ in Equations (2.23) and (2.24) is related to the hydraulic conductivity $\boldsymbol{K}$ [m/s]

$$\boldsymbol{k} = \frac{\mu}{\rho g} \boldsymbol{K}. \tag{2.25}$$

The input parameter values for the equations are given in Tables 2.14 and 2.15.

Table 2.13. Classification of the hydrogeological zones by transmissivity.

Class	Hydrogeological zones
A	R3, R4, R5, R6, R7, R19HY, R20HY, R21, R24HY, R25, R27, R28, R29, AR-zones
B	R1, R2, R8, R9HY, R10HY, R11, R16, R17HY, R18, R22, R23

Table 2.14. The transmissivity of the hydrogeological zones $[\mathrm{m}^2/\mathrm{s}]$ *and the hydraulic conductivity of the sparsely fractured rock* $[\mathrm{m}/\mathrm{s}]$*. The transmissivity of* $5.0 \cdot 10^{-8}[\mathrm{m}^2/\mathrm{s}]$ *was used for the repository located at a depth of 500 metres. The thickness of the zones and the repository were selected to be 10 and 5 m, respectively.*

Depth [m]	Zones (class A)	Zones (class B)	Sparsely fractured rock
$0-100$	$2.53 \cdot 10^{-4}$	$5.75 \cdot 10^{-6}$	$2.88 \cdot 10^{-9}$
$100-200$	$9.14 \cdot 10^{-5}$	$2.08 \cdot 10^{-6}$	$1.04 \cdot 10^{-9}$
$200-400$	$2.53 \cdot 10^{-5}$	$5.74 \cdot 10^{-7}$	$2.87 \cdot 10^{-10}$
$400-900$	$3.18 \cdot 10^{-6}$	$7.23 \cdot 10^{-8}$	$3.61 \cdot 10^{-11}$
$900-1500$	$5.87 \cdot 10^{-7}$	$1.33 \cdot 10^{-8}$	$6.66 \cdot 10^{-12}$

Table 2.15. The flow porosity $[-]$ *of the hydrogeological zones and the sparsely fractured rock.*

Depth [m]	Flow porosity
$0-100$	$5.19 \cdot 10^{-4}$
$100-200$	$3.36 \cdot 10^{-4}$
$200-400$	$1.93 \cdot 10^{-4}$
$400-900$	$7.33 \cdot 10^{-5}$
$900-1500$	$2.44 \cdot 10^{-5}$

Numerical solution method

The finite element method with linear elements was applied in solving the case numerically with FEFTRA. All 33 fracture zones were included explicitly in the modelled volume, which was meshed with 537 000 hexahedral elements for the sparsely fractured rock and 106 000 triangular/quadrilateral elements for the hydrogeological zones and repository (Figure 2.25). The mesh was created by adding the 2D elements on the faces and/or diagonals of the 3D elements in the existing base mesh consisting of the 3D elements only. Due to the (finite) element size of the base mesh, the surfaces representing the hydrogeological zones in the mesh (Figure 2.25) are somewhat stepped compared to the corresponding planes defined in the bedrock model (Figure 2.22). As the 2D elements did not have physical thickness, the thickness of the zones and repository was assigned in the transmissivity of Equations (2.23) and (2.24). The size of the 3D elements in the inner

refined area at the centre of the island was 27 m $\times$ 27 m $\times$ 25 m down to a depth of 1000 metres.

The partial differential equation (2.23) describing groundwater flow was solved numerically employing the conventional Galerkin technique (Huyakorn & Pinder 1983). The matrix equations resulting from the finite element formulation of Equation (2.23) was solved employing the conjugate-gradient method (Atkinson 1988). The flow paths and travel times were computed with the algorithm that uses the continuous Darcy velocity field obtained by treating $\boldsymbol{q}$ as an unknown variable and applying the finite element method to Equation (2.24).

In the NAMMU finite element model the hydrogeological zones are represented implicitly (Hartley et al. 2002) by manipulating the hydraulic conductivity tensor of the 3D elements crossed by the planes of the zones. The apparent inconsistency arising from the representation of the zones (of thickness 10 m) by 3D elements (of size about 25 m) was resolved by assigning an average permeability to the elements crossed by the zones, which ensures that the flow through the elements is correct. However, the porosity was not averaged, but the porosity of the sparsely fractured rock was assigned to all the elements (whether crossed by the zones and repository or not).

The finite elements around the repository in the NAMMU mesh were of size 25 m by 27 m by 5 m (Hartley et al. 2002). The horizontal discretisation is similar to the FEFTRA mesh, but there is greater vertical discretisation in the NAMMU model. In particular: the vertical element size is 10 m from -400 m to -480 m and 5 m from -480 m to -520 m, while below -520 m a graded discretisation was used, which starts with finite elements of size 5 m increasing to elements of size about 20 m. The NAMMU mesh consisted of 863 000 elements. Similarly to FEFTRA, a preconditioned conjugate gradient method was used to obtain the solution for groundwater flow.

Results

The result quantities calculated in the test case were:

- pressure along the boreholes KR1–KR5,
- flow paths starting at three points near the repository,
- flow rates through a box surrounding the repository (the box is intersected by the zones R10HY and R16) , and
- infiltration based on the computed flow rate through a horizontal plane at a depth of 10 metres.

The pressures along the boreholes KR1–KR5 are presented in Figure 2.26 showing an excellent agreement between the FEFTRA and NAMMU results. The computed net flow rates through a box surrounding the repository (Table 2.16) are also essentially in good agreement. The differences on the north-west and north-east side of the box can likely

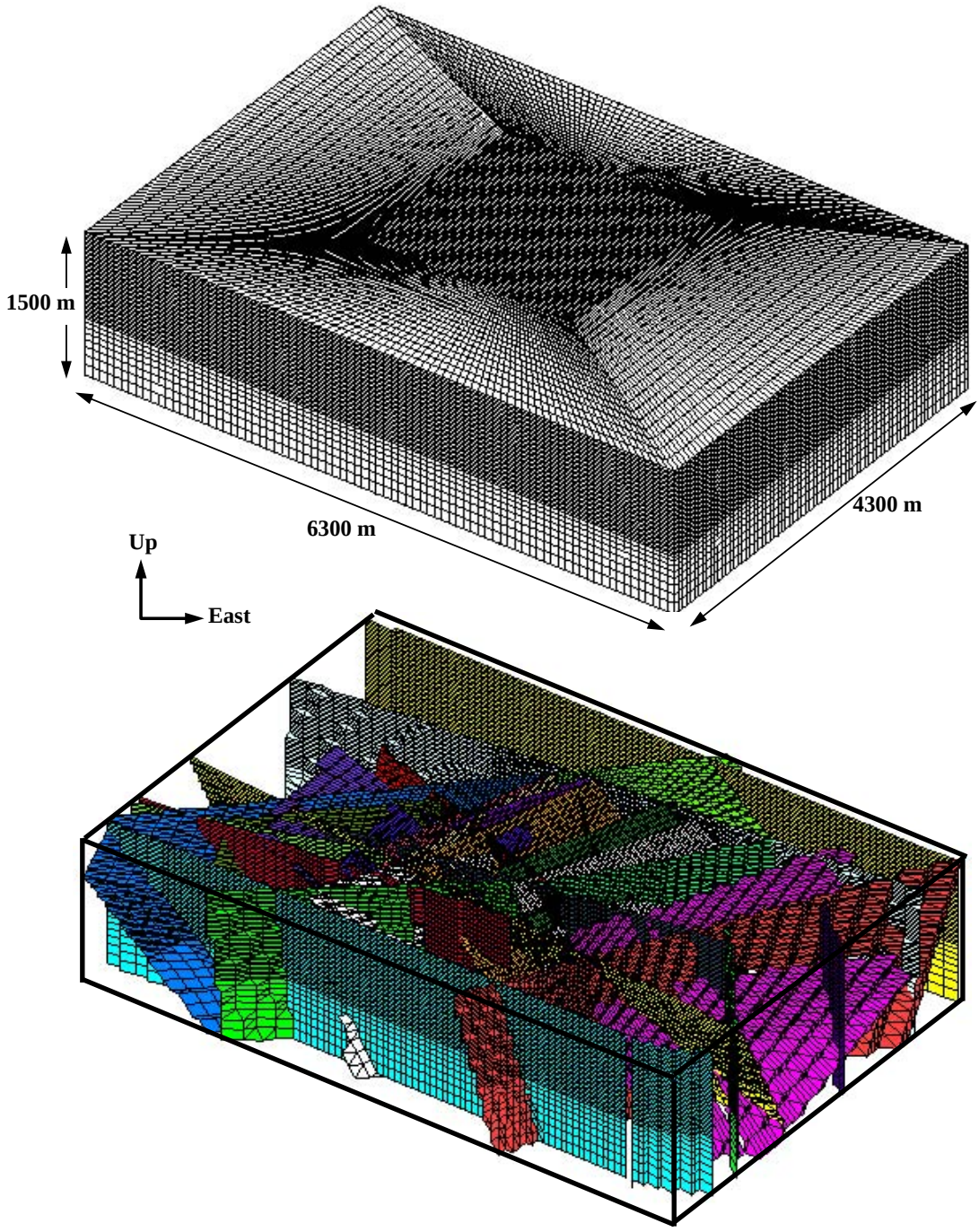

Figure 2.25. Finite element mesh for the Olkiluoto site in the FEFTRA model. The three-dimensional elements (537 000) represent the sparsely fractured rock (top) and the two-dimensional elements (106 000) the hydrogeological zones (bottom). Compare to Figure 2.22.

Table 2.16. Computed net flow rates [m^3/a] through a box surrounding the repository (+ denotes inflow and - outflow). The height of the box is 50 metres and the area of the top and bottom faces is 800000 m^2, whereas the distance between the repository and the faces of the box is about 20–30 metres. The box is intersected by the zones R10HY and R16. The inaccuracy of mass balance in the NAMMU flows results from the fact that the box was not coincident with finite elements (Hartley et al. 2002).

Face	FEFTRA	NAMMU
Bottom face	-24.98	-21.82
South-west side	0.58	0.58
South-east side	0.53	0.70
North-east side	-0.11	-0.20
North-west side	-0.60	-1.48
Top face	24.51	21.64
Mass balance	-0.07	-0.58

be attributed to the the different representation of the hydrogeological zones between the two models, which results in the northern corner of the box clipping several zones in the NAMMU model and gives different local flows in this area (Hartley et al. 2002). The computed infiltrations (34.3 mm/a in the FEFTRA and 33.5 mm/a in the NAMMU model) are in excellent agreement.

The final positions and lengths of the flow paths (Table 2.17 and Figure 2.27) show a pretty good agreement between the FEFTRA and NAMMU models. However, the travel times of the flow paths computed with FEFTRA are shorter than the corresponding NAMMU times. After leaving the repository the NAMMU paths (especially path 1 and 3) seem to stay much longer in the sparsely fractured rock than the FEFTRA paths. Due to the low velocity of the sparsely fractured rock, a small change in the path through the sparsely fractured rock may lead to a disproportionately large change in the travel time. Thus, the times are sensitive to the behaviour of the flow field in the sparsely fractured rock between the repository and the nearest zones. The discrepancies in the local flow field, on the other hand, can probably be attributed to the different representations of the hydrogeological zones and/or different discretisation in the vicinity of the repository (see subsection "*Numerical solution method*" above). Especially, the implicit representation of the zones in the NAMMU model may overestimate the travel times, because the permeability of the zones was reduced by averaging the permeability over the volumes of the finite elements crossed by the zones (Hartley et al. 2002).

The results proved that the representation of the hydrogeological zones by lower dimensional elements (2D elements in the 3D mesh) is a feasible and efficient alternative to the use of uniform dimensional elements, which was already shown in Section 2.4.

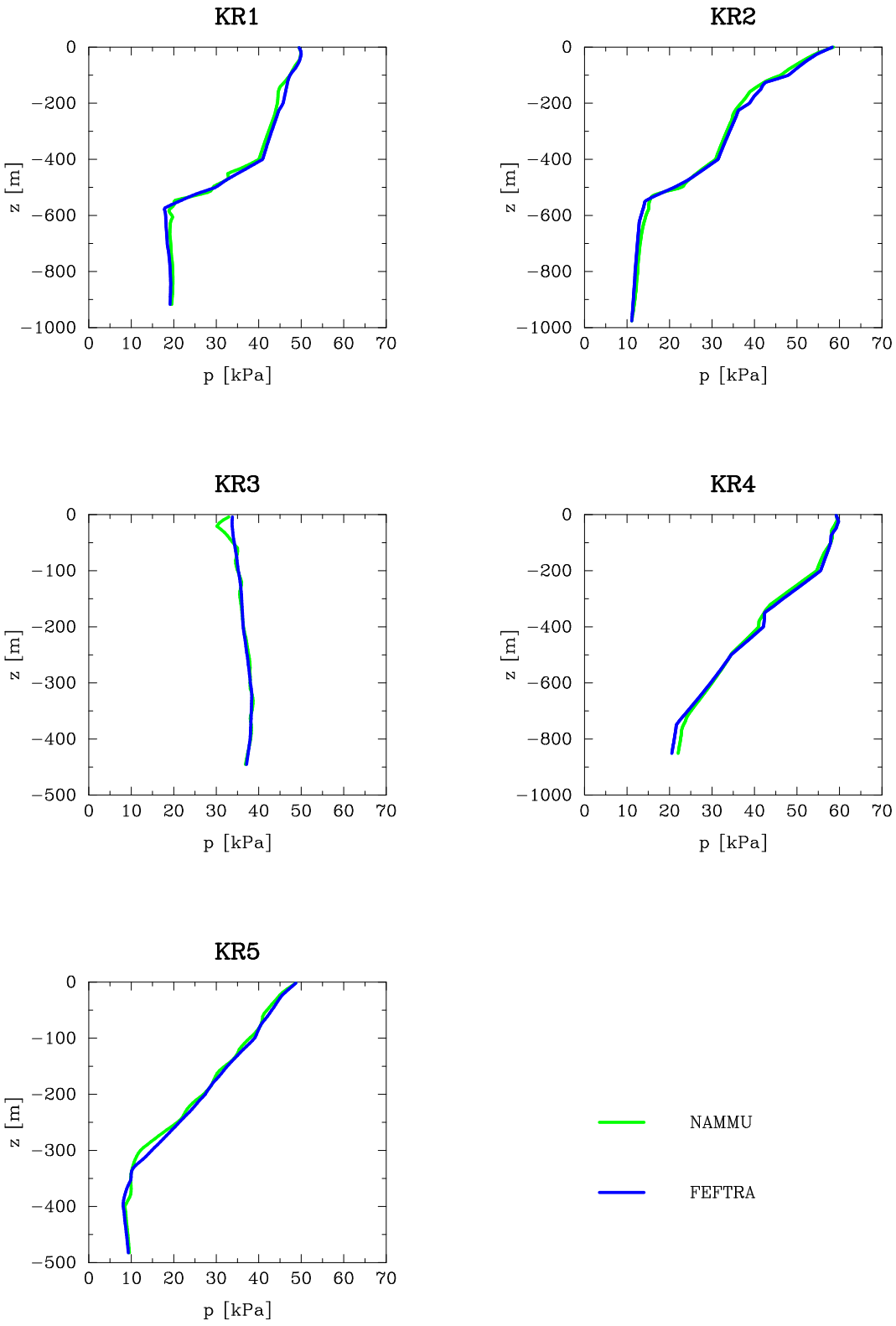

Figure 2.26. Residual pressure along the cored boreholes KR1–KR5 at the Olkiluoto site.

Table 2.17. Flowpaths computed with FEFTRA and NAMMU.

		FEFTRA			NAMMU		
		Path 1	Path 2	Path 3	Path 1	Path 2	Path 3
Initial position [m]	x	5596	5596	5596	5596	5596	5596
	y	2288	2288	2288	2288	2288	2288
	z	-500	-475	-525	-500	-475	-525
Final position [m]	x	5683	5680	5677	5697	5690	5693
	y	3526	3545	3554	3503	3521	3505
	z	0	0	0	0	0	0
Pathlength [m]		1677.7	1680.4	1723.8	1738.1	1745.4	1747.1
Travel time [a]		1321.0	1097.8	1614.9	2487.0	1358.9	2582.0

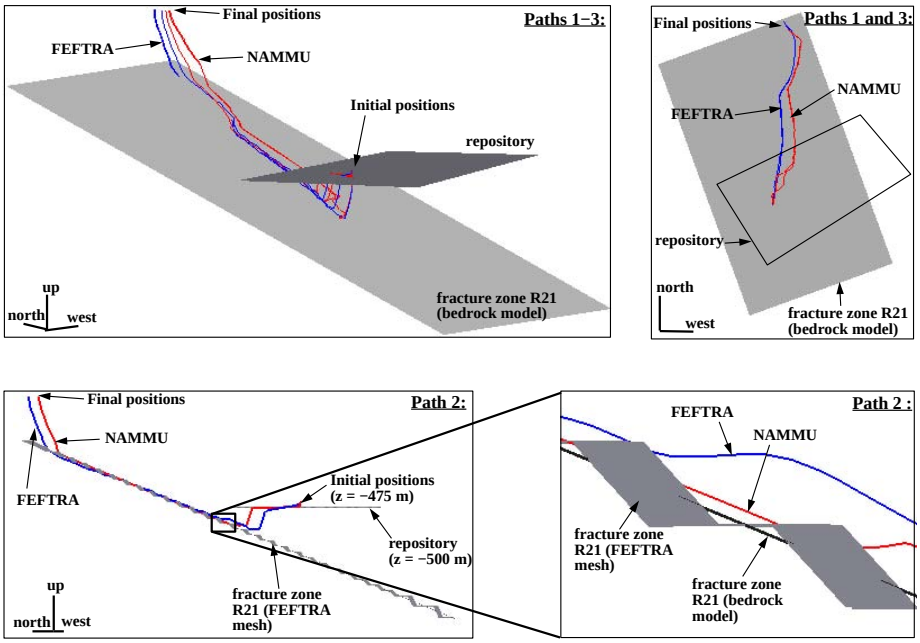

Figure 2.27. Computed flowpaths in the FEFTRA and NAMMU models. All three paths with the repository and hydrogeological zone R21 (the bedrock model) are presented on top-left. Flow path 1 and 3 are shown on top-right, whereas flow path 2 is presented at the bottom.

3. Coupled groundwater flow and solute transport

During the hydrogeochemical field investigations at the coastal sites (Olkiluoto, Hästholmen) in the Finnish site evaluation programmes, saline groundwater was observed. Salt content of groundwater usually increases with depth, but high salinity concentrations have also been observed relatively close to the ground surface. The variations in salt concentration not only affect the chemical stability of the bentonite clay surrounding the disposal canisters but also groundwater flow through the variations in the density. Thus, the simulation of coupled groundwater flow and solute transport constitute an important part of the ongoing site investigation programme as well as repository design and safety assessment.

3.1 Henry's seawater intrusion problem

One of the classic tests for variable density groundwater models is Henry's seawater intrusion problem (Henry 1964), which concerns a coupled groundwater flow and salt transport in a coastal aquifer. The problem describes an advance of a saltwater front in a confined aquifer initially charged with freshwater, for which Henry (1964) provided a semianalytic steady-state solution. Henry's problem has subsequently been widely used as a test case for numerical groundwater flow - salt transport codes (Lee & Cheng 1974; Voss & Souza 1987; Ségol 1994; Croucher & O'Sullivan 1995; Oldenburg & Pruess 1995; Ackerer et al. 1999).

Although the case is two-dimensional, the corresponding case with 3D elements was computed as well. The test case is located in the FEFTRA program path as follows:

- *feftra/solvit/t/press_conc/tpc2Dst_Henry* (2D mesh)
- *feftra/solvit/t/press_conc/tpc3Dst_Henry* (3D mesh)

Definition of the problem

The case is comprised of a vertical cross section (2 m $\times$ 1 m) taken through a homogeneous isotropic aquifer confined above and below by impermeable boundaries (Figure 3.1). Freshwater enters the aquifer at a constant rate from the left inland boundary, mixes with intruding salt water, and discharges to the sea through the upper right boundary. Salt water intrudes from the sea side until an equilibrium is reached with the opposing freshwater inflow. At the inland side the concentration is zero corresponding freshwater, while along the coastal boundary it is equal to the seawater concentration. The hydrostatic pressure based on the seawater density is assumed along the right vertical boundary.

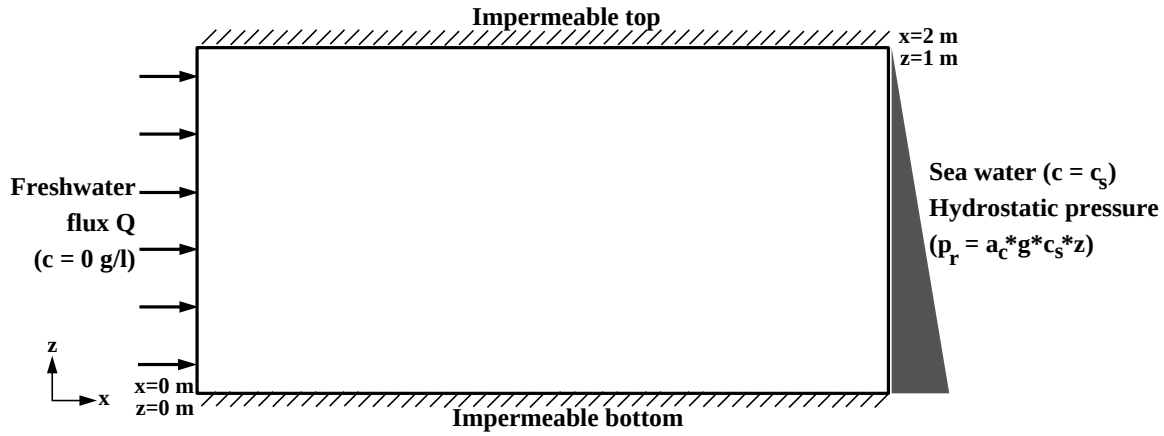

Figure 3.1. Schematic description of Henry's problem.

Mathematical model

The steady-state flow equation is written for the residual pressure p_r [Pa] (total pressure without the hydrostatic component of freshwater) as follows (Bear 1979; Huyakorn & Pinder 1983; de Marsily 1986)

$$\nabla \cdot \left(\frac{\rho \boldsymbol{k}}{\mu} \big(\nabla p_r + (\rho - \rho_0) g \nabla z \big) \right) = 0, \tag{3.1}$$

where $\boldsymbol{K}$ is the hydraulic conductivity tensor of rock [$\mathrm{m/s}$], g is the gravitational acceleration [$\mathrm{m/s^2}$], ρ is the density of water [$\mathrm{kg/m^3}$], ρ_0 is the density of freshwater [$\mathrm{kg/m^3}$], and z is the elevation relative to the sea level [m].

The equation describing salt transport is written in terms of salt concentration c [g/l] as follows (Bear 1979; Huyakorn & Pinder 1983; de Marsily 1986)

$$\nabla \cdot (\boldsymbol{D} \nabla c) - \nabla \cdot (\boldsymbol{q} c) = 0, \tag{3.2}$$

where $\boldsymbol{q}$ is the Darcy velocity [m/s], $\boldsymbol{D}$ is the dispersion tensor [$\mathrm{m^2/s}$], which in this case includes only the molecular diffusion and is expressed as

$$D_{ij} = D_0 \delta_{ij}, \tag{3.3}$$

where D_0 is the molecular diffusion coefficient [$\mathrm{m^2/s}$] and δ_{ij} is the Kronecker delta function [-].

Equations (3.1) and (3.2) are coupled by the Darcy velocity $\boldsymbol{q}$ [m/s]

$$\boldsymbol{q} = -\frac{\boldsymbol{k}}{\mu} (\nabla p_r + (\rho - \rho_0) g \nabla z) \tag{3.4}$$

and the density ρ [$\mathrm{kg/m^3}$], which is expressed as a linear function of the salt concentration c [g/l] as

$$\rho = \rho_0 + a_c c. \tag{3.5}$$

Table 3.1. Input parameters for Henry's problem (Henry 1964; Voss & Souza 1987; Ségol 1994).

Symbol	*Parameter*	*Equation*	*Value*
$\boldsymbol{K}$	Hydraulic conductivity	3.6	$1.0 \cdot 10^{-2}$ m/s
g	Gravitational acceleration	3.1, 3.4	9.81 m/s^2
ρ_0	Freshwater density	3.1, 3.4–3.7	1000 kg/m^3
D_0	Effective diffusion coefficient	3.2, 3.8	$6.6 \cdot 10^{-6}$ m^2/s
a_c	Coefficient for density dependence on salinity	3.5	0.7
Q	Freshwater flux	3.7, 3.8	$6.6 \cdot 10^{-5}$ m^2/s
c_s	Salt concentration in seawater		35.714 g/l
d	Aquifer thickness	3.7	1.0 m

where a_c is the coefficient of density dependence on concentration $[-]$. The permeability $\boldsymbol{k}$ in Equations (3.1) and (3.4) is related to the hydraulic conductivity $\boldsymbol{K}$ [m/s]

$$\boldsymbol{k} = \frac{\mu}{\rho g}\boldsymbol{K}. \tag{3.6}$$

The input parameter values for equations are given in Table 3.1.

Henry (1964) introduced two dimensionless parameters a and b for the problem as follows

$$a = \frac{Q}{d} \cdot \frac{\rho_0}{K(\rho_s - \rho_0)}, \tag{3.7}$$

$$b = \frac{D_0}{Q} = 0.1. \tag{3.8}$$

where Q is the freshwater flux from the inland boundary [m^2/s], d the aquifer thickness [m], and ρ_s the density of seawater [kg/m^3]. The input parameters (Table 3.1) and Equation (3.5) result in the values ρ_s=1025 kg/m^3, $a = 0.263$ and $b = 0.1$ for the seawater density and Henry's parameters.

Numerical solution method

The finite element method with linear elements was applied in solving the case numerically. The modelled region was discretised to a uniform mesh with 5000 quadrangular elements of size 0.02 m $\times$ 0.02 m (Figure 3.2). The mesh consisted of 5151 nodes. The corresponding 3D mesh consisted of hexaedral elements.

The partial differential equation (3.1) describing groundwater flow was solved numerically employing the conventional Galerkin technique (Huyakorn & Pinder 1983), whereas the streamline-upwind/Petrov-Galerkin (SUPG) method (Brooks & Hughes 1992; Laitinen 1995) was applied for the transport equation (3.2). The Darcy velocity (3.4) for the transport equation (3.2) was computed by taking directly the derivative of the computed

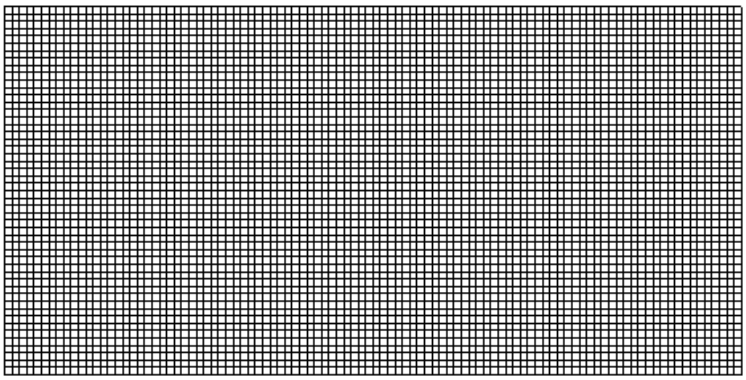

Figure 3.2. Finite element mesh (2D) for Henry's problem (5000 elements, 5151 nodes).

finite element approximation for the pressure (3.1). The resulting matrix equations for the flow and transport equations were solved employing the conjugate-gradient and Gauss-Seidel methods (Atkinson 1988).

The steady-state solution was attained with the Picard iteration scheme (Huyakorn & Pinder 1983), which was applied sequentially for the flow and the transport equations until the convergence was attained (50 iteration sweeps). At the end of each iteration sweep the concentration result was updated using an underrelaxation scheme to reduce the oscillations of concentration changes from iteration to iteration

$$c_i = c_{i-1} + 0.2(c - c_{i-1}), \tag{3.9}$$

where c_{i-1} and c denote the result of the previous iteration and the current iteration, respectively, and c_i is the final value of concentration at the current iteration sweep. The coefficient 0.2 in Equation (3.9) was found by trial and error.

Results

Henry (1964) developed a semianalytic steady-state solution for this problem, but no numerical model so far has been able to closely match his solution. On the other hand, several numerical models based on the different methods have given nearly identical results for the problem, which has indicated some inaccuracy in the original result by Henry. However, Ségol (1994) presented a revised calculation of Henry's semianalytic solution, and the previously observed differences between numerical and analytic results seem to be disappeared.

The computed FEFTRA results were compared to Henry's original and revised (Ségol 1994) solution as well as some numerical (Lee & Cheng 1974; Voss & Souza 1987; Croucher & O'Sullivan 1995) results. The contours of the nondimensional concentration $c' = c/c_s$ presented in Figure 3.3 show that the FEFTRA results compare very well with the revised analytic solution. On the other hand, Figure 3.4, which summarises

Henry's original solution with some numerical results for the contour of $c' = 0.5$, reveal the similarity of the FEFTRA results to the ones computed by Voss & Souza (1987) and Croucher & O'Sullivan (1995). Some slight differences to the Voss & Souza (1987) result can be observed near the coastal boundary, because they used the different boundary condition on the upper part of the boundary. However, it is clear that Henry's original analytic and numerical solution by Lee & Cheng (1974) do not match the other results; this can probably be attributed to some inconsistencies in the models by Henry and Lee & Cheng (1974). The computed FEFTRA results in 3D were identical to the 2D results.

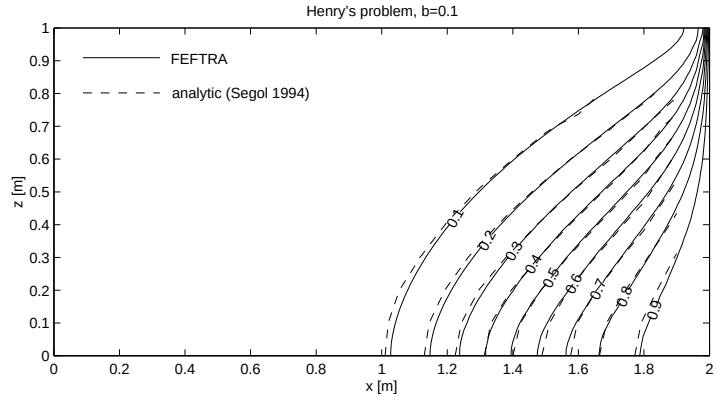

Figure 3.3. The FEFTRA and revised analytical solution to the Henry's problem for the contours of $c' = c/c_s = 0.1 - 1.0$ (step 0.1).

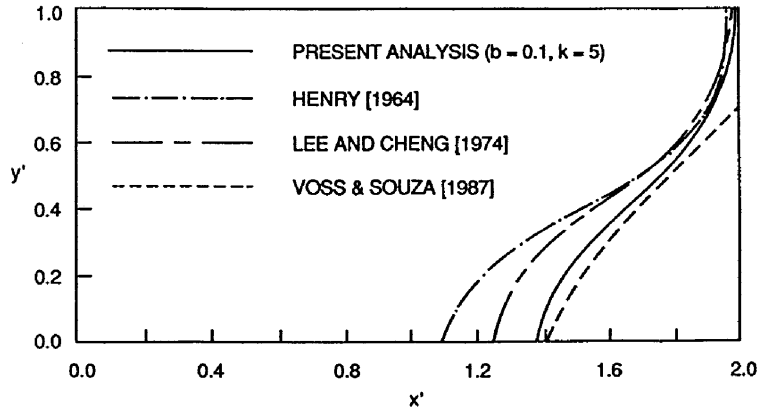

Figure 3.4. Henry's original and some previous numerical solutions to Henry's problem for the contour of $c' = c/c_s = 0.5$ ($b = 0.1$). The label 'present analysis' denotes the results by Croucher & O'Sullivan (1995).

3.2 Elder's free convection problem

Elder (1967) presented experimental and numerical studies concerning thermal convection produced by heating a base of a porous layer. Elder conducted the studies to verify his finite difference model for the numerical analysis of thermally driven convection. The numerical results of Elder (1967) for the problem of complex natural convection was suggested by Voss & Souza (1987) as a basis for verification of transport simulators as well. The objective of the solute analogue of Elder's problem was to verify the models in representing fluid flow driven purely by density differences. The large maximum density change (20 %) makes this a strongly coupled flow and solute transport problem, which has become a widely used test for variable density groundwater models (Oldenburg & Pruess 1995; Kolditz et al. 1998; Ackerer et al. 1999; Frolkovič & De Schepper 2001).

Although the case is two–dimensional, the corresponding case with 3D elements was computed as well. The test case is located in the FEFTRA program path as follows:

- *feftra/solvit/t/press_conc/tpc2Dtr_elderS* (coarse 2D mesh)
- *feftra/solvit/t/press_conc/tpc2Dtr_elderL* (fine 2D mesh)
- *feftra/solvit/t/press_conc/tpc3Dtr_elderL* (fine 3D mesh)

Definition of the problem

The problem concerns transient and coupled groundwater flow and solute transport in a closed box, where a dense fluid lies on top of the less dense fluid (Figure 3.5). The box is assumed to be a rectangular, vertical cross section (600 m $\times$ 150 m) taken through a homogeneous and isotropic medium. A source of solute with constant concentration (1 g/l) is specified at the top of the domain (150 m $\leq x \leq$450 m), while a zero concentration is maintained along the entire base. Pressure is initially hydrostatic and a zero pressure is held at the two upper corners of the domain. Solute enters the initially freshwater by diffusion, increases its density, and thereby begins a circulation process.

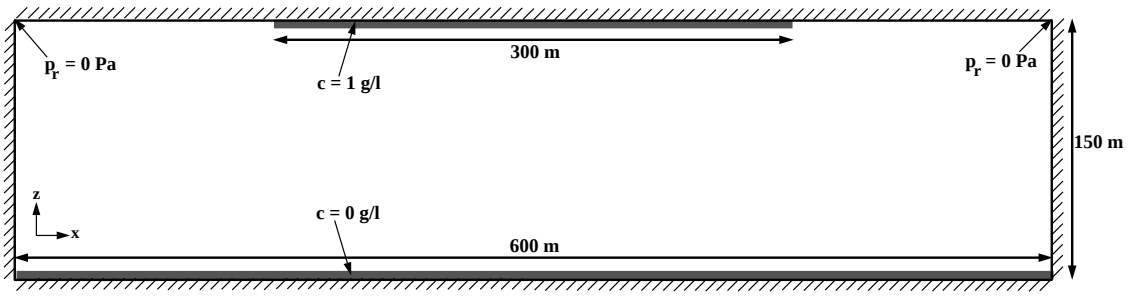

Figure 3.5. Schematic description of Elder's free convection problem.

Mathematical model

The transient flow equation is written for the residual pressure p_r [Pa] (total pressure without the hydrostatic component of freshwater) as follows (Bear 1979; Huyakorn & Pinder 1983; de Marsily 1986)

$$\nabla \cdot \left(\frac{\rho \boldsymbol{k}}{\mu} \big(\nabla p_r + (\rho - \rho_0) g \nabla z \big) \right) = \frac{\partial}{\partial t} (\rho \phi) \tag{3.10}$$

where $\boldsymbol{k}$ is the permeability tensor of rock [m^2], μ is the dynamic viscosity of water [kg/m/s], ρ is the density of water [kg/m^3], ρ_0 is the density of freshwater [kg/m^3], g is the gravitational acceleration [m/s^2], z is the elevation relative to the sea level [m], and ϕ is the porosity [$-$].

The equation describing transient salt transport is written in terms of salt concentration c [g/l] as follows (Bear 1979; Huyakorn & Pinder 1983; de Marsily 1986)

$$\nabla \cdot (\boldsymbol{D} \nabla c) - \nabla \cdot (\boldsymbol{q} c) = \phi \frac{\partial c}{\partial t}, \tag{3.11}$$

where $\boldsymbol{q}$ is the Darcy velocity [m/s] and $\boldsymbol{D}$ is the dispersion tensor [m^2/s], which in this case includes only the molecular diffusion and porosity, and is expressed as

$$D_{ij} = \phi D_0 \delta_{ij}, \tag{3.12}$$

where D_0 is the molecular diffusion coefficient [m^2/s] and δ_{ij} is the Kronecker delta function [$-$].

Equations (3.10) and (3.11) are coupled by the Darcy velocity

$$\boldsymbol{q} = -\frac{\boldsymbol{k}}{\mu} (\nabla p_r + (\rho - \rho_0) g \nabla z) \tag{3.13}$$

and the density ρ, which is expressed as a linear function of the salt concentration c as

$$\rho = \rho_0 + a_c c, \tag{3.14}$$

where a_c is the coefficient of density dependence on concentration [$-$].

Assuming the medium incompressible and the porosity only a function of pressure, and employing Equation (3.14), the right-hand side of Equation (3.10) can be written with salt concentration as follows

$$\frac{\partial}{\partial t} (\rho \phi) = \phi \frac{\partial \rho}{\partial t} + \rho \frac{\partial \phi}{\partial t} = \phi a_c \frac{\partial c}{\partial t}. \tag{3.15}$$

The last equality follows from the assumption that fluid flow is driven purely by density differences. The input parameter values for equations are given in Table 3.2.

Table 3.2. Input parameters for Elder's free convection problem (Voss & Souza 1987).

Symbol	*Parameter*	*Equation*	*Value*
$\boldsymbol{k}$	Permeability tensor of the medium	3.10, 3.13	$4.845 \cdot 10^{-13}$ m^2
ϕ	Porosity	3.10, 3.11, 3.12	0.1
μ	Dynamic viscosity of water	3.10, 3.13	$1.0 \cdot 10^{-3}$ kg/m/s
g	Gravitational acceleration	3.10, 3.13	9.81 m/s^2
ρ_0	Density of freshwater	3.10, 3.13, 3.14	1000 kg m^{-3}
D_0	Molecular diffusion coefficient	3.12	$3.565 \cdot 10^{-6}$ m^2/s
a_c	Density dependence on concentration	3.14	200.0

Numerical solution method

The finite element method with linear elements was applied in solving the case numerically. Although the problem is symmetrical with respect to the central vertical plane, the whole modelled region was discretised to check the ability of the code to produce symmetric results. As the problem has been reported to be sensitive to coarse discretisation (Oldenburg & Pruess 1995; Kolditz et al. 1998) two uniform quadrangular meshes (Figure 3.6) were employed: a coarse mesh (1100 elements of size 13.6 $\times$ 6 m) similar to the discretisation used by Elder (1967), Voss & Souza (1987) and Kolditz et al. (1998) and a fine mesh (4400 elements of size 6.8 $\times$ 3 m) similar to the fine discretisation used by Kolditz et al. (1998). The 3D mesh corresponding to the fine 2D mesh consisted of 4400 hexaedral elements. The simulation period of 10 years was discretised into 101 uniform time steps of size 0.1 years.

The partial differential equation (3.10) describing groundwater flow was solved numerically employing the conventional Galerkin technique (Huyakorn & Pinder 1983), whereas the streamline-upwind/Petrov-Galerkin (SUPG) method (Brooks & Hughes 1992; Laitinen 1995) was applied for the transport equation (3.11). The Darcy velocity (3.13) for the transport equation (3.11) was computed by taking directly the derivative of the computed finite element approximation for the pressure (3.10). The resulting matrix equations for the flow and transport equations were solved employing the conjugate-gradient and Gauss-Seidel methods (Atkinson 1988). The solution was attained with the Picard iteration scheme (Huyakorn & Pinder 1983), which was applied sequentially for the flow and the transport equations until the convergence was attained (5 iteration sweeps per time step). The fully implicit difference scheme was applied in the time discretisation.

Results

As there is no analytic solution for the problem, the numerical solution can only be assessed by comparison to other numerical solutions. Elder's free convection problem has been studied by many authors employing various numerical methods. Elder (1967) used a finite difference method for his original thermal convection problem, while Voss & Souza

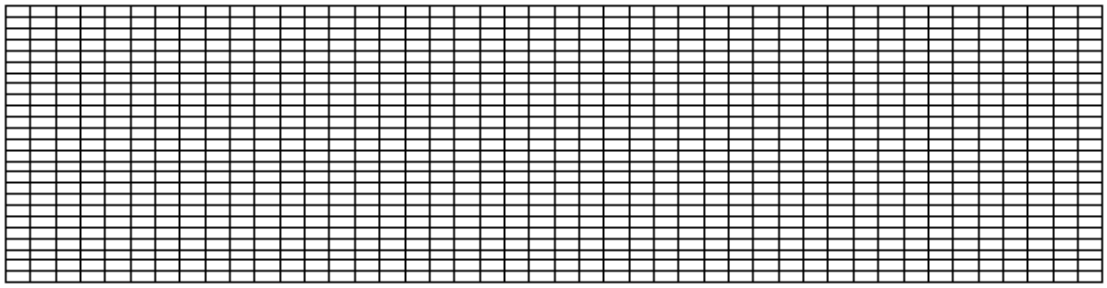

(a) Coarse mesh (1170 nodes, 1100 elements)

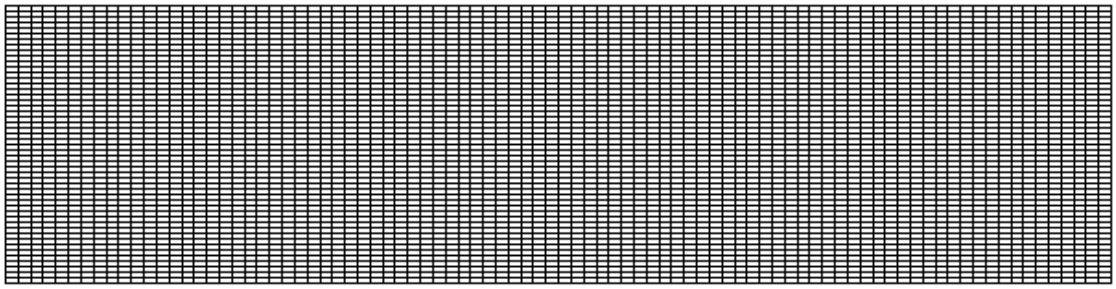

(b) Fine mesh (4539 nodes, 4400 elements)

Figure 3.6. Finite element meshes (2D) for Elder's free convection problem.

(1987) developed the first finite element model for the corresponding salt transport problem. Subsequently, Oldenburg & Pruess (1995) implemented a standard finite difference model for the problem, whereas Kolditz et al. (1998) studied the case with two Galerkin finite element models employing various numerical techniques. On the other hand, new numerical models were applied for the problem by Ackerer et al. (1999), whose model was based on a mixed hybrid and discontinuous finite element methods, and by Frolkovič & De Schepper (2001), who used a barycentre-based finite volume method. Although the various numerical solutions show general agreement, there are differences between the solutions, which show the complexity of Elder's problem. On the other hand, a perfect agreement cannot be expected, because of the different numerical methods and/or spatial discretisations.

The FEFTRA results were compared to the original results by Elder (1967) and Voss & Souza (1987) applying the coarse mesh (Figure 3.6(a)) as well as the subsequent results by Kolditz et al. (1998), who applied the fine mesh (Figure 3.6(b)) and similar numerical method (the Galerkin finite element method) as FEFTRA. The contours of 20 % and 60 % concentration for the coarse mesh at t = 2, 4 and 10 years are presented in Figure 3.7, which show that the FEFTRA results compare reasonably well with the results by Elder (1967) and Voss & Souza (1987), especially at t = 10 years. Although there are some differences at early times, all three solutions indicate similar physical behaviour of the system. The FEFTRA results computed with the fine mesh (Figure 3.8) are in excellent agreement with those given by Kolditz et al. (1998). The application of two different

spatial discretisation also confirms observations of the sensitivity of Elder's problem to the discretisation (Oldenburg & Pruess 1995; Kolditz et al. 1998).

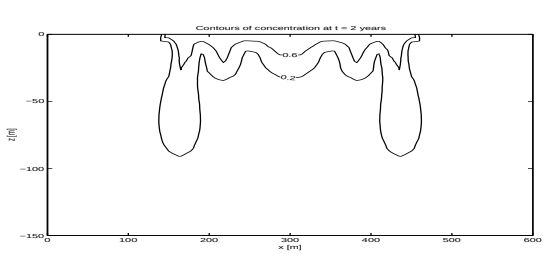

(a) FEFTRA ($t = 2$ years)

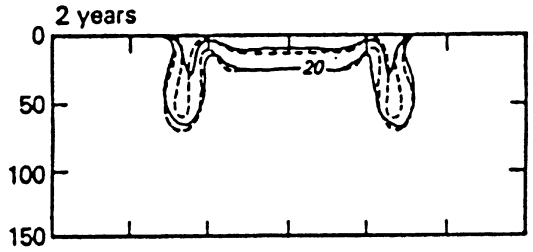

(b) Voss & Souza (1987) and Elder (1967)

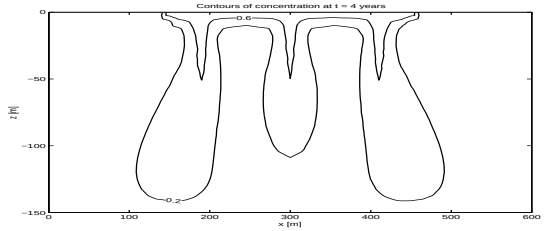

(c) FEFTRA ($t = 4$ years)

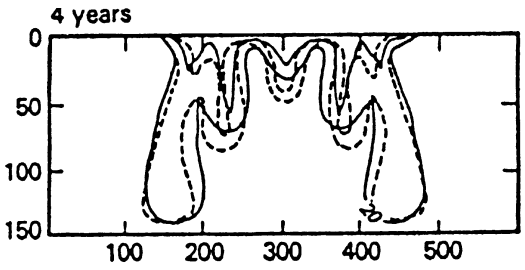

(d) Voss & Souza (1987) and Elder (1967)

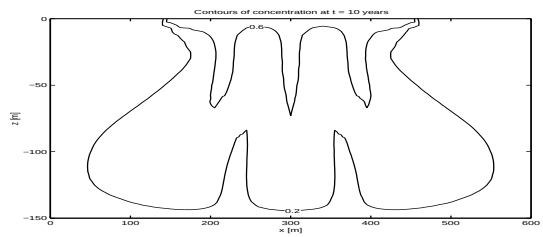

(e) FEFTRA ($t = 10$ years)

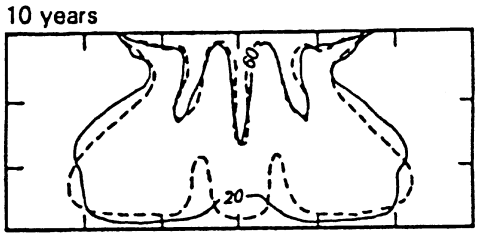

(f) Voss & Souza (1987) and Elder (1967)

Figure 3.7. Contours of 20 % and 60 % concentration for Elder's free convection problem. The FEFTRA results on the left side have been computed with the coarse mesh presented in Figure 3.6(a). The solid lines on the right side are the finite element results by Voss & Souza (1987), while the dashed lines are the finite difference results by Elder (1967) for the analogous temperature problem.

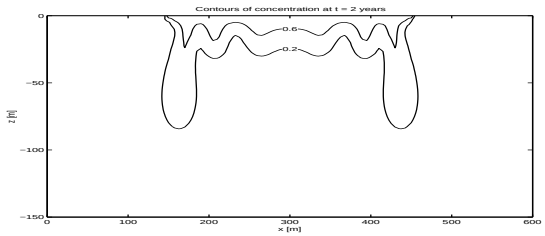

(a) FEFTRA ($t = 2$ years)

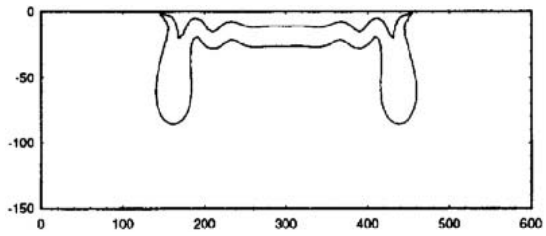

(b) Kolditz et al. (1998)

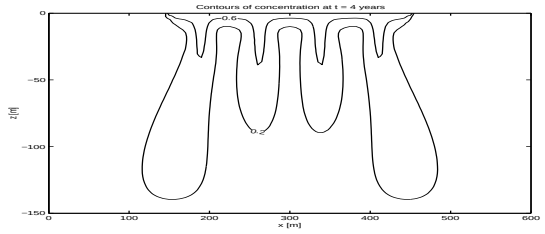

(c) FEFTRA ($t = 4$ years)

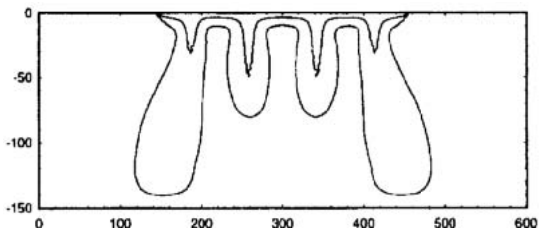

(d) Kolditz et al. (1998)

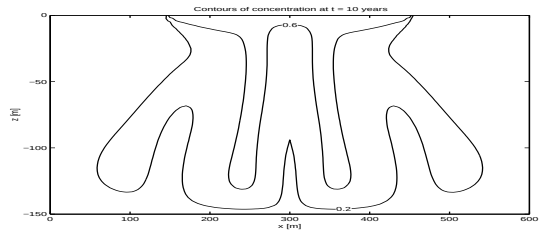

(e) FEFTRA ($t = 10$ years)

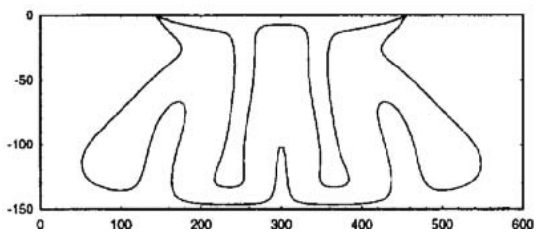

(f) Kolditz et al. (1998)

Figure 3.8. Contours of 20 % and 60 % concentration for Elder's free convection problem. The FEFTRA results on the left side have been computed with the fine mesh presented in Figure 3.6(b). The dimensions are vertically exaggerated to match the plots by Voss & Souza (1987).

3.3 Salt dome problem

This test case was introduced in the international hydrologic code intercomparison project (HYDROCOIN 1988) as the Case 5 of Level 1, and it concerns variable density groundwater flow over a hypothetical salt dome with a largely simplified geometry. The case was designed to simulate coupled groundwater flow and solute transport with density of water strongly dependent on concentration. Although the highly non-linear salt dome problem has its deficiencies, it has still been a subject of interest to many authors (Herbert et al. 1988; Oldenburg & Pruess 1995; Konikow et al. 1997; Kolditz et al. 1998; Younès et al. 1999) and it has become one of the standard tests for variable density groundwater models.

Although the case was two-dimensional, the corresponding case with 3D elements was computed as well (flow paths were computed only in 3D case). The test case is located in the FEFTRA program path as follows:

- *feftra/solvit/t/press_conc/tpc_hydrocoin_l1c5* (pressure and concentration in 2D)
- *feftra/solvit/t/press_conc/tpc_hydrocoin_l1c5_3D* (pressure and concentration in 3D)
- *feftra/solvit/t/velo/tq_hydrocoin_l1c5* (velocity in 2D)
- *feftra/solvit/t/velo/tq_hydrocoin_l1c5_3D* (velocity in 3D)
- *feftra/flowpath/t/tq_hydrocoin_l1c5_3D* (flow paths in 3D)

Definition of the problem

The problem is an idealisation of the geological conditions and groundwater flow over the salt dome, which is a potential site for a deep repository in bedrock. The case concerns steady-state flow in a vertical two-dimensional slice (900 m $\times$ 300 m) of a homogeneous isotropic rock (Figure 3.9). Impermeable lateral and bottom boundaries as well as a linearly varying pressure (from 10^5 Pa to 0 Pa) on the top boundary induce an inflow of freshwater into the domain on the top left and outflow on the top right. The salt concentration on the top is zero for the inflow region (0 m $\leq x \leq$ 202.5 m). The middle third of the bottom represents the top of the salt dome, where a constant concentration of 1 g/l is assumed. The rest of the bottom and the side walls as well as the outflow region of the top are taken as impermeable to dispersive salt transport. Eventually, the dispersing salt water reaches an equilibrium with the opposing freshwater inflow.

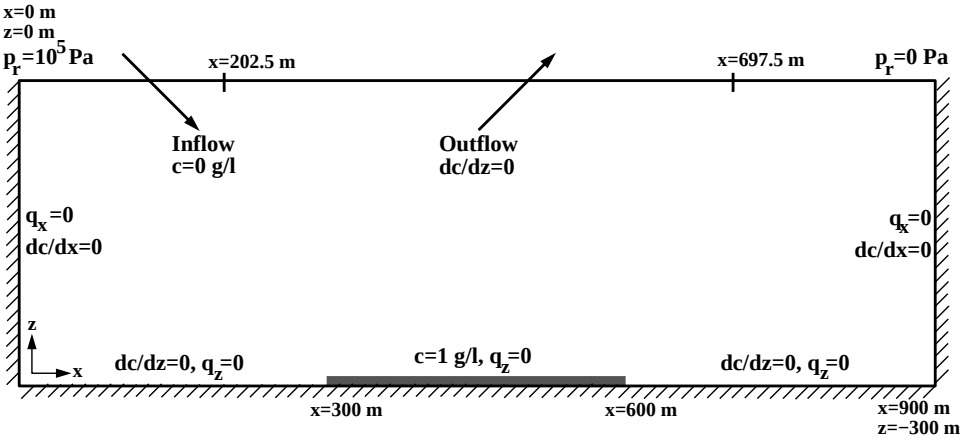

Figure 3.9. Schematic description of the salt dome problem.

Mathematical model

The steady-state flow equation is written for the residual pressure p_r [Pa] (total pressure without the hydrostatic component of freshwater) as follows (Bear 1979; Huyakorn & Pinder 1983; de Marsily 1986)

$$\nabla \cdot \left(\frac{\rho \boldsymbol{k}}{\mu} \big(\nabla p_r + (\rho - \rho_0) g \nabla z \big) \right) = 0, \tag{3.16}$$

where $\boldsymbol{k}$ is the permeability tensor of rock [m^2], μ is the dynamic viscosity of water [kg/m/s], ρ is the density of water [$\mathrm{kg/m}^3$], ρ_0 is the density of freshwater [$\mathrm{kg/m}^3$], g is the gravitational acceleration [$\mathrm{m/s}^2$], and z is the elevation relative to the sea level [m].

The equation describing salt transport is written in terms of salt concentration c [g/l] as follows (Bear 1979; Huyakorn & Pinder 1983; de Marsily 1986)

$$\nabla \cdot (\boldsymbol{D} \nabla c) - \nabla \cdot (\boldsymbol{q} c) = 0, \tag{3.17}$$

where $\boldsymbol{q}$ is the Darcy velocity [m/s] and $\boldsymbol{D}$ is the dispersion tensor [m^2/s], which is expressed as

$$D_{ij} = \varepsilon_T |\boldsymbol{q}| \delta_{ij} + (\varepsilon_L - \varepsilon_T) \frac{q_i q_j}{|\boldsymbol{q}|}, \tag{3.18}$$

where ε_L is the longitudinal dispersion length [m], ε_T is the transversal dispersion length [m] and δ_{ij} is the Kronecker delta function [-].

Equations (3.16) and (3.17) are coupled by the Darcy velocity $\boldsymbol{q}$ [m/s]

$$\boldsymbol{q} = -\frac{\boldsymbol{k}}{\mu} (\nabla p_r + (\rho - \rho_0) g \nabla z) \tag{3.19}$$

and the density ρ [$\mathrm{kg/m}^3$], which is expressed as a function of salt concentration c [g/l] as

$$\frac{1}{\rho} = \frac{c}{\rho_s} + \frac{1 - c}{\rho_0}, \tag{3.20}$$

Table 3.3. Input parameters for the salt dome problem (HYDROCOIN 1988).

Symbol	*Parameter*	*Equation*	*Value*
$\boldsymbol{k}$	Permeability tensor of the medium	3.16, 3.19	$1.0 \cdot 10^{-12}$ m^2
μ	Dynamic viscosity of water	3.16, 3.19	$1.0 \cdot 10^{-3}$ kg m^{-1}s^{-1}
g	Gravitational acceleration	3.16, 3.19	9.81 m s^{-2}
ρ_0	Freshwater density	3.16, 3.19, 3.20	1000 kg m^{-3}
ρ_s	Salt water density	3.20	1200 kg m^{-3}
ε_L	Longitudinal dispersion length	3.3	20 m
ε_T	Transversal dispersion length	3.3	2 m

where ρ_s is the salt water density [kg/m^3]. The input parameter values for equations are given in Table 3.3.

Numerical solution method

The finite element method with linear elements was applied in solving the case numerically. The modelled region was discretised to a mesh with 12899 triangular and quadrangular elements (Figure 3.10). The mesh was refined near the salt dome so that the size of the smallest elements were of order of 1 metre. The corresponding 3D mesh consisted of wedge and hexaedral elements.

The partial differential equation (3.16) describing groundwater flow was solved numerically employing the conventional Galerkin technique (Huyakorn & Pinder 1983), whereas the streamline-upwind/Petrov-Galerkin (SUPG) method (Brooks & Hughes 1992; Laitinen 1995) was applied for the transport equation (3.17). The Darcy velocity (3.19) for the transport equation (3.17) was computed by taking directly the derivative of the computed finite element approximation for the pressure (3.1). The resulting linear matrix equations for the flow and transport equations were solved employing the conjugate-gradient and Gauss-Seidel methods (Atkinson 1988).

The steady-state solution was attained with the Picard iteration scheme (Huyakorn & Pinder 1983), which was applied sequentially for the flow and the transport equations until the convergence was attained (60 iteration sweeps). At the end of each iteration sweep the concentration result was updated using an underrelaxation scheme to reduce the oscillations of concentration changes from iteration to iteration

$$c_i = c_{i-1} + 0.49(c - c_{i-1}), \tag{3.21}$$

where c_{i-1} and c denote the result of the previous iteration and the current iteration, respectively, and c_i is the final value of concentration at the current iteration sweep. The coefficient 0.49 in Equation (3.21) was found by trial and error.

The flow paths (in 3D cases) were computed with the algorithm that uses the continuous

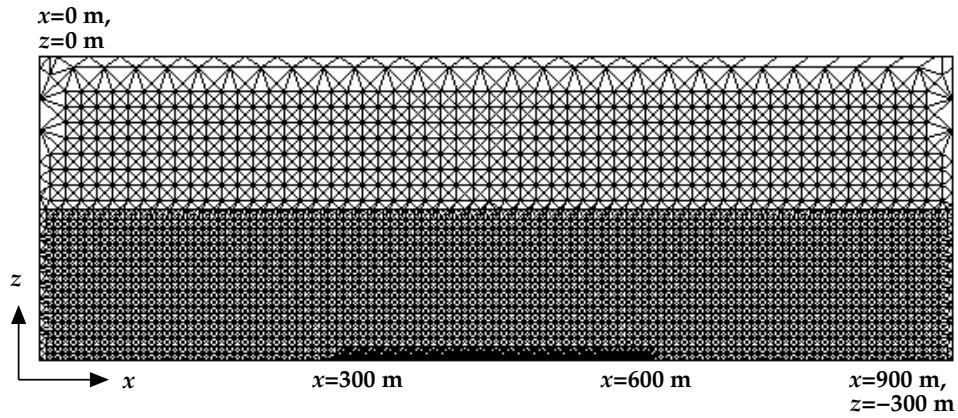

Figure 3.10. Finite element mesh for the salt dome problem (12900 elements, 6700 nodes).

Darcy velocity field obtained by treating $\boldsymbol{q}$ as an unknown variable and applying the finite element method to Equation (3.19).

Results

As there is no analytic solution for the the salt dome problem, the numerical solution of the problem can only be assessed on the basis of the expected physical behaviour of the system and the other numerical solutions. On the basis of the nature of the case, pressure should decrease from left to right and from the bottom to the top across the domain, whereas salt should form a plume flowing to the right and upwards from the salt dome. On the other hand, the pathlines starting at the top-left of the domain should first descend downwards and then move to the right and upwards across the domain.

The HYDROCOIN (1988) project indicated that the salt dome problem is numerically very difficult to solve. In the project the problem was solved by five different teams (Table 3.4) employing various computer codes with various special numerical methods. Although the overall flow field computed by the teams showed general agreement, there were significant differences in pressure and concentration fields as well as pathlines. On the other hand, it was concluded that the results of teams 1, 2 and 4 (Table 3.4) were reliable, because they were fairly close to each other and included all the expected physical features.

Since the HYDROCOIN project the salt dome problem has been tackled by several authors (Herbert et al. 1988; Oldenburg & Pruess 1995; Konikow et al. 1997; Kolditz et al. 1998; Younès et al. 1999), who have corrected deficiencies in the original specification of the problem and provided some variations for the input parameters. However, the subsequent solutions still have some differences, which show the difficulty of the problem. On the other hand, a perfect agreement between the numerical solutions cannot be expected, because the codes employ different numerical methods.

The computed FEFTRA results were compared with the numerical solutions by the original HYDROCOIN (1988) teams (Table 3.4). The result quantities were pressure and salinity distribution along horizontal lines at different depths, the vertical Darcy velocity along the top boundary, contours of salt concentration and pathlines starting at the top-left of the domain. The computed pressure at the depths of 50 m and 250 m is presented in Figure 3.11 showing a good agreement between the FEFTRA results and those of teams 1, 2 and 4, although the differences in the pressure increase downwards. The vertical Darcy velocities (Figure 3.12) are in excellent agreement. The five FEFTRA pathlines (Figure 3.13) are also essentially in line with those computed by the HYDROCOIN teams 1, 2 and 4. However, the computed salt concentration distribution indicates some discrepancies between the FEFTRA and other results. The concentrations along the horizontal lines (Figure 3.14) show a more dispersive solution by FEFTRA than teams 1, 2 and 4. FEFTRA overestimates the salt concentrations near the top-right corner and towards the right boundary at the depths of 100 and 200 m. On the other hand, the FEFTRA concentration compared well with that of team 1 at the bottom boundary. The same observations can also be made on the basis of the contours of the salt concentration (Figure 3.15). The computed FEFTRA results in 3D were identical to the 2D results.

The possible reasons for the discrepancies might be the use of non-continuous Darcy velocity in the transport equation (3.17) by taking directly the derivative of the computed finite element approximation for the pressure. On the other hand, the Picard iteration scheme with underrelaxation may not have ended up to full convergence. In addition, there were some inconsistencies in the original specification of the case that may have caused numerical problems.

The salt dome case also proved to be very difficult to solve for the FEFTRA code. In the first efforts, FEFTRA resulted in a significant overestimation of the salt concentration near the top-right corner of the domain. This was finally overcome only by assigning convective mass flux through the right side of the top boundary (697.5 m $\leq x \leq$ 900 m, Figure 3.9). The flux was calculated self-consistently by the code from the Darcy velocity and concentration. It should be noted that the two top corners constitute a source of inconsistency in the original problem specification (HYDROCOIN 1988; Herbert et al. 1988).

Table 3.4. HYDROCOIN (1988) teams and computer codes used in the salt dome problem.

No	*Team*	*Computer code*
1	CFEONW	CFEST
2	NAMAER	NAMMU
3	MTRRIV	METROPOL
4	SWITUB	SWIFT
5	SW2SAN	SWIFT2

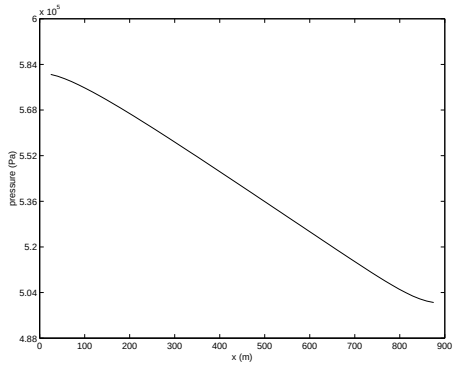

(a) FEFTRA ($z = -50$ m)

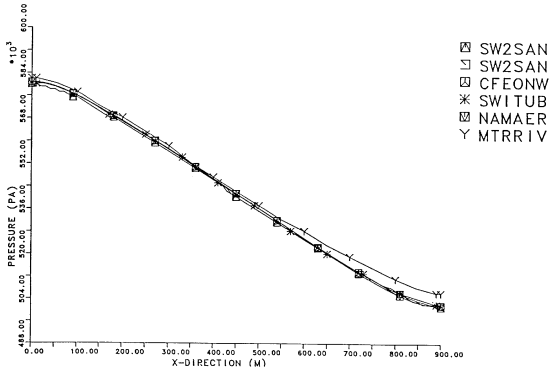

(b) HYDROCOIN teams ($z = -50$ m)

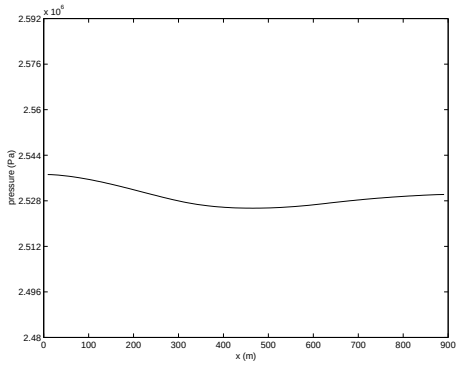

(c) FEFTRA ($z = -250$ m)

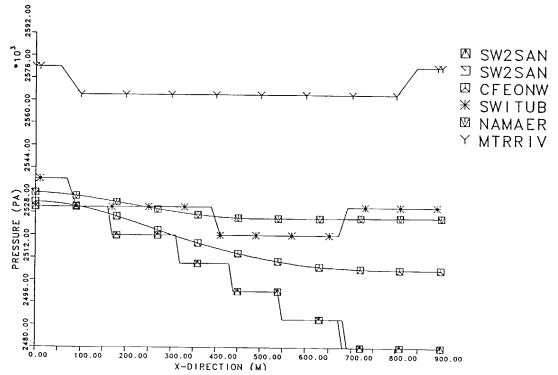

(d) HYDROCOIN teams ($z = -250$ m)

Figure 3.11. Computed pressures along two horizontal lines. The HYDROCOIN (1988) teams with corresponding computer codes are summarised in Table 3.4.

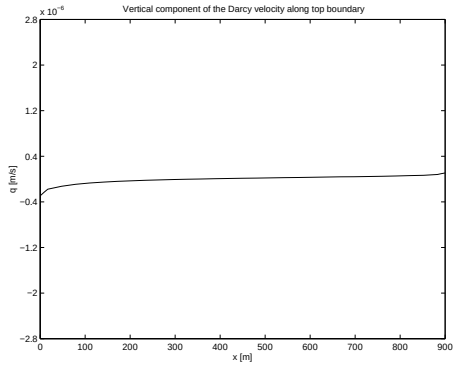

(a) FEFTRA

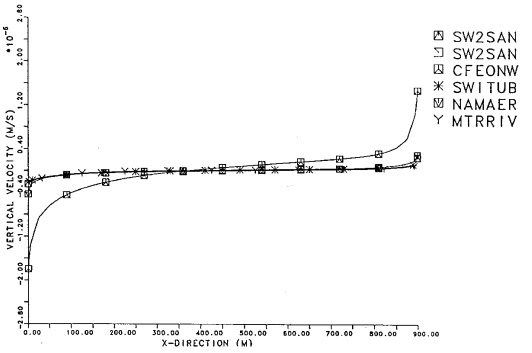

(b) HYDROCOIN teams

Figure 3.12. Computed vertical component of the Darcy velocity along top boundary. The HYDROCOIN (1988) teams and computer codes are summarised in Table 3.4.

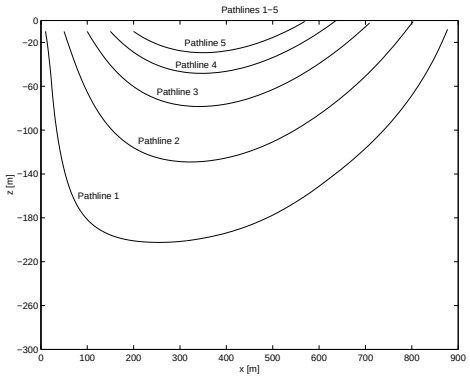

(a) FEFTRA (pathlines 1-5)

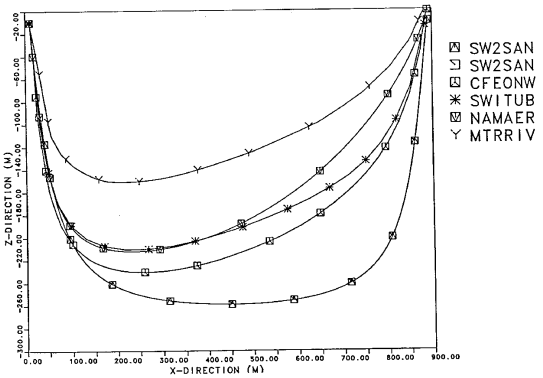

(b) HYDROCOIN teams (pathline 1, starting point at $x = 10$ m, $z = -10$ m)

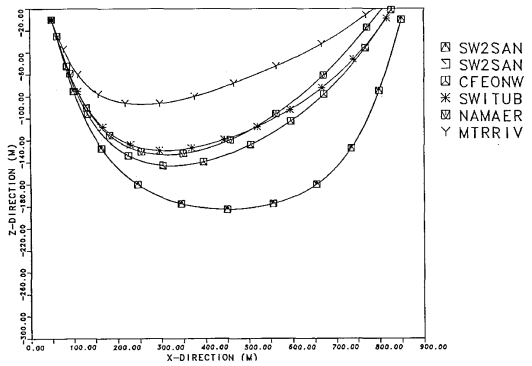

(c) HYDROCOIN teams (pathline 2, starting point at $x = 50$ m, $z = -10$ m)

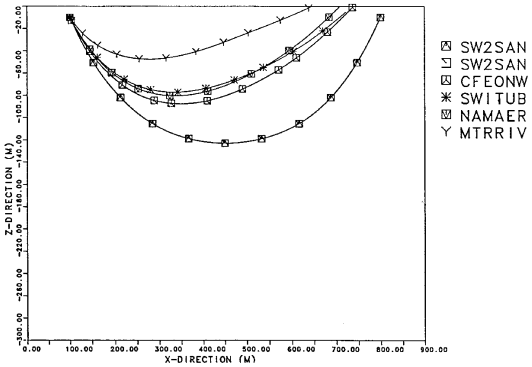

(d) HYDROCOIN teams (pathline 3, starting point at $x = 100$ m, $z = -10$ m)

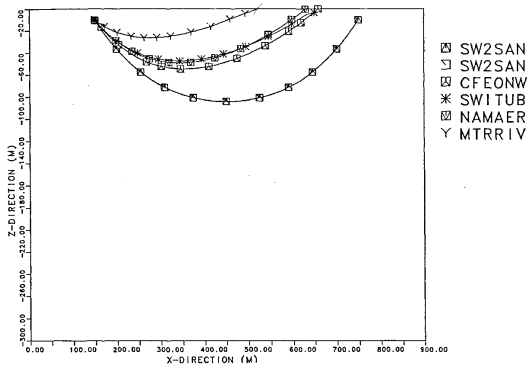

(e) HYDROCOIN teams (pathline 4, starting point at $x = 150$ m, $z = -10$ m)

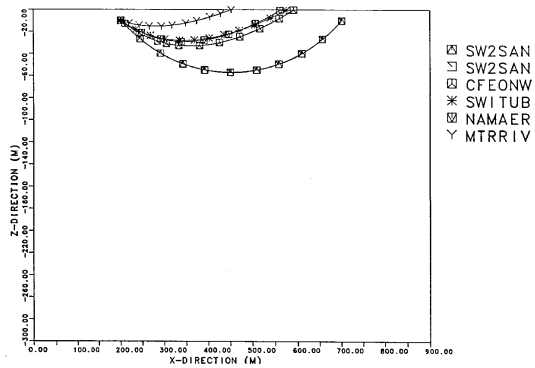

(f) HYDROCOIN teams (pathline 5, starting point at $x = 200$ m, $z = -10$ m)

Figure 3.13. Computed pathlines for five starting points. The HYDROCOIN (1988) teams with corresponding computer codes are summarised in Table 3.4.

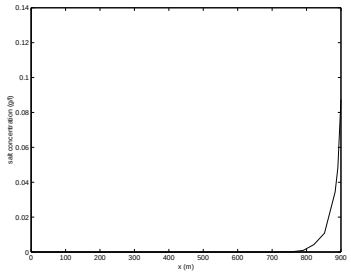

(a) FEFTRA ($z = 0$ m)

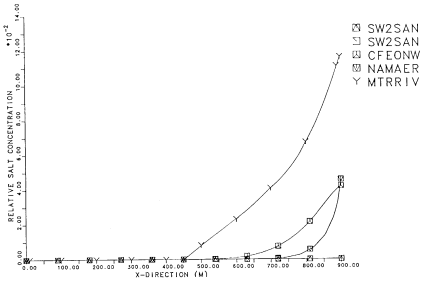

(b) HYDROCOIN teams ($z = 0$ m)

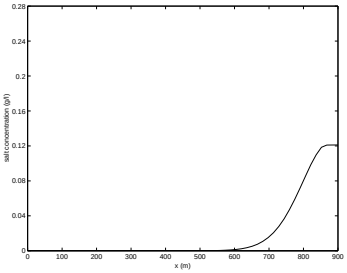

(c) FEFTRA ($z = -100$ m)

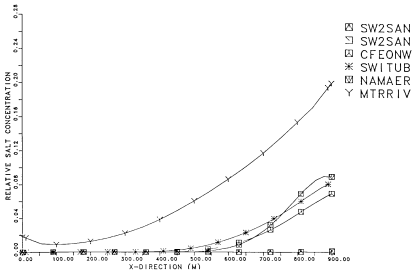

(d) HYDROCOIN teams ($z = -100$ m)

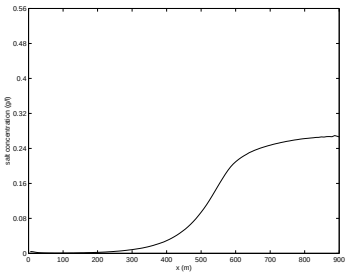

(e) FEFTRA ($z = -200$ m)

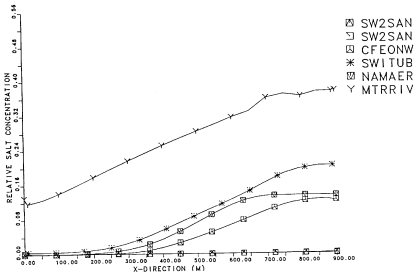

(f) HYDROCOIN teams ($z = -200$ m)

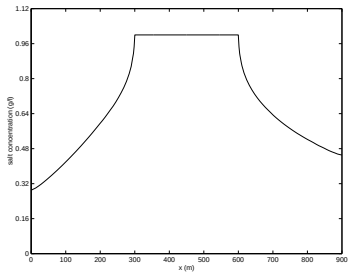

(g) FEFTRA ($z = -300$ m)

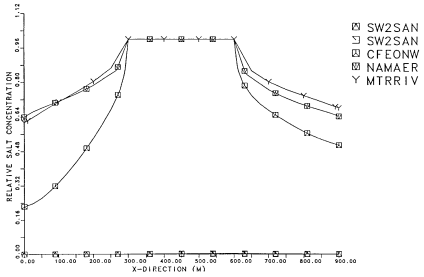

(h) HYDROCOIN teams ($z = -300$ m)

Figure 3.14. Computed salt concentration along four horizontal lines. The HYDROCOIN (1988) teams with corresponding computer codes are summarised in Table 3.4.

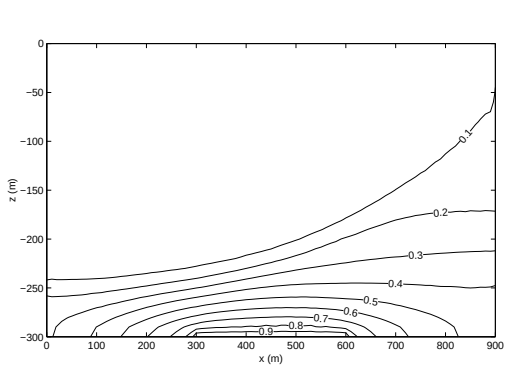

(a) FEFTRA

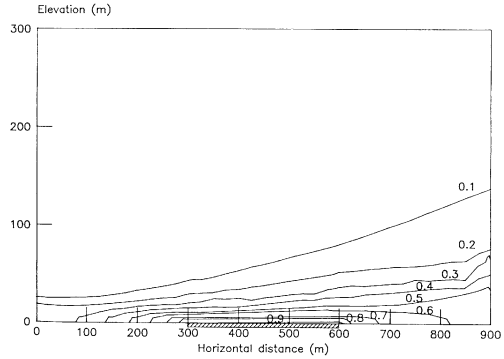

(b) CFEST

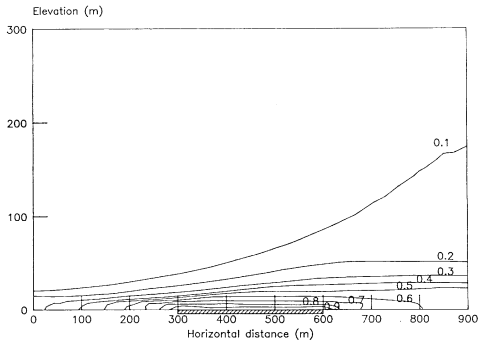

(c) SUTRA

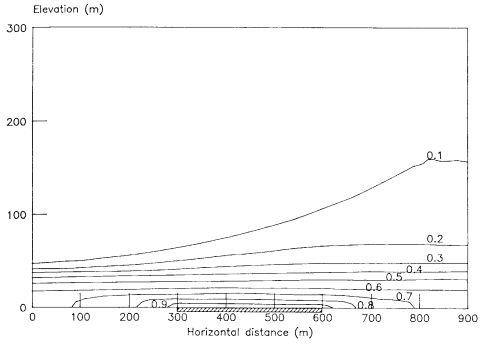

(d) NAMMU

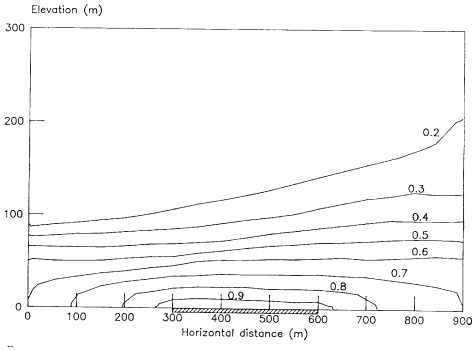

(e) METROPOL

Figure 3.15. Contours of salt concentration computed by FEFTRA and other codes used by the HYDROCOIN (1988) teams (Table 3.4).

3.4 Saltwater upconing beneath a pumping well

As a part of seeking a final repository for spent nuclear fuel an underground rock characterization facility, to be potentially extended with the drifts of the repository, is currently being excavated in the bedrock of Olkiluoto. The open tunnel system will constitute a hydraulic disturbance to the site's natural groundwater system. In particular, the upward flow below the tunnels may give rise to the upconing of more saline groundwater observed deep in the bedrock of Olkiluoto. Saline water is a major concern with regard to the performance of the tunnel backfill material after tunnel closure, because it may significantly decrease the swelling pressure and increase the hydraulic conductivity of the backfill.

Zhou et al. (2005) have investigated the effect of dispersion in saltwater upconing and decay beneath a pumping well. They simulated a constant-rate pumping of an axisymmetric, anisotropic and confined aquifer, equipped with a layer of seawater underlying freshwater. Their model was a modification of the model introduced by Voss & Souza (1987). The simulations were carried out using FEAS code, which uses a Eulerian-Lagrangian framework for solving the advective-dispersive salt transport equation and should produce an accurate salinity distribution near sharp concentration fronts. Although not originally presented as a case for testing of groundwater simulation software, this case is suitable for cross-code testing of FEFTRA for the simulation of the saline water upconing phenomenon.

The test case is located in the FEFTRA program path *feftra/solvit/t/press_conc/tpc_upconing*.

Definition of the problem

The case concerns upconing of saline water in an axisymmetric disc of radius of 2000 m, with a 20 m long well screen centred at the top and set to pump at a constant rate (Figure 3.16). Recharge of water occurs only at the external radial boundary. Initially, a 20 m thick layer of saltwater rests at the bottom of the domain and a 2 m thick transition zone separates the saltwater from freshwater in the upper part. A hydrostatic pressure distribution is assumed as an initial condition for the flow equation. The inner radial boundary as well as the top and bottom of the domain are impermeable, while at the external boundary dynamic boundary conditions are used to maintain a zero concentration gradient normal to the boundary. At the external boundary the pressure distribution is hydrostatic thorough the simulation.

Mathematical model

Transient flow equation is written for residual pressure p_r [Pa] as (Bear 1979; Huyakorn & Pinder 1983; de Marsily 1986)

$$\nabla \cdot \left(\frac{\rho \boldsymbol{k}}{\mu} (\nabla p_r + (\rho - \rho_0) g \nabla z) \right) - \rho Q_{out} = \frac{\partial}{\partial t}(\rho \phi), \tag{3.22}$$

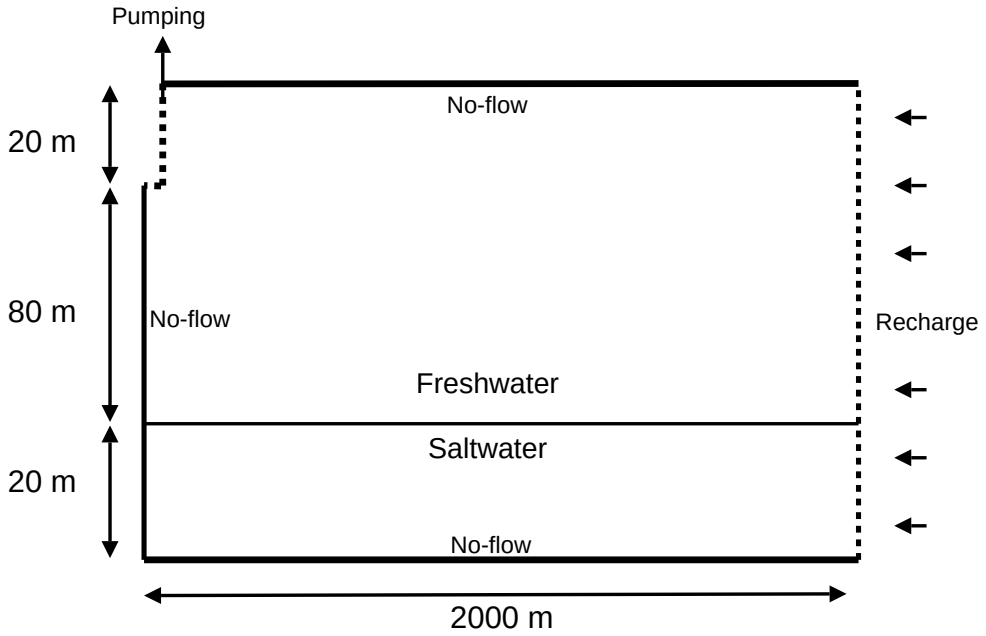

Figure 3.16. Schematic description of the axially (the vertical side on the left) symmetric saltwater upconing problem. The inner boundary as well as the top and bottom are impermeable, whereas the external boundary on the right is open for recharge of water.

where $\boldsymbol{k}$ is the permeability tensor of the porous media [m^2], μ is the dynamic viscosity of water [kg/m/s], ρ is the density of water [$\mathrm{kg/m}^3$], ρ_0 is the density of freshwater [$\mathrm{kg/m}^3$], g is the gravitational acceleration [$\mathrm{m/s}^2$], z is the elevation relative to the top of the modelled domain [m], and ϕ is the porosity of the media [-]. The term ρQ_{out} represents the sink in the model domain, where Q_{out} is the volumetric outflow rate [m^3/s].

The transient salt transport equation is written as (Bear 1979; Huyakorn & Pinder 1983; de Marsily 1986)

$$\nabla \cdot (\boldsymbol{D} \nabla c) - \nabla \cdot (\boldsymbol{q} c) + c_{in} Q_{in} - c Q_{out} = \phi \frac{\partial c}{\partial t}, \tag{3.23}$$

where $\boldsymbol{q}$ is the Darcy velocity [m/s] and $\boldsymbol{D}$ is the dispersion tensor [m^2/s]. The dispersion tensor is expressed as

$$D_{ij} = \varepsilon_T |\boldsymbol{q}| \delta_{ij} + (\varepsilon_L - \varepsilon_T) \frac{q_i q_j}{|\boldsymbol{q}|}, \tag{3.24}$$

where ε_L is the longitudinal dispersion length [m], ε_T is the transversal dispersion length [m] and δ_{ij} is the Kronecker delta function [-].

Equations (3.22) and (3.23) are coupled by the Darcy velocity

$$\boldsymbol{q} = -\frac{\boldsymbol{k}}{\mu} (\nabla p_r + (\rho - \rho_0) g \nabla z), \tag{3.25}$$

the density

$$\rho = \rho_0 + a_c c, \tag{3.26}$$

Table 3.5. Input data for the Case A and Case C of the saltwater upconing problem.

Symbol	*Parameter*	*Equation*	*Value*
k_x, k_y	Horizontal permeability	3.22	2.56×10^{-11} m/s
k_z	Vertical permeability	3.22	1.00×10^{-11} m/s
ϕ	Porosity	3.22	0.2
μ	Viscosity	3.22	1.0×10^{-3} kg/ms
Q_w	Pumping rate of the well	3.28	2400 m^3/d
c_{sw}	Concentration of saltwater	3.29	35.0 g/l
c_{fw}	Concentration of freshwater	3.29	0.0 g/l
ε_L	Longitudinal dispersivity, Case A	3.24	1.0 m
	Longitudinal dispersivity, Case C	3.24	10.0 m
ε_T	Transverse dispersivity, Case A	3.24	0.5 m
	Transverse dispersivity, Case C	3.24	1.0 m
ΔT	Time-step size	-	5 d
n_{it}	Number of Picard iterations	-	200
ω	Relaxation in Picard iterations		0.08

where a_c is the coefficient of density dependence on concentration $[-]$, and the dynamic viscosity

$$\mu = \mu_0 \left(1 + 1.85 \frac{c}{1000} - 4.1 (\frac{c}{1000})^2 + 44.5 (\frac{c}{1000})^3 \right). \tag{3.27}$$

The input parameters for the equations are given in Table 3.5.

Numerical solution method

The finite element method with linear elements was applied in solving the case numerically. Due to the axial symmetry of the problem, it is sufficient to select the computational domain as a 2000 m wide wedge with opening angle of 5 degrees. At the inner radial boundary wedge elements are used, while the rest of the domain is discretized using brick elements. The computation mesh is extensively refined at the location of the pumping well, and also at the location of the initial interface of seawater and freshwater as well as near the top and bottom of the domain. The characteristic element size varies between 0.5 m at the well and 25 m at the distant parts of the model. The total number of elements in the mesh is $34\ 000$ and the total number of nodes is $68\ 000$.

To model the pumping well, equidistant nodal sinks are placed at the top of the inner radial boundary. The pumping rate at the well is adjusted to produce the correct outflow rate at the inner boundary of the model,

$$Q_{out} = Q_w \times \frac{5^\circ}{360^\circ} = 33.3 \text{ m}^3/\text{d} \,. \tag{3.28}$$

The outflow rate is distributed uniformly along the 20 m long line of nodes.

The partial differential equation (3.22) describing groundwater flow was solved numerically employing the conventional Galerkin technique (Huyakorn & Pinder 1983), whereas the streamline-upwind/Petrov-Galerkin (SUPG) method (Brooks & Hughes 1992; Laitinen 1995) was applied for the transport equation (3.23). The Darcy velocity (3.25) for the transport equation was computed by taking directly the derivative of the computed finite element approximation for the pressure (3.22). The resulting matrix equations for the flow and transport equations were solved employing the conjugate-gradient and Gauss-Seidel methods (Atkinson 1988). The non-linear coupling of the equations is resolved using 200 Picard iterations with underrelaxation. A suitable relaxation parameter to ensure convergence was found to be $\omega = 0.08$. Time-steps are of the constant size of 5 days and total simulation time is approximately 4 years, comprising of 300 time-steps.

Results

Zhou et al. (2005) presented three different cases with regard to the dispersion parameters. For Case A they defined the longitudinal dispersivity $\varepsilon_L = 1$ m and, for Case B $\varepsilon_L = 0.2$ m and for Case C they used the value $\varepsilon_L = 10$ m. Only the upconing part of Cases A and C are simulated with FEFTRA. Case B is excluded since the extremely long period of time to be simulated would have reserved excessive amounts of computational resources.

The results are presented using a normalized mass-fraction as the primary quantity, defined as

$$C = \frac{c - c_{fw}}{c_{sw} - c_{fw}}, \tag{3.29}$$

where $c_{fw} = 0$ g/l is the TDS of freshwater and $c_{sw} = 35$ g/l is the TDS of the saline water.

When the FEFTRA results were checked against the ones computed with the FEAS code in the simulation of Case A, the contour line of 0.02 mass-fraction does not extend as close to the well along the inner radial boundary as in the reference results for time step 1 year (Figure 3.17). However, at 2 years, the 0.02 mass-fraction has already reached the pumping well at $z = 100$ m, which corresponds well with the reference result. At distances 20 m and 100 m from the inner boundary the FEFTRA distribution of mass-fraction compares almost identically with the FEAS code values (Figure 3.18). Similarly, in Case C (Figure 3.19), the salinity contour lines calculated with the FEFTRA and FEAS codes match very well. As a conclusion, all of the results compare well with the results obtained by Zhou et al. (2005), indicating good consistency between the two codes FEAS and FEFTRA.

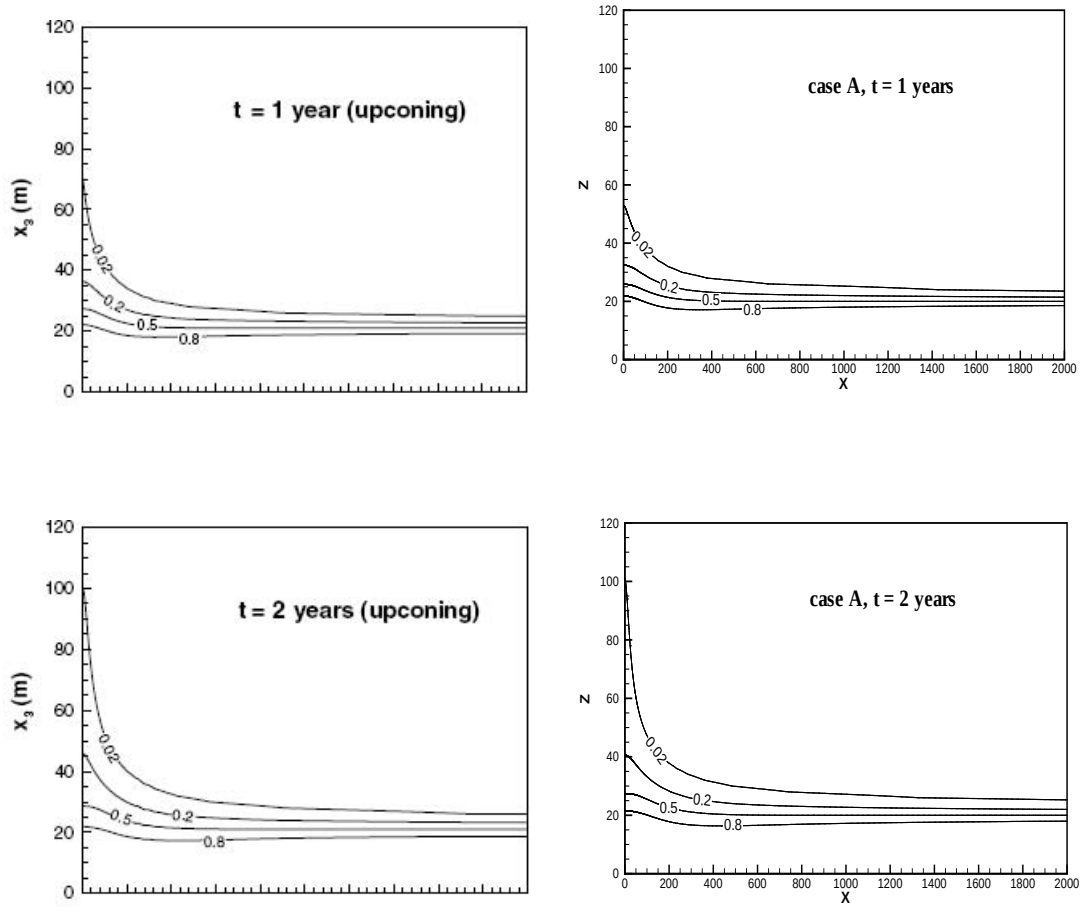

Figure 3.17. The computed mass-fraction distribution in Case A of the saltwater upconing problem. On the left, the reference results by Zhou et al. (2005); on the right, those computed with FEFTRA.

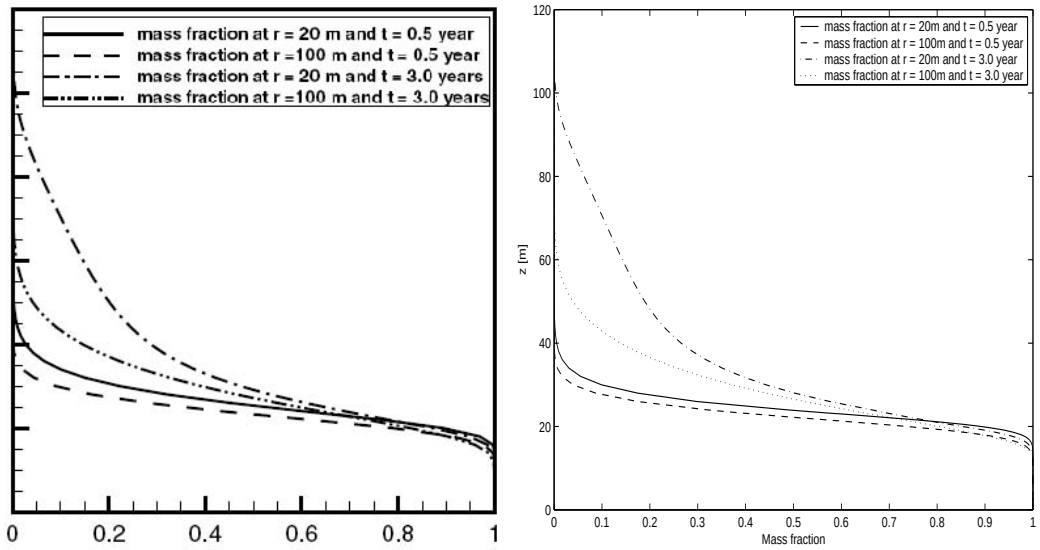

Figure 3.18. The computed mass fraction along vertical lines at two locations and time-steps in Case A of the saltwater upconing problem. On the left, reference results by Zhou et al. (2005); on the right, those computed with FEFTRA.

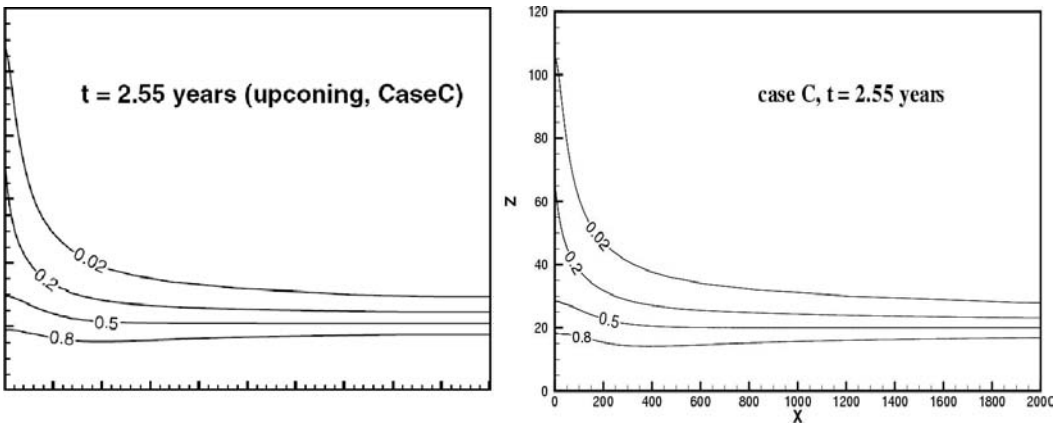

Figure 3.19. The computed mass-fraction distribution in Case C of the saltwater upconing problem. On the left, the reference results by Zhou et al. (2005); on the right, those computed with FEFTRA.

4. Heat transfer

The heat output of spent fuel will raise the temperature of the repository and the surrounding bedrock several tens of degrees. The temperature rise not only affects the chemical stability of the bentonite clay surrounding the disposal canisters but also may cause changes to flow conditions over distances of several hundred metres for many centuries. Thus, the simulation of heat transfer separately or coupled to flow constitute an important part of the ongoing repository design and safety assessment.

4.1 Heat transfer induced by repository

Rae & Robinson (1979) and Ratigan (1977) introduced simple test cases in which the repository-induced heat transfer in a homogeneous rock was considered. The cases are used to verify the capability of the FEFTRA code to simulate heat transfer by both conduction through rock and convection with flowing water. The test cases are located in the FEFTRA program path as follows:

- *feftra/solvit/t/temp/tt2DcondC* (Case 1: constant source)
- *feftra/solvit/t/temp/tt2DcondE* (Case 2: decaying source)
- *feftra/solvit/t/temp/tt2DcondEF* (Case 3: decaying source with imposed flow)

Definition of the problem

The case consists of a planar uniform repository located in an isotropic and homogeneous rock at a depth of 500 metres (Figure 4.1). The repository, which has the same properties as the surrounding rock, acts as a heat source, which raises temperature in the surroundings. The modelled region is comprised of a quadratic vertical cross section of size 3 km $\times$ 3 km with a line source representing the repository. Three different cases are considered. In two cases, the heat transfer mechanism is assumed to be conduction through rock induced by a constant (Case 1) and decaying (Case 2) source. In the third case a decaying source and a constant horizontal flow across the modelled region is assumed resulting in heat transfer by both conduction through rock and convection with flowing water.

Mathematical model

The equation for heat conduction is written in terms of temperature T [K] as (Carslaw & Jaeger 1959; Huyakorn & Pinder 1983; de Marsily 1986)

$$\nabla \cdot \left(\boldsymbol{\lambda} \nabla T\right) - \nabla \cdot \left(\rho c_w \boldsymbol{q} \nabla T\right) + H = \rho_r c_r \frac{\partial T}{\partial t}, \tag{4.1}$$

where $\boldsymbol{\lambda}$ is the thermal conductivity tensor of rock $[\mathrm{W/m/K}]$, $\boldsymbol{q}$ is the Darcy velocity $[\mathrm{m/s}]$, c_w is the specific heat of water $[\mathrm{J/kg/K}]$ H is the heat source $[\mathrm{W/m^3}]$, ρ_r is the

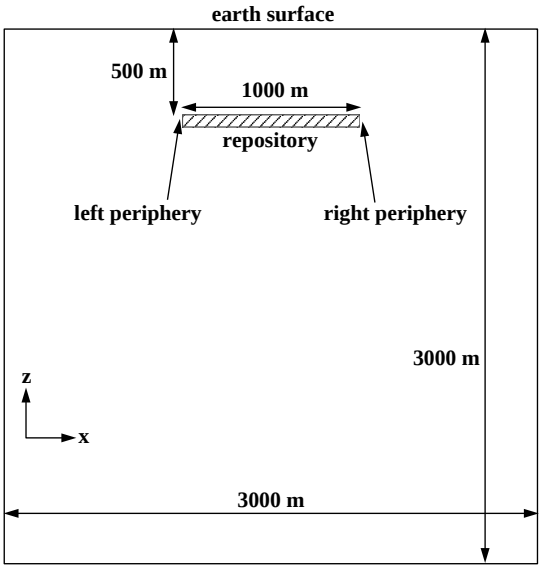

Figure 4.1. Schematic description of a test case with the repository induced heat transfer.

density of rock [$\mathrm{kg/m^3}$], c_r is the specific heat of rock [$\mathrm{J/kg/K}$] and t is time [s]. The second term in the left-hand side of Equation (4.1) represents the convective heat flux, which is not considered in Cases 1 and 2, assuming only conductive heat transfer.

The heat source H in Equation (4.1) is assumed to be as follows

$$H = \begin{cases} H_0 & \text{in Case 1} \\ H_0(0.882e^{\lambda_1 t} + 0.118e^{\lambda_2 t}) & \text{in Case 2 and 3,} \end{cases} \tag{4.2}$$

where H_0 is the initial heat power of the repository [$\mathrm{W/m^3}$], and λ_1 and λ_2 are the decay coefficients [$1/\mathrm{s}$].

The prescribed zero temperature rise is applied on the earth surface and no heat flow on other boundaries. The input parameter values are given in Table 4.1.

Table 4.1. Input parameters for the repository-induced heat transfer case.

Symbol	*Parameter*	*Equation*	*Value*
λ	Thermal conductivity of rock	4.1	2.05 W m^{-1} K^{-1}
ρ_r	Density of rock	4.1	2800 kg m^{-3}
c_r	Specific heat of rock	4.1	735 J kg^{-1}K^{-1}
c_w	Specific heat of water	4.1	4180 J kg^{-1}K^{-1}
H_0	Initial heat power of the repository	4.2	5.25 W/m^3
λ_1	Decay coefficient of heat power (Case 2 and 3)	4.2	$7.3 \cdot 10^{-10}$ s^{-1}
λ_2	Decay coefficient of heat power (Case 2 and 3)	4.2	$4.4 \cdot 10^{-11}$ s^{-1}
q_x	Darcy velocity in x-direction (Case 3)	4.1	$2.0 \cdot 10^{-9}$ m/s
q_y	Darcy velocity in y-direction	4.1	0.0 m/s
q_z	Darcy velocity in z-direction	4.1	0.0 m/s

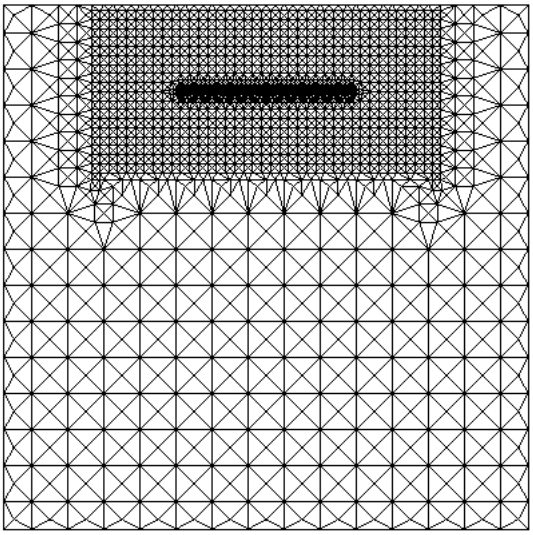

Figure 4.2. Finite element mesh with 3200 elements and 6400 nodes.

Numerical solution method

The finite element method with linear elements was applied in solving the case numerically. The modelled volume was discretised into mesh with 3 200 triangular (rock) and line (repository) elements (Figure 4.2). The mesh was refined near the repository so that the smallest elements were of an order of 5 metres. In Case 1 (constant source), the simulation period was discretised into 45 time steps, while 93 steps were applied in Cases 2 and 3 (decaying source with and without imposed flow).

The partial differential equation (4.1) describing heat transfer was solved numerically employing the conventional Galerkin technique (Huyakorn & Pinder 1983). The fully implicit difference scheme was applied in the time discretisation for Equation (4.1). The mass matrix resulting from the transient finite element formulation of Equation (4.1) was formed by a diagonalisation procedure known as "lumping" (Huyakorn & Pinder 1983), which gives a more stable solution to practical problems than a "consistent" matrix. Finally, the linear matrix equation was solved employing the conjugate-gradient method (Atkinson 1988).

Results

The simulated temperature rises were compared against the analytical and numerical solutions given by Rae & Robinson (1979) at the repository centre and peripheries. The numerical comparison values were calculated with the NAMMU program package. The results as a function of time are presented in Figure 4.3, which shows a good agreement between FEFTRA and other solutions.

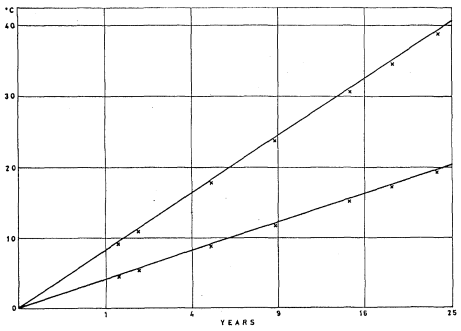

(a) Analytical and NAMMU: case 1.

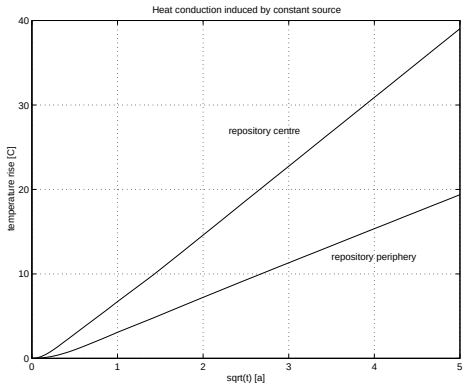

(b) FEFTRA: case 1.

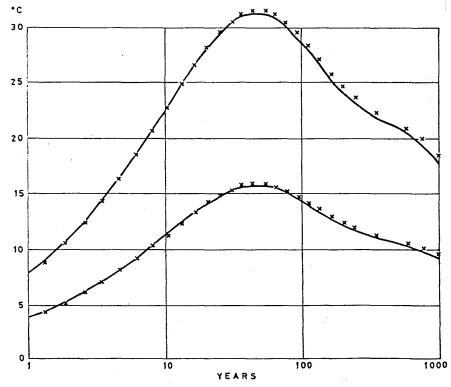

(c) Analytical and NAMMU: case 2.

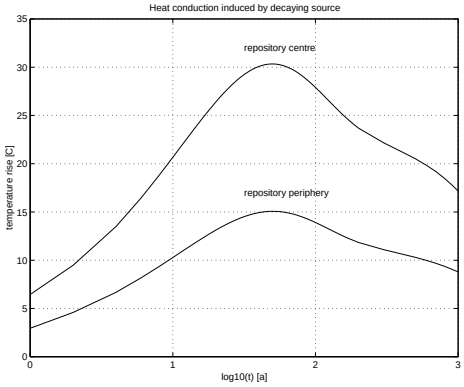

(d) FEFTRA: case 2.

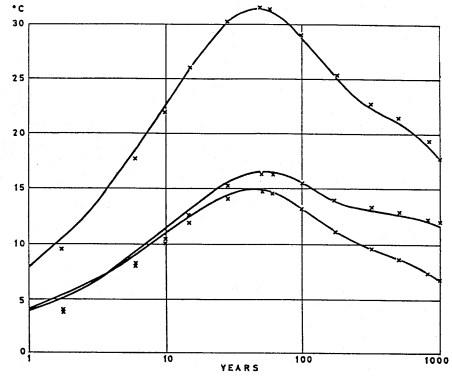

(e) Analytical and NAMMU: case 3.

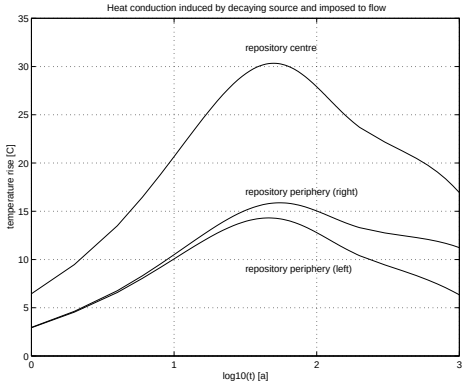

(f) FEFTRA: case 3.

Figure 4.3. Analytical and computed temperature rises as a function of time at the repository centre and peripheries in Case 1 (constant source), Case 2 (decaying source) and Case 3 (decaying source with flow). The analytical (crosses) and numerical (NAMMU, solid) comparison values on the left were taken from Rae & Robinson (1979).

4.2 Heat conduction in an anisotropic medium

The thermal properties of bedrock surrounding the disposal canisters are essential factors in the repository design. The geological field investigations in the boreholes at the Olkiluoto site have indicated that the thermal conductivity tends to be dependent on the direction of measurement. The anisotropic nature of conductivity results from anisotropic structures of rock such as foliation and layering, which prevent heat to transfer as effectively perpendicular to the structures as it does parallel to the structures.

Carslaw & Jaeger (1959) presented analytical solutions for various heat conduction problems. The case with a continuous point source is employed to verify the capability of FEFTRA for anisotropic heat conduction problems. For comparison, an isotropic case is considered too. The test cases are located in the FEFTRA program path as follows:

- *feftra/solvit/temp/tt3DcontPa* (anisotropic case)
- *feftra/solvit/temp/tt3DcontP* (isotropic case)

Definition of the problem

The problem is comprised of a point source, which releases heat at a constant rate per unit time resulting in temperature rise in an infinite, anisotropic porous rock (Carslaw & Jaeger 1959). The thermal conductivities were assumed to be different along each principal direction located parallel to the global coordinate axes. The time period to be considered starts from the release of heat and continues up to 70 days onward.

Mathematical model

The equation governing heat conduction in a porous medium is based on the law of conservation of energy; it can be written in terms of the temperature T [K] as follows (Carslaw & Jaeger 1959; Huyakorn & Pinder 1983; de Marsily 1986):

$$\nabla \cdot \left(\boldsymbol{\lambda} \nabla T\right) + H = \rho c \frac{\partial T}{\partial t}, \tag{4.3}$$

where $\boldsymbol{\lambda}$ is the thermal conductivity tensor of medium [$\mathrm{W/m/K}$], H is the internal heat source [$\mathrm{W/m^3}$], ρ is the density of the medium [$\mathrm{kg/m^3}$], and c is the specific heat of the medium [$\mathrm{J/kg/K}$]. The first term in the left-hand side of Equation (4.3) represents conductive heat flux to or from the system, while the right-hand side describes the temporal change in the heat content.

The thermal conductivity tensor $\boldsymbol{\lambda}$ in Equation (4.3), which takes into account the anisotropy of the medium, is expressed as

$$\boldsymbol{\lambda} = \boldsymbol{A}^T \boldsymbol{\lambda'} \boldsymbol{A}, \tag{4.4}$$

where

$$\boldsymbol{\lambda'} = \begin{pmatrix} \lambda_{x'} & 0 & 0 \\ 0 & \lambda_{y'} & 0 \\ 0 & 0 & \lambda_{z'} \end{pmatrix} \tag{4.5}$$

is a diagonal matrix including the thermal conductivities $\lambda_{x'}, \lambda_{y'}, \lambda_{z'}$ [$\mathrm{W/m/K}$] along the principal directions (x', y', z') rotated from the global coordinate system (x, y, z). $\boldsymbol{A}$ is a general rotation matrix, which transforms the conductivities along the principal directions to the global coordinate system. Thus, the consideration of an arbitrary directed anisotropic thermal conductivity requires the knowledge of six different parameters: the conductivities along the principal directions $\lambda_{x'}, \lambda_{y'}, \lambda_{z'}$ and the corresponding Euler's angles (α, β, γ). However, if the principal axes (x', y', z') are parallel to the global coordinate axes (x, y, z) the Euler's angles are zero and the global conductivity matrix (4.4) reduces to the diagonal matrix (4.5) (Löfman 2001).

The thermal properties of bedrock and the heat source are presented in Table 4.2. The properties of the rock were based on the averages of the measurements of Olkiluoto mica gneiss at the temperature of 60 °C (Kukkonen 2000). The conductivities along the principal directions were modified from an average value. The heat power of the point source was assumed to be approximately the power of one disposal canister for the fuel of burnup of 35 $\mathrm{MWd/kg}$ after cooling for 30 years (Raiko 1996).

Numerical solution method

Due to the symmetry of the case, only 1/8 of the volume around the point source was included into the model of cubic shape (Figure 4.4). The length of the edges of the cube were chosen to be 10 metres, which was sufficient considering the short duration (70 days) of the simulation. No heat is assumed to transfer through the faces of the cube. The modelled volume was discretised into mesh with 3400 linear hexaedral elements (Figure 4.4), while the simulation period was discretised into 31 time steps.

Table 4.2. The thermal properties of rock at the temperature of 60 °C (Kukkonen 2000) and the heat power in the test case with continuous point source. The conductivity of 2.61 $\mathrm{W/m/K}$ *is used for the isotropic case.*

Symbol	Parameter	Equation	Value
$\lambda_{x'}$	Thermal conductivity along the principal axis x'	4.5, 4.6	3.61 $\mathrm{W/m/K}$
$\lambda_{y'}$	Thermal conductivity along the principal axis y'	4.5, 4.6	2.61 $\mathrm{W/m/K}$
$\lambda_{z'}$	Thermal conductivity along the principal axis z'	4.5, 4.6	1.61 $\mathrm{W/m/K}$
ρ_r	Density of rock	4.3	2749 $\mathrm{kg/m^3}$
c_r	Specific heat of rock	4.3	784 $\mathrm{J/kg/K}$
P	Power of heat source	4.3, 4.6	1600 W
(x_0, y_0, z_0)	Location of heat source	4.6	(0, 0, 0)

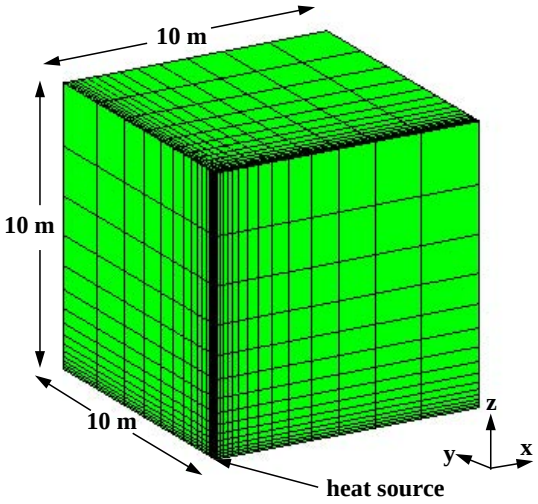

Figure 4.4. Finite element mesh with 3375 elements in the test case with continuous point source.

The partial differential equation (4.3) describing the heat conduction was solved numerically employing the conventional Galerkin technique (Huyakorn & Pinder 1983), and the fully implicit difference scheme for the time discretization. The mass matrix resulting from the transient finite element formulation of the heat conduction equation was formed by a diagonalization procedure known as "lumping" (Huyakorn & Pinder 1983), which gives a more stable solution in practical problems than a "consistent" matrix. Finally, the resulting linear matrix equation is solved employing the conjugate-gradient method (Atkinson 1988).

Results

The simulated values were compared against the analytical solution provided by Carslaw & Jaeger (1959) as follows

$$T(x,y,z,t) = \frac{P}{4\pi\sqrt{\lambda_{y'}\lambda_{z'}(x-x_0)^2+\lambda_{x'}\lambda_{z'}(y-y_0)^2+\lambda_{x'}\lambda_{y'}(z-z_0)^2}} \cdot$$

$$\mathrm{erfc}\sqrt{\frac{\rho_r c_r}{4t}\left(\frac{(x-x_0)^2}{\lambda_{x'}}+\frac{(y-y_0)^2}{\lambda_{y'}}+\frac{(z-z_0)^2}{\lambda_{z'}}\right)}, \qquad (4.6)$$

where P is the power of the heat source $[W]$, (x_0, y_0, z_0) is the location of the point heat source $[\mathrm{m}]$, and erfc is the complementary error function (Zwillinger 1996).

The results at the distance of 0.88 metres from the source as a function of time and after 37 days as a function of distance from the source are presented in Figures 4.5 and 4.6, which show that the numerically computed temperatures compare well with the analytical solutions both in the isotropic and anisotropic cases.

.

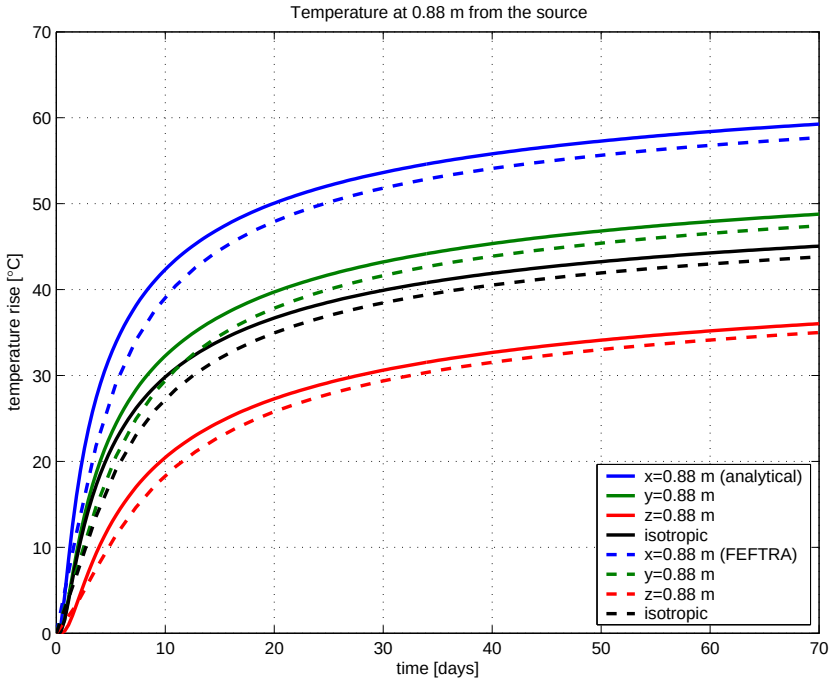

Figure 4.5. Temperature at the distance of 0.88 metres from the source in the test case with continuous point source.

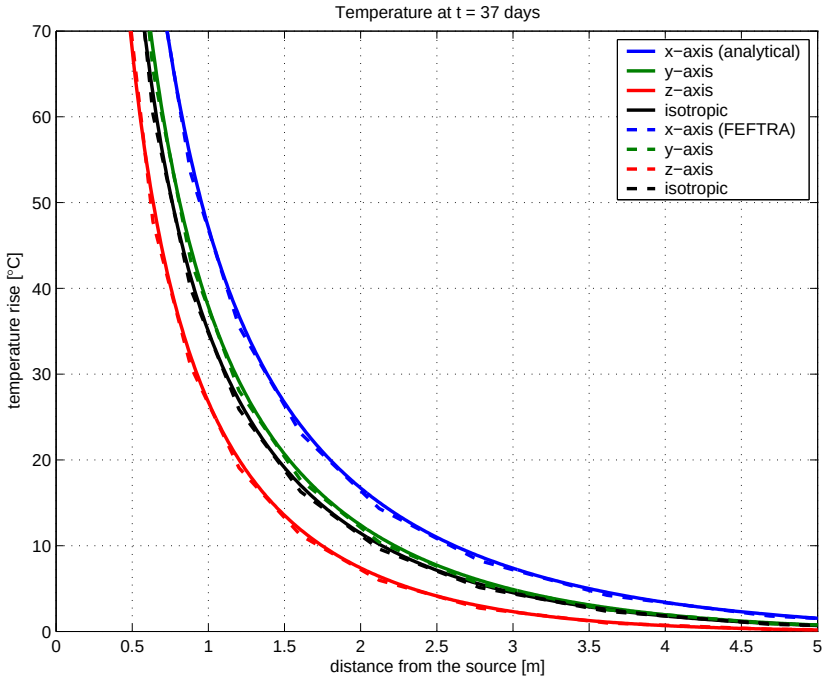

Figure 4.6. Temperature at 37 days in the test case with continuous point source.

4.3 Heat conduction induced by disposal canister

The spent nuclear fuel will be encapsulated in final disposal canisters made of cast iron enclosed in a copper shell. The canisters will be emplaced in holes drilled at the bottom of the repository tunnels. The canisters are surrounded with bentonite clay, which expands when it absorbs water. The clay not only prevents direct groundwater flow to the surface of the canister, but also protects the canister against minor bedrock movements. In order to guarantee the chemical stability of the bentonite, one of the basic design requirements for the repository is that the surface temperature of the disposal canisters will not be allowed to exceed a limit of 100 °C. The heat production of spent nuclear fuel will raise the temperature of the canisters and the surrounding bedrock several tens of degrees. Thus, in order to avoid too high temperatures in the bentonite layer the thermal analyses of the canisters is an important part of the repository design.

This case is employed to verify the capability of the FEFTRA code to simulate detailed canister-scale heat conduction problems required in the repository design. The case is located in *feftra/solvit/temp/tt3Dcanister* in the FEFTRA program path.

Definition of the problem

The case is comprised of one disposal canister surrounded by a bentonite clay layer (Figure 4.7), and located in an infinite porous rock with an isotropic and homogeneous properties. The canister acts as a cylindrical and exponentially decreasing heat source, which raises temperature in the canister, bentonite and surrounding bedrock. The real disposal canister consists of a cast iron insert with an outer shell of copper. Because the thermal conductivity of the metal canister is two orders of magnitude higher than the surrounding bentonite and rock, the canister will be practically at a uniform temperature and all the thermal gradients will prevail in the bentonite and rock around the canister. Thus, the canister can be assumed to be homogeneous in the simulations. The period to be considered starts from the moment of disposal and continues up to 20 years onward.

Mathematical model

The equation governing heat conduction in a porous medium is based on the law of conservation of energy; it can be written in terms of the temperature T [K] as follows (Carslaw & Jaeger 1959; Huyakorn & Pinder 1983; de Marsily 1986)

$$\nabla \cdot \big(\boldsymbol{\lambda} \nabla T\big) + H = \rho c \frac{\partial T}{\partial t}, \tag{4.7}$$

where $\boldsymbol{\lambda}$ is the thermal conductivity tensor of medium [$\mathrm{W/m/K}$], H is the internal heat source [$\mathrm{W/m^3}$], ρ is the density of medium [$\mathrm{kg/m^3}$], and c is the specific heat of medium [$\mathrm{J/kg/K}$]. The first term in the left-hand side of Equation (4.7) represents conductive heat flux to or from the system, while the right-hand side describes the temporal change in the heat content.

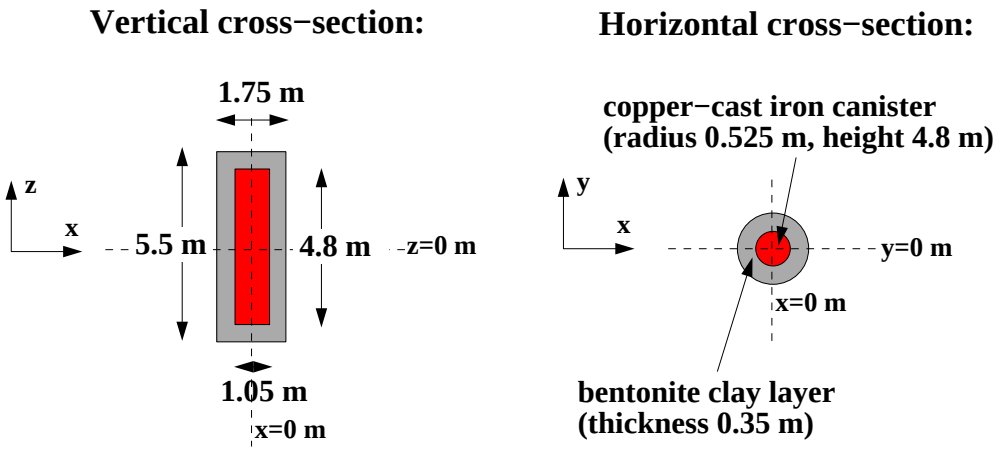

Figure 4.7. Schematic description of the test case with one disposal canister. The boundaries of the cubic-shaped model are located at a distance of 100 metres from the mid-point of the canister. The dimensions of the canister are based on Raiko (1996) and Raiko & Salo (1999).

The thermal conductivity tensor $\boldsymbol{\lambda}$ in Equation (4.7) is a diagonal matrix

$$\boldsymbol{\lambda} = \begin{pmatrix} \lambda & 0 & 0 \\ 0 & \lambda & 0 \\ 0 & 0 & \lambda \end{pmatrix}, \tag{4.8}$$

in which λ is the isotropic thermal conductivity $[\mathrm{W/m/K}]$.

The thermal properties of the canister were assumed to be those of copper, while the properties of rock were based on the averages of the measurements of Olkiluoto mica gneiss at the temperature of 60 °C (Kukkonen 2000). The saturation of the bentonite clay around the canister varies depending on the heat of the canisters and the supply of water in the surrounding rock. The thermal conductivity varies with saturation and can be nearly twice as high in a fully saturated bentonite than in the dry one. However, as the degree of saturation is very uncertain, a conservative assumption was made and the properties of dry bentonite were employed in this work (Raiko 1996; Ageskog & Jansson 1999). The thermal properties of the canister, bentonite clay and rock, as well as the dimensions of the canister, are presented in Table 4.3.

The heat generation of the disposal canister depends on the amount, burnup and cooling time of the fuel. In this study, the cooling time of 30 years was assumed, and an exponentially decreasing fit for the heat power of one canister was constructed on the basis of the computations on the heat output of spent nuclear fuel of burnup of 35 $\mathrm{MWd/kg}$ during the period between 20 and 200 years of cooling time (Raiko 1996). The fit is defined (as years after disposal) by

$$P(t) = 2319e^{-0.0245t} + 620.7e^{-0.0028t},\ -10 \leq t \leq 170 \text{ years after disposal}, \tag{4.9}$$

which is presented with the corresponding data points in Figure 4.8.

Table 4.3. The thermal properties of the canister, bentonite clay around the canister and rock in the test case with one disposal canister.

Symbol	Parameter	Equation	Value
λ_c	Thermal conductivity of the canister (copper)	4.8	380 $\mathrm{W/m/K}$
ρ_c	Density of the canister (copper)	4.7	8930 $\mathrm{kg/m^3}$
c_c	Specific heat of the canister (copper)	4.7	390 $\mathrm{J/kg/K}$
r_c	Diameter of the canister		1.05 m
h_c	Height of the canister		4.8 m
λ_b	Thermal conductivity of the bentonite clay	4.8	0.75 $\mathrm{W/m/K}$
$\rho_b c_b$	Heat capacity of the bentonite clay	4.7	2.2 $\mathrm{MJ/m^3/K}$
d_b	Thickness of the bentonite clay		0.35 m
λ_r	Thermal conductivity of rock	4.8	2.61 $\mathrm{W/m/K}$
ρ_r	Density of rock	4.7	2749 $\mathrm{kg/m^3}$
c_r	Specific heat of rock	4.7	784 $\mathrm{J/kg/K}$

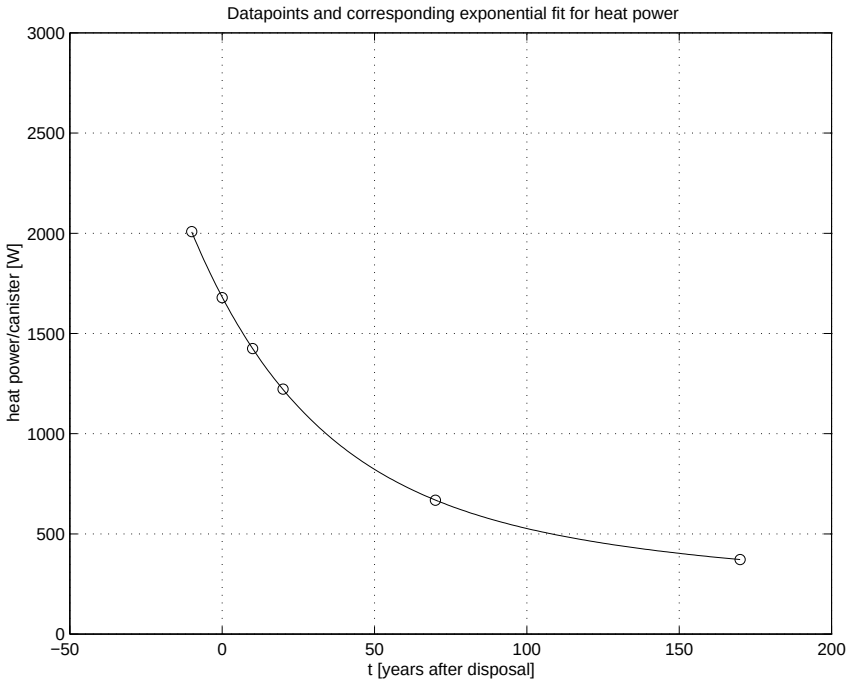

Figure 4.8. An exponential fit for heat power of one disposal canister for the fuel of burnup of 35 $\mathrm{MWd/kg}$ *based on the data by Raiko (1996) during the period between 20 and 200 years of cooling time (i.e. between -10 and 170 years after disposal).*

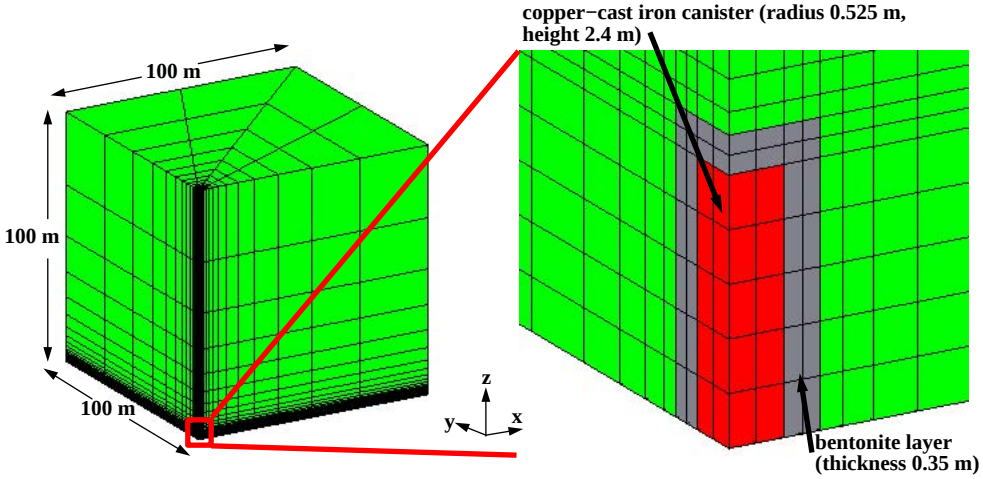

Figure 4.9. Finite element mesh with 1584 elements in the case with one disposal canister. Due to symmetry the mesh contains only 1/8 of modelled volume (see Figure 4.7).

Numerical solution method

Due to the symmetry of the case, only 1/8 of the volume around the mid-point of the canister was included into the model of the cubic shape (Figure 4.9). As the simulation was carried out from the moment of disposal to up to 20 years onward, the length of the edges of the cube was chosen to be 100 metres, which is far enough from the canister not to have any effect on the temperature distribution in the model during the simulation period. No heat is assumed to transfer through the boundaries of the model. The modelled volume was discretised into mesh with 1600 linear hexaedral elements (Figure 4.9), while the simulation period was discretised into 45 time steps.

The partial differential equation (4.3) describing the heat conduction was solved numerically employing the conventional Galerkin technique (Huyakorn & Pinder 1983), and the fully implicit difference scheme for the time discretization. The mass matrix resulting from the transient finite element formulation of the heat conduction equation was formed by a diagonalization procedure known as "lumping" (Huyakorn & Pinder 1983), which gives a more stable solution in practical problems than a "consistent" matrix. Finally, the resulting linear matrix equation is solved employing the conjugate-gradient method (Atkinson 1988).

Results

The simulated values were compared against the analytical solution given by the analytical REPTEM code (Hautojärvi et al. 1987; Carslaw & Jaeger 1959). The results in the canister as well as in rock at a distance of 1.8 and 12.3 metres from the centre of the canister are presented in Figure 4.10, from which a good agreement is observed between the numerical and analytical solution. Small discrepancies can be attributed to the different fit in the analytical and numerical models for the heat power. In addition, differences be-

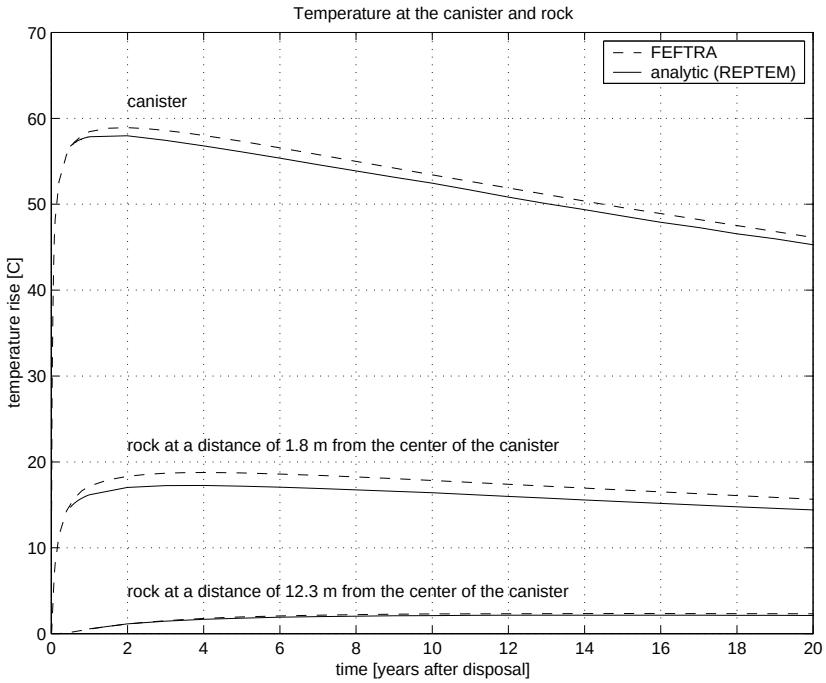

Figure 4.10. Temperature at the canister and rock in the test case with one canister.

tween the line source model employed in the REPTEM code for the canister and the fully three-dimensional canister model employed in the FEFTRA code may have some effects on the results, although the surface area of the canister in both models has been adjusted to correspond to each other.

4.4 Thermally induced groundwater flow in a saturated permeable medium

The heat output of spent nuclear fuel will raise the temperature of the repository and the surrounding bedrock several tens of degrees, which may cause changes to the flow conditions over distances of several hundred metres for many centuries. Although the effects of temperature rise can usually be considered to be short-term, there are situations that require the estimation of the phenomenon. The international Hydrologic Code Intercomparison project (HYDROCOIN 1988) introduced a test case (Level 1, Case 4), in which thermally induced groundwater flow in a saturated permeable medium was considered. The case is used to verify the capability of the FEFTRA code to simulate buoyancy-driven groundwater flow coupled with heat transfer. The test case is located in the FEFTRA program path as follows:

- *feftra/solvit/t/press_temp/tpt_hydrocoin_l1c4* (base case)
- *feftra/solvit/t/press_temp/tpt_hydrocoin_l1c4s* (coarse mesh)
- *feftra/solvit/t/temp/tt_hydrocoin_l1c4s* (coarse case with temperature only)

Definition of the problem

The case consists of a spherically idealised uniform repository located in an infinite rock with isotropic and homogeneous properties (Figure 4.11). The repository, which has the same properties as the surrounding rock, acts as an exponentially decaying heat source, which raises the temperature in the surroundings. Due to low permeability of the rock, the effect of convection with flowing water was considered insignificant, and the dominant heat transfer mechanism could be assumed to be conduction through rock. The temporal variations of the flow field were assumed to follow solely from the time-dependent heat output of the repository. In addition, the density of water was assumed to be dependent on temperature, whereas constant viscosity and the thermal expansion coefficient of water were applied.

Mathematical model

The flow equation is written for the residual pressure p_r [Pa] (the total pressure without the hydrostatic component of freshwater) as follows (Bear 1979; Huyakorn & Pinder 1983; de Marsily 1986)

$$\nabla \cdot \left(\frac{\rho \boldsymbol{k}}{\mu} \big(\nabla p_r + (\rho - \rho_0) g \nabla z \big) \right) = 0, \tag{4.10}$$

where ρ is the density of water [$\mathrm{kg/m^3}$], ρ_0 is the density of the freshwater [$\mathrm{kg/m^3}$], $\boldsymbol{k}$ is the permeability tensor of rock [$\mathrm{m^2}$], μ is the dynamic viscosity of water [$\mathrm{kg/m/s}$], g is the gravitational acceleration (= 9.81 $\mathrm{m/s^2}$), and z is the elevation relative to the sea level [m]. The flow equation (4.10) was written in a steady-state form, because the temporal variations of the flow field were assumed to follow solely from the heat output of the repository.

The equation for heat conduction is written in terms of temperature T [K] as (Carslaw & Jaeger 1959; Huyakorn & Pinder 1983; de Marsily 1986)

$$\nabla \cdot \big(\boldsymbol{\lambda} \nabla T \big) + H = \rho_r c_r \frac{\partial T}{\partial t}, \tag{4.11}$$

where $\boldsymbol{\lambda}$ is the thermal conductivity tensor of rock [$\mathrm{W/m/K}$], H is the heat source [$\mathrm{W/m^3}$], ρ_r is the density of rock [$\mathrm{kg/m^3}$], c_r is the specific heat of rock [$\mathrm{J/kg/K}$] and t is time [s].

The heat source H in Equation (4.11) is assumed to decay exponentially as

$$H = \frac{3 W_0}{4 \pi r^3} e^{\lambda t}, \tag{4.12}$$

where W_0 is the initial heat power of the repository, r is the radius of the sphere representing the repository and λ is the decay constant of the heat power.

Table 4.4. Input parameters for the HYDROCOIN Level 1, Case 4 (HYDROCOIN 1988).

Symbol	*Parameter*	*Equation*	*Value*
$\boldsymbol{k}$	Permeability of rock	4.10	10^{-16} m^2
λ	Thermal conductivity of rock	4.11	2.51 W m^{-1} K^{-1}
ρ_r	Density of rock	4.11	2600 kg m^{-3}
c_r	Specific heat of rock	4.11	879 J kg^{-1}K^{-1}
ρ_0	Density of freshwater	4.10, 4.13	992.2 kg m^{-3}
β	Thermal expansion coefficient of water	4.13	$3.85 \cdot 10^{-4}$K^{-1}
μ	Dynamic viscosity of water	4.10	$6.529 \cdot 10^{-4}$ kg m^{-1}s^{-1}
r	Radius of the sphere (repository)	4.12	250 m
W_0	Initial heat power of the repository	4.12	10 MW
λ	Decay constant of heat power	4.12	$7.3215 \cdot 10^{-10}$ s $^{-1}$

Equations (4.10) and (4.11) are coupled with the density of water ρ, which is dependent on temperature T as follows

$$\rho = \rho_0 + \rho_0 \beta T, \tag{4.13}$$

where β is the thermal expansion coefficient of water.

Initially, both residual pressure and temperature are assumed to be zeros in the repository and rock. The input parameter values are given in Table 4.4.

Numerical solution method

The finite element method with linear elements was applied in solving the case numerically. Due to the symmetry of the case, it was not necessary to consider the whole sphere, but only the vertical slice of the angle of 12.5° was included into the model (Figure 4.11). As the repository was assumed to locate in an infinite rock, the radius of the vertical slice was chosen to be 7000 metres, which was considered to be far enough to avoid the boundary conditions having an effect on the results during the simulation period of 10000 years. Neither heat nor water was assumed to transfer through the boundaries of the model. The modelled volume was discretised into mesh with 5900 tetrahedral and hexahedral elements (Figure 4.11), while the simulation period was discretised into 104 time steps.

The partial differential equations (4.10) and (4.11) describing flow and heat conduction were solved numerically employing the conventional Galerkin technique (Huyakorn & Pinder 1983). The fully implicit difference scheme was applied in the time discretisation for Equation (4.11). The mass matrix resulting from the transient finite element formulation of Equation (4.11) was formed by a diagonalisation procedure known as "lumping" (Huyakorn & Pinder 1983), which gives a more stable solution in practical problems than a "consistent" matrix. Finally, the linear matrix equations resulting from the finite element formulation of Equations (4.10) and (4.11) were solved, employing the conjugate-gradient method (Atkinson 1988).

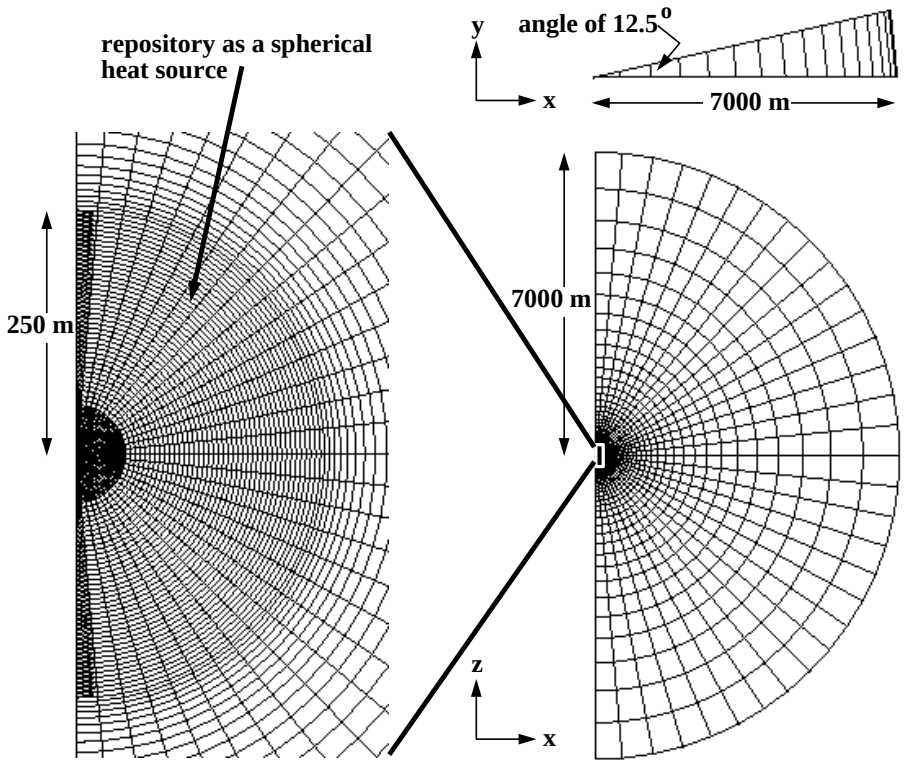

Figure 4.11. Finite element mesh for the HYDROCOIN Level 1 Case 4 (5900 elements, 4300 nodes).

Results

The simulated pressure and temperature rises were compared against the analytical solutions given in HYDROCOIN (1988) on the vertical centreline ($x = 0$, $y = 0$) of the sphere. The results as a function of time between 1 and 10000 years for $z = 0$, 125, 250 and 375 metres and as a function of distance between $z = 0$ and $z = 750$ metres for times of 50, 100, 500 and 1000 years are presented in Figures 4.12 and 4.13, which show an excellent agreement between FEFTRA and analytical solutions.

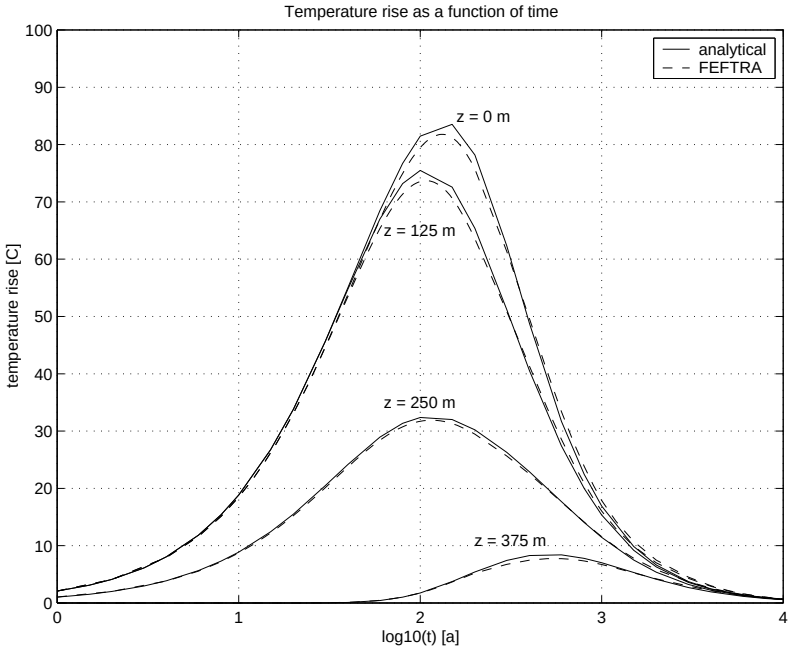

(a) Temperature rise as a function of time at four points on the vertical centreline of the sphere.

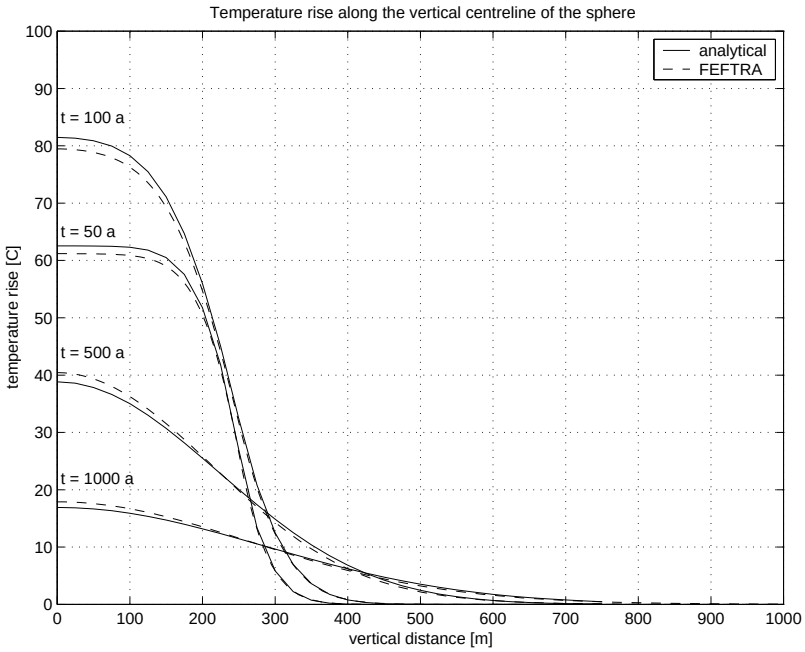

(b) Temperature rise as a function of vertical distance at four points in time.

Figure 4.12. Temperature rises as a function of time and distance. Analytical values taken from HYDROCOIN (1988).

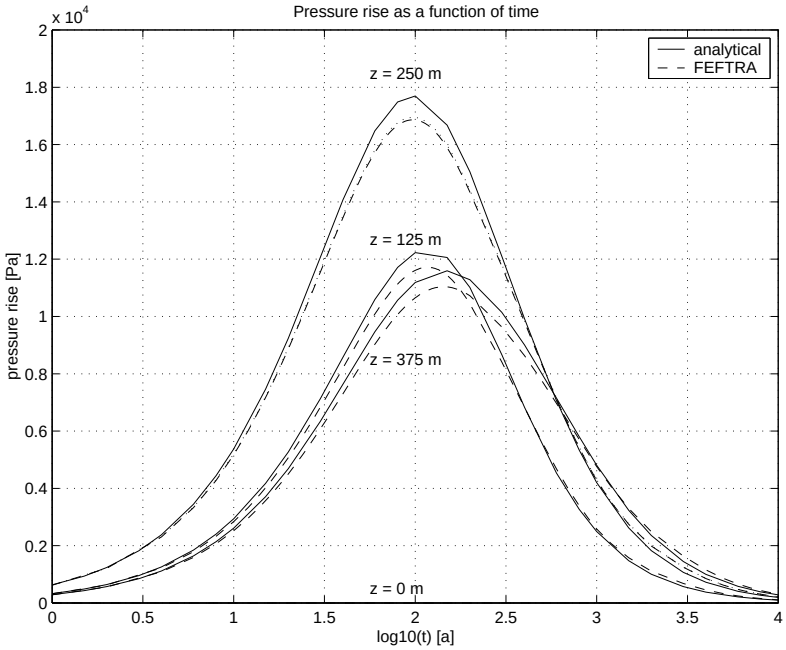

(a) Pressure rise as a function of time at four points on the vertical centreline of the sphere.

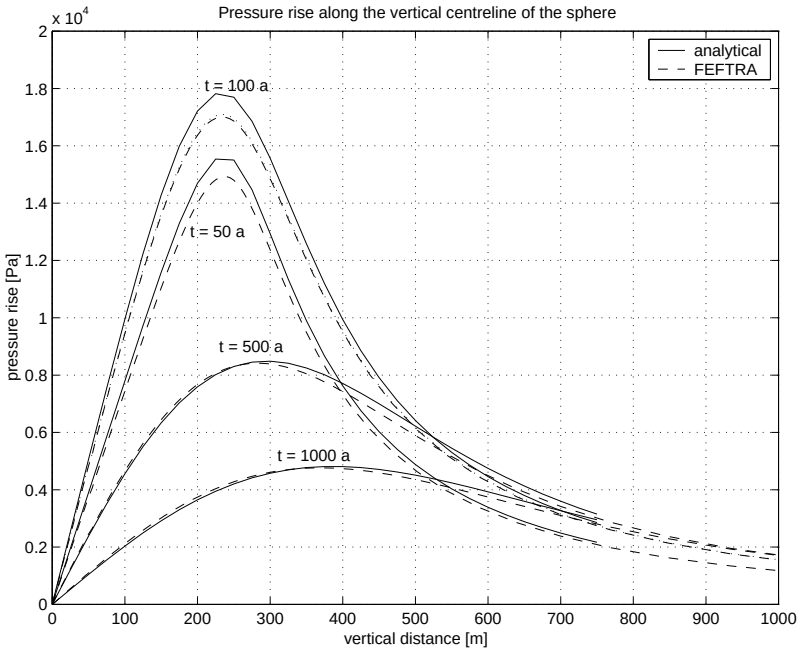

(b) Pressure rise as a function of vertical distance at four points in time.

Figure 4.13. Pressure rises as a function of time and distance. Analytical values taken from HYDROCOIN (1988).

5. Summary

FEFTRA is a finite element program package developed at VTT for groundwater flow analyses in the site investigation programme seeking for a final repository of spent nuclear fuel. The code is capable of modelling steady-state or transient groundwater flow, solute transport and heat transfer as coupled or separate phenomena. Being a typical research tool used only by its developers, the FEFTRA code has so far been short of a competent testing system and a precise documentation of the verification of the code.

The objective of this work was to reorganise all the material related to the existing verification cases and place them into the FEFTRA program path under the version control system. The work also included a development of a new testing system, which automatically computes the selected cases, checks the new results against the old approved results (i.e. the results that have been compared with analytic or other numerical results) and constructs a summary of the test run. All the existing cases were gathered together, checked and added into the new testing system. The documentation of each case was rewritten and added into the system in a way that the whole test documentation (this report) can easily be generated with one command in a postscript or pdf-format. The report is available both in a printed and electronic format. As the report is in a constant state of evolution resulting from the current code development, the printed form represents a "snapshot" of its content at the date of publishing, while the electronic format represents always the most up-to-date version of the report.

At the moment the report includes mainly the cases related to the testing of the primary result quantities (i.e. hydraulic head, pressure, salinity concentration, temperature). The selected cases, however, represent typical hydrological applications in which the program package has been employed in the Posiva site evaluation programme.

Groundwater flow

The simplest cases related to groundwater flow with constant density were comprised of steady-state and transient flow problems in a homogeneous and fractured bedrock. The cases with a radial steady-state (Section 2.1) and transient (Section 2.2) flow in a homogeneous and isotropic discoid structure were the simplest problems and they were selected to verify the use of various types of elements and boundary conditions (flow rates and fluxes) in 2D and 3D. The modelling of transient pumping tests was considered with the case (Section 2.3) in which the pumping of water results in a flow from the borehole to a single fracture and rock matrix. In all cases the FEFTRA results compared well with the analytical solutions (Figures 2.3, 2.5, 2.8(a) and 2.8(b)).

The problem (Section 2.4) concerning a steady-state flow in a two-dimensional slice of a fractured bedrock intersected by two hydrogeological zones was introduced to verify the code for heterogeneous flow problems with large permeability contrasts. The case, which is an idealisation of the hydrogeological conditions at a potential site for a deep repository in bedrock, was also employed to assess the performance of different representations of

zones in the finite element mesh. The representation of rock matrix and zones by uniform dimensional elements were compared to the two approaches, in which the elements of different dimensions can be used in the same mesh, i.e. 1D (2D) elements for zones and 2D (3D) elements for rock matrix. The computed results showed a good agreement between the FEFTRA and other numerical results. The results proved also that the representation of the zones by lower dimensional elements is a feasible and efficient alternative to the use of uniform dimensional elements

The study by Hartley et al. (2002) consisted of a site-scale model testing, in which a steady-state groundwater flow in 3D was computed with NAMMU and FEFTRA program packages for the Olkiluoto site and the results compared. In this work, the case was documented and examined with regard to the modelling performed with FEFTRA (Section 2.7). The result quantities computed in the test case were pressure along the boreholes KR1-KR5, flow paths starting at three points near the repository, flow rates through a box surrounding the repository and infiltration. Pressure (Figure 2.26), flow rates (Table 2.16), infiltration and the final positions and lengths of the flow paths (Table 2.17 and Figure 2.27) showed an excellent agreement between the FEFTRA and NAMMU models. On the other hand, the travel times of the flow paths computed with FEFTRA were shorter than the corresponding NAMMU times, which can probably be attributed to the different representations of the hydrogeological zones and/or different discretisation in the vicinity of the repository. However, the case verified further the capability of the FEFTRA code to simulate real-life site-scale groundwater flow problems employing 2D elements for the zones in the 3D mesh.

The underground rock characterization facility ONKALO, which is currently being excavated in the bedrock of Olkiluoto, will constitute hydraulic disturbances to the site's groundwater system. In particular, an inflow of groundwater into the open tunnels may cause a drawdown of the groundwater table. The FEFTRA code employs a free surface approach to simulate the water table drawdown and its recovery back to the undisturbed conditions. The code's free surface approach was verified with two test cases. In the first, a pumping at a horizontal well in an unconfined aquifer results in the water table drawdown (Section 2.5), whereas the Mariño's experiment considers the growth and decay of a groundwater ridge caused by the infiltration (Section 2.6). In the horizontal well case, the results were evaluated with the semianalytical solution (Zhan & Zlotnik 2002), which compared very well with the one from FEFTRA (Figure 2.16 and Figure 2.17). Only at the beginning of the simulation did the results differ slightly in the immediate vicinity of the well; this was because the semianalytical solution is prone to errors close to strong sinks. The Mariño's experiment was realized with FEFTRA as 2D and 3D simulations, and results were compared with the analytical solution (Ségol 1994). In the 2D case the results are well in line with the analytical solution (Figure 2.20). In the 3D case there is a slight deviation, which is probably due to insufficient discretization of the free surface.

Coupled groundwater flow and solute transport

The capability of FEFTRA to simulate coupled groundwater flow and solute transport was verified with three classic test cases designed for variable density flow and transport problems. Henry's seawater intrusion problem (Section 3.1) concerns a steady-state flow and an advance of a saltwater front in a coastal aquifer initially charged with fresh water. Freshwater enters the aquifer from the inland boundary and mixes with salt water intruding from the sea side until an equilibrium is reached. Elder's free convection problem (Section 3.2) deals with flow driven purely by density differences. In a closed box, solute enters the initially freshwater by diffusion, increases its density, and thereby begins a circulation process. The salt dome problem (Section 3.3) is an example of a steady-state flow in idealised geological conditions over the salt dome, which is a potential site for a deep repository in bedrock. A linearly varying pressure on the top boundary induces an inflow of freshwater into the domain, while the middle third of the bottom represents the top of the salt dome. Eventually, the dispersing saltwater reaches an equilibrium with the opposing freshwater inflow. In Henry's problem the density variations are small (2.5 %). However, in addition to the highly non-linear density dependence on salt concentration in the salt dome problem, Elder's and the salt dome problem are strongly coupled cases due to the large density variations (20 %), thus they present a challenge to the codes.

Due to their non-linear nature, there are generally no analytic solutions for the variable density flow and transport problems, with the exception of the semianalytic solution for Henry's problem. Thus, the numerical solution can usually be assessed by comparison to other numerical solutions only. In Henry's case the computed FEFTRA results (Figure 3.3) compared very well with a revised semianalytic solution. In Elder's case the FEFTRA and other solutions computed with the coarse mesh compared reasonably well (Figure 3.7), while the results computed with the fine discretisation were in excellent agreement (Figure 3.8).

In the salt dome problem the FEFTRA results were compared with the numerical solutions by the original HYDROCOIN (1988) teams 1, 2 and 4 (Table 3.4). The problem proved to be very difficult to solve. Although pressure (Figure 3.11), the Darcy velocity (Figure 3.12) and pathlines (Figure 3.13) were in line with those computed by the HYDROCOIN teams, salt concentration distribution (Figures 3.14 and 3.15) indicated some discrepancies, which may be attributed to the use of non-continuous Darcy velocity, the possible unconvergence of the Picard iteration scheme and/or the inconsistencies in the original specification of the case.

The open underground rock characterization facility ONKALO may also give rise to the upconing of deep saline groundwater observed in the bedrock of Olkiluoto. Saline water is a major concern with regard to the performance of the tunnel backfill material after tunnel closure. The capability of the FEFTRA code to produce the correct behaviour of the upconing phenomenon was verified with the case, which considers a vertical pumping well in an aquifer with a saline water layer residing at depth (Section 3.4). A cross-code verification was performed by comparing the results from FEFTRA with the ones calculated with another simulation code, FEAS, Voss & Souza (1987). The results from

FEFTRA and FEAS are in good agreement, which can be observed from the contour lines of salinity distribution (Figure 3.17 and Figure 3.19) and the mass-fractions at different locations and time steps (Figure 3.18).

Heat transfer

The capability of the FEFTRA code to simulate various heat transfer problems was verified with cases that concern conduction through isotropic (Section 4.1) and anisotropic rock (Section 4.2) as well as convection with flowing water. In the simplest cases, the repository is represented by a point or line-like heat sources, but a detailed cylindrical disposal canister surrounded by bentonite clay layer is considered in one case as well (Section 4.3). Heat output is assumed to be either constant or it decayed exponentially. In all cases the computed FEFTRA results compared well with the analytical or other numerical solutions (Figures 4.3, 4.5 and 4.6 and 4.10).

Simulation of coupled groundwater flow and heat transfer was verified in the case in which the decay heat of spent nuclear fuel induces a buoyancy-driven groundwater flow in an infinite rock with an isotropic and homogeneous properties (Section 4.4). Conduction is the dominant heat transfer mechanism and the temporal variations of the flow field follow solely from the exponentially decaying heat output of the repository. The simulated pressure (Figure 4.13) and temperature (Figure 4.12) rises agreed very well with the analytical solutions.

References

Ackerer, P., Younès, A., & Mosé, R., 1999. Modeling Variable Density Flow and Solute Transport in Porous Medium: 1. Numerical Model and Verification. Transport in Porous Media, 35:345–373.

Ageskog, L. & Jansson, P., 1999. Thermal calculations applied to three hypothetical sites: Aberg, Beberg and Ceberg. Technical Report TR-99-02, Swedish Nuclear Fuel and Waste Management Co (SKB), Stockholm.

Atkinson, K. E., 1988. An Introduction to Numerical Analysis. John Wiley & Sons, Inc., New York. Second Edition.

Bathe, K.-J., 1982. Finite Element Procedures in Engineering Analysis. Prentice-Hall, New Jersey.

Bear, J., 1979. Hydraulics of Groundwater. McGraw-Hill, Israel.

Brooks, A. N. & Hughes, T. J. R., 1992. Streamline Upwind/Petrov-Galerkin Formulations for Convection Dominated Flows with Particular Emphasis on the Incompressible Navier-Stokes Equations. Computer Methods in Applied Mechanics and Engineering, 32:199–259.

Carslaw, H. S. & Jaeger, J. C., 1959. Conduction of Heat in Solids, Second Edition. Clarendon Press, Oxford.

Croucher, A. E. & O'Sullivan, M. J., 1995. The Henry Problem for Saltwater Intrusion. Water Resources Research, 31(7):1809–1814.

CVS, 2007. CVS – The Concurrent Versions System.
`http://www.nongnu.org/cvs/`
`http://ximbiot.com/cvs/`
`http://cvsbook.red-bean.com`.

de Marsily, G., 1986. Quantitative Hydrogeology – Groundwater Hydrology for Engineers. Academic Press INC, Orlando.

Elder, J. W., 1967. Transient Convection in a Porous Medium. Journal of Fluid Mechanics, 27(3):609–623.

Frolkovič, P. & De Schepper, H., 2001. Numerical Modelling of Convection Dominated Transport Coupled with Density Driven Flow in Porous Media. Advances in Water Resources, 24:63–72.

Gradshteyn, I. S. & Ryzhik, I. M., 1980. Table of Integrals, Series, and Products. Academic Press, London.

Grundfelt, B., 1984. Proposal for a Test Problem for HYDROCOIN Level 1 Case 2: Steady-State Flow in a Rock Mass Intersected by Permeable Fracture Zones. Technical report, KEMAKTA Consultants Co., Stockholm, Sweden.

Hartley, L., Hoch, A., & Holton, D., 2002. An integrated approach to groundwater flow modelling on different scales. Working Report 2002-33, Posiva Oy, Helsinki.

Hautojärvi, A., Anttila, M., & Taivassalo, V., 1987. Effects of Fuel Burn-Up and Cooling Periods on Thermal Responses in a Repository for Spent Nuclear Fuel. Report YJT-87-21, Nuclear Waste Commission of Finnish Power Companies, Helsinki.

Henry, H. R., 1964. Effects of Dispersion on Salt Encroachment in Coastal Aquifers. U.S. Geological Survey Water Supply Paper, 1613-C, C71–C84.

Herbert, A. W., Jackson, C. P., & Lever, D. A., 1988. Coupled Groundwater Flow and Solute Transport with Fluid Density Strongly Dependent upon Concentration. Water Resources Research, 24(10):1781–1795.

Hinton, E. & Owen, D. R. J., 1977. Finite Element Programming. Academic Press, London.

Hodgkinson, D. P. & Barker, J., 1985. Specification of a Test Problem for HYDROCOIN Level 1 Case 1: Transient Flow from a Borehole in a Fractured Permeable Medium. Report AERE R-11574, U. K. Atomic Energy Authority, Harwell Laboratories, United Kingdom.

Huyakorn, P. S. & Pinder, G. F., 1983. Computational Methods in Subsurface Flow. Academic Press INC, Orlando.

HYDROCOIN, 1988. The International HYDROCOIN Project – Level 1: Code Verification. Organization for Economic Co-operation and Development (OECD), Paris.

Kolditz, O., Ratke, R., Diersch, H.-J. G., & Zielke, W., 1998. Coupled Groundwater Flow and Transport: 1. Verification of Variable Density Flow and Transport Models. Advances in Water Resources, 21(1):27–46.

Konikow, L. F., Sanford, W. E., & Campbell, P. J., 1997. Constant-Concentration Boundary Condition: Lessons from the HYDROCOIN Variable-Density Groundwater Benchmark Problem. Water Resources Research, 33(10):2253–2261.

Koskinen, L., Laitinen, M., Löfman, J., Meling, K., & Mészáros, F., 1996. FEFLOW – A Finite Element Code for Simulating Groundwater Flow, Heat Transfer and Solute Transport. In Zannetti, P. & Brebbia, C. A., editors, Development and Application of Computer Techniques Environmental Studies VI, Proceedings of the 6th International Conference on Development and Application of Computer Technique to Environmental Studies, Envirosoft96. Computational Mechanics Publications, New York.

Kukkonen, I., 2000. Thermal Properties of the Olkiluoto Mica Gneiss: Results of Laboratory Measurements. Working Report 2000-40, Posiva Oy.

Laitinen, M., 1995. Modelling Convection Dominated Transport Problems with Improved Galerkin Finite Element Formulations. VTT Julkaisuja - Publikationer 804 VTT-JULK-804, Technical Research Centre of Finland, Espoo. (in Finnish, abstract in English). 70 p.

Lee, C. & Cheng, R., 1974. On Seawater Encroachment in Coastal Aquifers. Water Resources Research, 10(5):1039–1043.

Löfman, J., 1999. Site Scale Groundwater Flow in Olkiluoto. Posiva Report POSIVA-99-03, Posiva Oy.

Löfman, J., 2001. The effect of an anisotropic bedrock on the temperature rise of the repository – Preliminary study. Working Report 2001-17, Posiva Oy, Helsinki.

Löfman, J., 2005. Simulation of Hydraulic Disturbances Caused by the Decay Heat of the Repository in Olkiluoto. Posiva Report 2005-07, Posiva Oy, Olkiluoto.

Löfman, J. & Mészáros, F., 2002. Integration of equivalent continuum and discrete fracture network approaches in groundwater flow modelling – Preliminary study. Working Report 2002-39, Posiva Oy, Helsinki.

Löfman, J. & Mészáros, F., 2005a. Simulation of Hydraulic Disturbances Caused by the Underground Rock Characterisation Facility in Olkiluoto. Posiva Report 2005-08, Posiva Oy, Olkiluoto.

Löfman, J. & Mészáros, F., 2005b. Simulation of Hydraulic Disturbances Caused by the Underground Rock Characterisation Facility in Olkiluoto, Finland. In Faybishenko, B., Witherspoon, P. A., & Gale, J., editors, Dynamics of Fluids and Transport in Fractured Rock, Geophysical Monograph 162. American Geophysical Union, Washington, DC.

Löfman, J. & Taivassalo, V., 1993. FEFLOW 1.10 – Solving of Coupled Equations for Flow, Heat and Solute Transport. Report Report YJT-93-30, Nuclear Waste Commission of Finnish Power Companies, Helsinki. (In Finnish).

NAMMU, 2007. A high performance software package for modelling groundwater flow and transport through porous media. Serco Assurance.
`http://www.nammu.co.uk`.

Neuman, S. P. & Witherspoon, P. A., 1971. Analysis of Nonsteady Flow with a Free Surface Using the Finite Element Method. Water Resources Research, 7(3):611–623.

Oldenburg, C. M. & Pruess, K., 1995. Dispersive Transport Dynamics in a Strongly Coupled Groundwater-Brine Flow System. Water Resources Research, 31(2):289–302.

Posiva, 2005. Olkiluoto Site Description 2004. Posiva Report POSIVA 2005-03, Posiva Oy, Olkiluoto.

Posiva, 2006a. Expected Evolution of a Spent Nuclear Fuel Repository at Olkiluoto. Posiva Report 2006-05, Posiva Oy, Olkiluoto.

Posiva, 2006b. Nuclear Waste Management of the Olkiluoto and Loviisa Power Plants: Programme for Research, Development and Technical Design for 2007–2009. TKS 2006, Posiva Oy, Olkiluoto.

Posiva, 2007. Olkiluoto Site Description 2006. Posiva Report 2007-03, Posiva Oy, Olkiluoto.

Rae, J. & Robinson, C., 1979. NAMMU: Finite element program for coupled heat and groundwater flow problems. Report AERE-R 9610, U. K. Atomic Energy Authority, Harwell Laboratories, United Kingdom.

Raiko, H., 1996. Thermal Optimisation of the Final Disposal of Spent Nuclear Fuel. Posiva Report POSIVA-96-03, Posiva Oy, Helsinki. (In Finnish).

Raiko, H. & Salo, J., 1999. Design report of the disposal canisters for twelve fuel assemblies. Posiva Report POSIVA 99-18, Posiva Oy, Helsinki.

Ratigan, J., 1977. Groundwater movements around a repository. Technical Report 54:02, Swedish Nuclear Fuel and Waste Management Co (KBS), Stockholm.

Saksa, P., Ahokas, H., Nummela, J., & Lindh, J., 1998. Bedrock Models of Kivetty, Olkiluoto and Romuvaara Sites, Revisions of the Structural Models during 1997. Work Report PATU-98-12, Posiva Oy, Helsinki. (In Finnish).

Ségol, G., 1994. Classic Groundwater Simulations: Proving and Improving Numerical Models. PTR Prentice Hall, Englewood Cliffs, New Jersey 07632.

Taivassalo, V., Koskinen, L., & Mészáros, F., 1991. Development of the FEFLOW Code for Transient Simulations. Work Report 91-14, Teollisuuden Voima Oy (TVO), Helsinki. (In Finnish).

Theis, C. V., 1935. The Relation between the Lowering of the Piezometric Surface and the Rate and Duration of Discharge of a Well Using Ground-Water Storage. Trans. Am. Geophys. Union, 16th Ann. Meet.

Voss, C. I. & Souza, W. R., 1987. Variable Density Flow and Solute Transport Simulation of Regional Aquifers Containing a Narrow Freshwater-Salt Water Transition Zone. Water Resources Research, 23(10):1851–1866.

WHI, 2003. The Fortran 77 program WHI used in the numerical calculations of the paper by Zhan and Zlotnik (2002).
`http://geoweb.tamu.edu/Faculty/Zhan/Software/pack5`.

Yeh, G.-T., 1981. On the Computation of Darcian Velocity and Mass Balance in the Finite Element Modeling of Groundwater Flow. Water Resources Research, 17(5):1529–1534.

Younès, A., Ackerer, P., & Mosé, R., 1999. Modeling Variable Density Flow and Solute Transport in Porous Medium: 2. Re-Evaluation of the Salt Dome Flow Problem. Transport in Porous Media, 35:375–394.

Zhan, H. & Zlotnik, V. A., 2002. Groundwater flow to a horizontal or slanted well in an unconfined aquifer. Water Resources Research, 38(7):13–1–13–11.

Zhou, Q., Bear, J., & Bensabat, J., 2005. Saltwater Upconing and Decay Beneath a Well Pumping Above and Interface Zone. Transport in Porous Media, 61:337–363.

Zwillinger, D., editor, 1996. CRC Standard Mathematical Tables and Formulae. 30th Edition. CRC Press, Inc., New York.

Appendix A

Automatic testing system

The FEFTRA program package includes a testing system that automatically computes and documents the test cases. The system has been implemented in Unix and Linux environments with the GNU's `(g)make` program (http://www.gnu.org) and the *awk* language. Each module of FEFTRA (e.g. *solvit, flowpath,* etc.) includes a test subdirectory *t* (e.g. *solvit/t, flowpath/t,* etc.), in which all the cases related to the module have been placed. All the material related to the individual cases is located in the their own subdirectory. Test cases are run by the command `(g)make test` in the current home directory of FEFTRA (Table A.1). The command results in a computation of all the test cases located in the directories defined in a variable `TESTDIR` in *feftra/Makefile*, a check of the new results against the old approved results (i.e. the results that have been compared with analytic or other numerical results) and a summary of the test run. The summary (see example in Appendices B–D) is written in the file *test.log* in the FEFTRA home directory and includes a version number of FEFTRA, information on the current computer system, a date of the test run, a list of all the cases computed, a name of a directory in which the cases are located and information as to whether the case has passed or failed testing, or if the case is not run by default, (`"Skipped by user (TEST_FEFTRA = NO)"`).

The tasks executed by the command `(g)make test` are defined in *Makefile*s in the current FEFTRA home directory and in the test directories of the modules. *Makefile*s execute the scripts `fef123` (cases for module *solvit*) and `prgtest` (cases for other modules) in the directory *feftra/bin*. The case is not run by default if the variable `TEST_FEFTRA = NO` in *Makefile* in the case-specific directory.

The documentation of the test cases (this report) is generated by the command `(g)make test.ps` (postscript format) or `(g)make test.pdf` (pdf format) in the FEFTRA home directory *feftra*. The command results in the generation of the whole document in the file *test.ps* or *test.pdf* in the directory *feftra/docs* (note that the size of the postscript file may be quite large i.e. about $\sim$50 MB). The tasks that the command executes are defined in *feftra/Makefile* and require the installation of the LaTeXdocumentation preparation system.

Table A.1. Summary of `(g)make test` *commands in the current home directory of FEFTRA. The summary of the test run is located in the current home directory, whereas the test document is located in* `docs` *directory.*

Command	*Results*
`gmake test`	Run all test cases and create summary of the test run
`gmake test.ps`	Build test document (this report) in postscript format
`gmake test.pdf`	Build test document (this report) in pdf format

Appendix B

Example of a run of the testing system

```
###
### Testing feftra-4.0
###
### system:
Linux vertigo.ketfys.vtt.fi 2.6.19-1.2288.2.4.fc5 #1 SMP
Sun Mar 4 15:57:52 EST 2007 x86_64 x86_64 x86_64 GNU/Linux
### date:
Thu Mar 15 16:14:41 EET 2007
### all output is also saved in test.log

### Cases for concentration in directory
    /users/waste/lofman/feftra/solvit/t/conc

   tc_hydrocoin_l1c2 :     ..............  Passed
tc_hydrocoin_l1c2_3D :     ..............  Passed

### Cases for hydraulic head in directory
    /users/waste/lofman/feftra/solvit/t/head

                t1h :     ..............  Passed
               t1h+ :     ..............  Skipped by user (TEST_FEFTRA = NO)
             th2Dst :     ..............  Passed
          th2Dst_is :     ..............  Passed
           th2Dst_v :     ..............  Passed
             th2Dtr :     ..............  Passed
           th2Dtr_v :     ..............  Passed
             th3Dst :     ..............  Passed
          th3Dst_is :     ..............  Passed
           th3Dst_v :     ..............  Passed
             th3Dtr :     ..............  Passed
           th3Dtr_v :     ..............  Passed
   th_hydrocoin_l1c1 :     ..............  Passed
   th_hydrocoin_l1c2 :     ..............  Passed
th_hydrocoin_l1c2_2Dr2Dfz :     ..............  Passed
th_hydrocoin_l1c2_3D :     ..............  Passed
th_hydrocoin_l1c2_3Dr3Dfz :     ..............  Passed
th_hydrocoin_l1c2_pa :     ..............  Passed
th_hydrocoin_l1c2_pa_3D :     ..............  Passed
     tfs_ZhanZlotnik :     ..............  Passed
          tfs_marino :     ..............  Passed

### Cases for pressure in directory
    /users/waste/lofman/feftra/solvit/t/press

             tp2Dst :     ..............  Passed
          tp2Dst_is :     ..............  Passed
           tp2Dst_v :     ..............  Passed
           tp2Dtr_v :     ..............  Passed
             tp3Dst :     ..............  Passed
    tp3Dst_olkiluoto :     ..............  Skipped by user (TEST_FEFTRA = NO)
           tp3Dst_v :     ..............  Passed
             tp3Dtr :     ..............  Passed
```

```
           tp3Dtr_v :     ..............  Passed
   tp_hydrocoin_l1c1 :     ..............  Passed
   tp_hydrocoin_l1c2 :     ..............  Passed
tp_hydrocoin_l1c2_3D :     ..............  Passed

### Cases for coupled pressure and concentration in directory
    /users/waste/lofman/feftra/solvit/t/press_conc

       tpc2Dst_Henry :     ..............  Passed Passed
          tpc2Dst_is :     ..............  Passed Passed
       tpc2Dst_is5x5 :     ..............  Skipped by user (TEST_FEFTRA = NO)
      tpc2Dtr_elderL :     ..............  Passed Passed
      tpc2Dtr_elderS :     ..............  Passed Passed
          tpc2Dtr_is :     ..............  Passed Passed
          tpc3Dst_is :     ..............  Passed Passed
          tpc3Dtr_is :     ..............  Passed Passed
  tpc_hydrocoin_l1c5 :     ..............  Passed Passed
tpc_hydrocoin_l1c5_3D :     ..............  Skipped by user (TEST_FEFTRA = NO)
        tpc_upconing :     ..............  Passed Passed

### Cases for coupled pressure and temperature in directory
    /users/waste/lofman/feftra/solvit/t/press_temp

  tpt_hydrocoin_l1c4 :     ..............  Skipped by user (TEST_FEFTRA = NO)
 tpt_hydrocoin_l1c4s :     ..............  Passed Passed

### Cases for temperature in directory
    /users/waste/lofman/feftra/solvit/t/temp

           tt2DcondC :     ..............  Passed
           tt2DcondE :     ..............  Passed
          tt2DcondEF :     ..............  Passed
           tt2Dst_is :     ..............  Passed
            tt2Dst_v :     ..............  Passed
            tt2Dtr_v :     ..............  Passed
        tt3Dcanister :     ..............  Passed
           tt3DcontP :     ..............  Passed
          tt3DcontPa :     ..............  Passed
            tt3Dst_v :     ..............  Passed
            tt3Dtr_v :     ..............  Passed
   tt_hydrocoin_l1c2 :     ..............  Passed
tt_hydrocoin_l1c2_3D :     ..............  Passed
  tt_hydrocoin_l1c4s :     ..............  Passed

### Cases for velocity in directory
    /users/waste/lofman/feftra/solvit/t/velo

    tp3Dst_olkiluoto :     ..............  Skipped by user (TEST_FEFTRA = NO)
     tq2Dh_hori_quad :     ..............  Passed
      tq2Dh_hori_tri :     ..............  Passed
       tq2Dh_is_quad :     ..............  Passed
    tq2Dh_is_quad_1d :     ..............  Passed
        tq2Dh_is_tri :     ..............  Passed
     tq2Dh_vert_quad :     ..............  Passed
  tq2Dh_vert_quad_1d :     ..............  Passed
      tq2Dh_vert_tri :     ..............  Passed
```

Appendix D

```
       tq2Dp_is_quad :     ..............  Passed
    tq2Dp_is_quad_1d :     ..............  Passed
      tq2Dpc_is_quad :     ..............  Passed
     tq3Dh_hori_hexa :     ..............  Passed
       tq3Dh_is_hexa :     ..............  Passed
    tq3Dh_is_hexa_2d :     ..............  Passed
      tq3Dh_is_wedge :     ..............  Passed
     tq3Dh_vert_hexa :     ..............  Passed
       tq3Dp_is_hexa :     ..............  Passed
    tq3Dp_is_hexa_2d :     ..............  Passed
tq_hydrocoin_l1c2_3D :     ..............  Passed
tq_hydrocoin_l1c2_3Dr3Dfz :     ..............  Passed
tq_hydrocoin_l1c2_pa_3D :     ..............  Passed
   tq_hydrocoin_l1c5 :     ..............  Passed
tq_hydrocoin_l1c5_3D :     ..............  Skipped by user (TEST_FEFTRA = NO)

### Cases for flowpath in directory
    /users/waste/lofman/feftra/flowpath/t

    tfp3Dq_hori_hexa :     ..............  Passed
   tfp3Dq_hori_wedge :     ..............  Passed
      tfp3Dq_is_hexa :     ..............  Passed
     tfp3Dq_is_wedge :     ..............  Passed
tfp_hydrocoin_l1c2_3D :     ..............  Passed
tfp_hydrocoin_l1c2_3Dr3Dfz :     ..............  Passed
tfp_hydrocoin_l1c2_pa_3D :     ..............  Passed
    tp3Dst_olkiluoto :     ..............  Skipped by user (TEST_FEFTRA = NO)

### Cases for dvelom in directory
    /users/waste/lofman/feftra/dvelom/t

    tdm2Dh_hori_quad :     ..............  Passed
       tdm2Dh_is_tri :     ..............  Passed
     tdm2Dpc_is_quad :     ..............  Passed

### Cases for frate in directory
    /users/waste/lofman/feftra/frate/t

           th3Dfrate :     ..............  Passed
           tp3Dfrate :     ..............  Passed
    tp3Dst_olkiluoto :     ..............  Skipped by user (TEST_FEFTRA = NO)

All tests done
```

Series title, number and
report code of publication

VTT Research Notes 2385
VTT-TIED-2385

Author(s)
Löfman, Jari, Keto, Vesa & Mészáros, Ferenc

Title

FEFTRA™ Verification

Abstract

FEFTRA is a finite element program package developed at VTT for the analyses of groundwater flow in Posiva's site evaluation programme that seeks a final repository for spent nuclear fuel in Finland. The code is capable of modelling steady-state or transient groundwater flow, solute transport and heat transfer as coupled or separate phenomena. Being a typical research tool used only by its developers, so far the FEFTRA code has been short of a competent testing system and precise documentation of the verification of the code.

The objective of this work was to reorganise all the material related to the existing verification cases and place them into the FEFTRA program path under the version-control system. The work also included development of a new testing system, which automatically calculates the selected cases, checks the new results against the old approved results and constructs a summary of the test run. All the existing cases were gathered together, checked and added into the new testing system. The documentation of each case was rewritten with the LaTeX document preparation system and added into the testing system in a way that the whole test documentation (this report) can easily be generated in a postscript or pdf-format.

At the moment the report includes mainly the cases related to the testing of the primary result quantities (i.e. hydraulic head, pressure, salinity concentration, temperature). The selected cases, however, represent typical hydrological applications, in which the program package has been and will be employed in the Posiva's site evaluation programme, i.e. the simulations of groundwater flow, solute transport and heat transfer as separate or coupled phenomena. The comparison of the FEFTRA results to the analytical, semianalytical and/or other numerical solutions proves the capability of FEFTRA to simulate such problems.

The report is available both in a printed and electronic format. As the report is in a constant state of evolution resulting from the current code development, the printed form represents a "snapshot" of its content at the date of publishing, while the electronic format represents always the most up-to-date version of the report.

ISBN
978-951-38-6919-9 (soft back ed.)
978-951-38-6920-5 (URL: http://www.vtt.fi/publications/index.jsp)

Series title and ISSN	Project number
VTT Tiedotteita – Research Notes 1235-0605 (soft back edition) 1455-0865 (URL: http://www.vtt.fi/publications/index.jsp)	16643

Date	Language	Pages
May 2007	English, Finnish abstr.	103 p. + app. 4 p.

Name of project	Commissioned by
FEFTRA07	VTT

Keywords	Publisher
modelling, groundwater flow, solute transport, heat transfer, nuclear waste, disposal	VTT P.O. Box 1000, FI-02044 VTT, Finland Phone internat. +358 20 722 4404 Fax +358 20 722 4374

Julkaisun sarja, numero ja raporttikoodi

VTT Tiedotteita 2385
VTT–TIED–2385

Tekijä(t)
Löfman, Jari, Keto, Vesa & Mészáros, Ferenc

Nimeke

FEFTRA™ Verifionti

Tiivistelmä

FEFTRA on VTT:llä kehitetty elementtimenetelmään perustuva numeerinen virtausten simulointiohjelmisto. Posiva Oy:n käytetyn ydinpolttoaineen loppusijoituspaikkatutkimuksiin liittyviin pohjaveden virtausongelmiin suunniteltua ohjelmistoa voidaan soveltaa moniin erityyppisiin tapauksiin, jotka edellyttävät esimerkiksi veteen liuenneiden aineiden ja/tai veden lämpötilaeroista aiheutuvien veden tiheyserojen huomioimista. Koska ohjelmisto on ollut ennenkaikkea kehittäjiensä ja ylläpitäjiensä käyttöön tarkoitettu työkalu, siitä on tähän asti puuttunut kunnollinen testijärjestelmä sekä yksityiskohtainen dokumentaatio verifioinnista.

Tämän työn tavoitteena oli järjestää uudelleen FEFTRAn hajallaan ollut verifiointimateriaali ja liittää se ohjelmistopakettiin versionhallintaohjelmiston hallintaan. Työssä kehitettiin testijärjestelmä, joka automaattisesti laskee halutut tapaukset, vertaa tuloksia aikaisemmin laskettuihin ja oikeaksi todettuihin tuloksiin sekä konstruoi yhteenvetoraportin suoritetuista testiajoista ja niiden tarkastuksesta. Olemassaoleva hajallaan oleva testimateriaali koottiin yhteen, tarkistettiin ja liitettiin uuteen järjestelmään. Kustakin tapauksesta kirjoitettiin LaTeX-ohjelmalla uusi yksityiskohtainen dokumentaatio, joka liitettiin kehitettyyn järjestelmään siten, että koko dokumentti (tämä raportti) voidaan helposti generoida joko postscript tai pdf-formaatissa.

Tämä raportti sisältää tällä hetkellä pääasiassa perustulossuureisiin (hydraulinen korkeus, paine, suolapitoisuus, lämpötila) liittyviä tapauksia, jotka kuitenkin edustavat sellaisia pohjaveden virtaukseen, suolan kulkeutumiseen ja lämmönsiirtymiseen liittyviä tilanteita, joiden simulointiin ohjelmistoa sovelletaan ydinjätteen loppusijoitukseen liittyvissä paikkatutkimuksissa. Lasketut tapaukset osoittavat FEFTRA-ohjelmiston soveltuvan hyvin kyseisten ongelmien simulointiin.

Raportti on saatavissa sekä painettuna että sähköisessä muodossa. Painettu versio kuitenkin edustaa ainoastaan julkaisuhetkeä, kun taas sähköistä versiota tullaan jatkuvasti päivittämään ohjelmankehityksen mukana.

ISBN
978-951-38-6919-9 (nid.)
978-951-38-6920-5 (URL: http://www.vtt.fi/publications/index.jsp)

Avainnimeke ja ISSN	Projektinumero
VTT Tiedotteita – Research Notes 1235-0605 (nid.) 1455-0865 (URL: http://www.vtt.fi/publications/index.jsp)	16643

Julkaisuaika	Kieli	Sivuja
Toukokuu 2007	Englanti, suom.kiel. tiiv.	103 s. + liitt. 4 s.

Projektin nimi	Toimeksiantaja(t)
FEFTRA07	VTT

Avainsanat	Julkaisija
modelling, groundwater flow, solute transport, heat transfer, nuclear waste, disposal	VTT PL 1000, 02044 VTT Puh. 020 722 4404 Faksi 020 722 4374

FEFTRA is a finite element program package developed at VTT for the analyses of groundwater flow in Posiva's site evaluation programme that seeks a final repository for spent nuclear fuel in Finland. The code is capable of modelling steady-state or transient groundwater flow, solute transport and heat transfer as coupled or separate phenomena. This report is a documentation of the verification cases that represent typical hydrological applications in which the program package has been and will be employed in the site evaluation programme. The comparison of the FEFTRA results to the analytical, semianalytical and/or other numerical solutions proves the capability of the code to simulate such problems.

Julkaisu on saatavana
VTT
PL 1000
02044 VTT
Puh. 020 722 4404
Faksi 020 722 4374

Publikationen distribueras av
VTT
PB 1000
02044 VTT
Tel. 020 722 4404
Fax 020 722 4374

This publication is available from
VTT
P.O. Box 1000
FI-02044 VTT, Finland
Phone internat. + 358 20 722 4404
Fax + 358 20 722 4374

ISBN 978-951-38-6919-9 (soft back ed.)
ISSN 1235-0605 (soft back ed.)
ISBN 978-951-38-6920-5 (URL: http://www.vtt.fi/publications/index.jsp)
ISSN 1455-0865 (URL: http://www.vtt.fi/publications/index.jsp)